University of Coimbra

Doctoral thesis

Contribution to the design of Multi-Functional Artificial Reefs

By Mechteld ten Voorde

Under scientific supervision of:

- Doctor José Simão Antunes do Carmo, Associate Professor in the Department of Civil Engineering of the University of Coimbra;

- Doctor Maria da Graça Neves, Research officer in the National Laboratory of Civil Engineering - Lisbon.

Coimbra, September 2009

I

ACKNOWLEDGEMENTS

ABSTRACT

Portugal is one of many countries in the world that suffers from coastal erosion. Conventional ways of protecting a coastline appear to entail some disadvantages. An innovative and interesting way of protecting a local coastal zone by means of multi-functional artificial reefs avoids some of them. A multi-functional artificial reef is a submerged breakwater which, besides the helping to protect the local coastline, can offer other purposes; in particular, it may enhance the surfing possibilities and the environmental value of the local area. The structure has several positive side-effects: first, it provides an unimpaired visual amenity; second, it offers tourist and economic benefits by improving the surfing conditions; third, it can enhance the environmental value of the area where it is built, and fourth, with a proper design the down drift erosion can be minimal.

An optimal reef design for the Leirosa beach, located to the south of Figueira da Foz, midway along the Portuguese West Atlantic coast, is investigated. In order to achieve this optimal design several steps were conducted. A preliminary design, as a result of a theoretical study, achieved step by step, is proposed for a multi-functional artificial reef making use of the theory and of the state of the art. The proposed reef geometry is used as initial design in the numerical and physical tests, which were executed to analyze the capacity of a multi-functional reef breakwater to protect the local coastline of Leirosa, Portugal, and to increase the local surfing possibilities. Further, a physical and a numerical 2DV study have been executed to get insight in the influence of the length of the reef and in the submergence on the Iribarren number, which is an indication for the breaker type. In this study, also the optimum height for the reef has been defined. Subsequently, in order to be able to investigate the three design parameters: the reef angle, the geometry of the reef (with or without a platform) and the horizontal dimensions in 2DH for the optimal geometry, the Boussinesq-type COULWAVE model was validated; finally, a 2DH numerical study has been conducted with COULWAVE to define the best values for these parameters.

In terms of surfability, and for the conditions of the local coastline of Leirosa, the following values for the main parameters were found: a reef angle of 66°, a structure height of 3.20 m, a reef geometry composed by a delta without platform, a reef submergence of 1.50 m and a structure seaward slope of 1:10.

The calibration of the numerical model COULWAVE has shown that it can be used very well to simulate the hydrodynamics around an MFAR. However, improvements are recommended on the actual version of COULWAVE. These improvements include mainly the introduction of bottom porous structures. Even though the mean velocity fields give an indication about the sediment transport, they are not sufficient to get a

deep insight about the influence of an MFAR on the morphology around the structure. For a proper design of the reef, particularly for the protection of a local coastline, a morphological study has to be executed.

RESUMO

Portugal é um dos muitos países no mundo que sofre os efeitos adversos da erosão costeira. É sabido que as formas convencionais de protecção costeira apresentam algumas desvantagens. Uma forma particularmente interessante de proteger ou contribuir para a protecção local de um troço da zona costeira, minimizando algumas das desvantagens das estruturas tradicionais, é através da construção de recifes artificiais multi-funcionais. Um recife artificial multi-funcional é um quebra-mar submerso construído com objectivos de ajudar a proteger localmente a zona costeira e oferecer outras valências, nomeadamente, aumentar as possibilidades locais para a prática de *surf* e contribuir para a valorização ambiental da região.

Um recife artificial com estas características apresenta diversos aspectos positivos. Com efeito, esta estrutura: (1) não tem qualquer impacto visual negativo; (2) oferece os benefícios económicos resultantes da atracção turística, ao melhorar as condições locais para práticas de *surf* e/ou outros desportos náuticos (mergulho e pesca); (3) permite aumentar o valor ambiental da região, e (4) com um projecto adequado permite reduzir ao mínimo os efeitos adversos da erosão local ou prolongar mesmo a praia por efeito de *tômbolo*.

Neste trabalho são investigados os parâmetros característicos de um recife artificial multi-funcional, tendo como caso de estudo um troço da zona costeira da Leirosa, situado a cerca de 15 km a sul da Figueira da Foz, Portugal. Para obter as características óptimas da estrutura a construir foram realizados vários estudos ao longo de diversas etapas. Como resultado do estado da arte e de um estudo teórico, realizado passo a passo, é proposta uma geometria preliminar de recife artificial multi-funcional. Esta geometria preliminar do recife é em seguida utilizada como projecto inicial de diversos testes em modelo numérico e em modelo físico para analisar a sua capacidade na protecção da praia e do cordão dunar da Leirosa e, em simultâneo, analisar as possibilidades locais para a prática de *surf*.

Além dos testes realizados em modelo físico, foi efectuado um estudo numérico utilizando o modelo 2DV COBRAS-UC para obter informações sobre a influência do comprimento do recife e da submersão do mesmo no número Iribarren, sendo este um parâmetro que fornece uma boa indicação do tipo de rebentação a esperar. Neste estudo foi igualmente investigada a altura ideal para o recife. Posteriormente, procedeu-se à validação de um modelo numérico 2DH do tipo Boussinesq, o modelo COULWAVE, tendo como objectivo analisar a influência de três parâmetros de projecto com particular desenvolvimento no plano horizontal: o ângulo do recife, a geometria do recife (com ou sem plataforma) e as suas dimensões horizontais. Uma vez validado, foi este modelo

numérico utilizado para analisar a influência daqueles parâmetros e identificar os seus valores mais adequados para a definição de uma geometria optimizada do recife.

Em termos de características para a prática de *surf*, e para as condições locais do litoral da Leirosa, foram identificados os seguintes valores para os principais parâmetros: uma estrutura de recife com ângulo de 66º, altura de 3.20 m e uma geometria composta por um delta sem plataforma, uma submersão do recife de 1.50 m e um declive de barlamar da estrutura de 1:10.

A calibração do modelo numérico COULWAVE mostrou que este pode ser usado com sucesso para simular a hidrodinâmica em torno de um recife artificial multi-funcional. No entanto, recomendam-se melhorias na actual versão deste modelo. Tais melhorias incluem principalmente a possibilidade de modelação com fundos porosos. Embora os campos da velocidade média forneçam uma primeira indicação sobre o transporte de sedimentos, esta informação não é por si só suficientemente profunda para obter conclusões definitivas quanto à influência de uma estrutura com estas características sobre a morfologia local. Para uma concepção mais adequada da estrutura final do recife, em particular para efeitos de protecção costeira, deverá ser elaborado um estudo morfodinâmico.

TABLE OF CONTENTS

LIST OF FIGURES

Chapter 1

Chapter 2

Chapter 3

Chapter 4

Chapter 5

Chapter 6

LIST OF TABLES

Chapter 2

Chapter 3

Chapter 4

Chapter 5

Chapter 6

LIST OF SYMBOLS

a	- amplitude
B	- length of structure
$\vec{c}$	- wave celerity vector
c_g	- wave group celerity
d	- water depth at start of reef
g	- gravity acceleration
h	- water depth at structure
h_b	- breaking depth
h_c	- water depth at crest of the structure
h_{fore}	- height of the foreshore
h_init	- water depth at the source
H	- wave height
H_b	- wave height at breakpoint
H_0	- deep water wave heigth
H_m	- mean zero up-crossing wave height
H_s	- significant wave height
H_{wm}	- wave height at the wave maker
h_{reef}	- height of the reef
H/L	- wave steepness
Ir	- Iribarren number
k	- wave number = $2\pi/L$
K_s	- shoaling factor
K_r	- refraction factor
L	- wavelength
L_{begin_reef}	- wavelength at the beginning of the reef
L_c	- length of the crest of the reef
L_{fore}	- length of the foreshore
L_{init}	- length of the initial plane area between the wave maker and the foreshore
$L_{initial}$	- wave length at the source
L_0	- deep water wave length
L_s	- length of reef that wave experiences before breaking
t	- time
T	- wave period, V_p = 'peel rate' of the wave
$\vec{V}_p$	- peel rate of the wave
$\vec{V}_S$	- down-line velocity vector
s	- bottom slope
s_reef	- the slope of the reef
S	- submergence
S_a	- distance from the apex of the structure to the undisturbed shoreline
S_u	- distance from undisturbed shoreline to structure
SZW	- natural surf zone width
T_z	- mean period of zero up-crossing
μ	- wave number times depth
U	- $x\_$horizontal velocity vector
V	- $y\_$horizontal velocity vector
W	- crest width
x	- horizontal axis in cross-shore direction
y	- horizontal axis in longshore direction
z	- vertical axis
α	- peel angle
α_1	- angle θ minus the decrease due to refraction on the reef slope
α_2	- difference of the angles for the cases with and without wave focusing
α_3	- angle due to deviation of the breaker line from the parallel to the bathymetry of the reef side
α_4	- angle θ minus the decrease due to refraction on the reef slope in the part of wave focusing

β - angle between the normal on the bathymetry and the wave ray ('wave angle')

θ - reef angle

ξ_b - inshore Iribarren number

ξ_0 - offshore Iribarren number

γ_b - breaker parameter

∇ - (∂/∂x, ∂/∂y), horizontal gradient vector

ς - surface elevation

LIST OF ABBREVIATIONS

AMD	- name of manufacturer of processors in workstation Corvus
ASR	- Artificial Surf Reef
CIRIA	- Construction Industry Research and Information Association
COBRAS-UC	- Cornell Breaking Waves and Structures, University of Cantabria)
COULWAVE	- Cornell University Long and Intermediate Wave Model
CPU	- Central Processing Unit
DELOS	- Environmental Design of Low Crested Coastal Defense Structures
FINA	- International Federation of Swimming
GSC	- Geotextile Sand Containers
LCS	- Low Crested Structures
MFAR	- Multi-Functional Artificial Reef
MPI	- Message Passing Interface
NLSW	- Non Linear Shallow Water
PC	- Personal Computer
POOC	- Planos de Ordenamento da Orla Costeira
RANS	- Reynolds-Averaged Navier-Stokes
REFDIF	- phase-resolving parabolic refraction-diffraction model
VOF	- Volume of Fluid
2DH	- 2-Dimensions (x,y) in the horizontal plane
2DV	- 2-Dimensional (x,z) in the vertical plane

Chapter 1 Introduction

1. INTRODUCTION

1.1 DEFINITION OF COASTAL ZONES

The nomenclature is not standardized, and various authors describe the same features using different names. This ambiguity is especially evident in the terminology used for the subzones of the shore and littoral areas. In the absence of a widely accepted standard nomenclature, coastal researchers would do well to accompany their reports and publications with diagrams and definitions to ensure that readers will fully understand their use of terms.

As shown in Figure 1.1 the coastal zone is divided into four main subzones: Coast, Shore, Nearshore or Shoreface and Continent shelf - Offshore.

Figure 1.1 - Landforms and terminology of coastal zones (Thurman and Trujillo, 1999).

Each of the following definitions applies (Army Corps of Engineers, 1992):

- The coast is a strip of land of indefinite width that extends from the coastline inland as far as the first major change in topography. Cliffs, frontal dunes, or a line of permanent vegetation usually mark this inland boundary. On barrier coasts, the distinctive back barrier lagoon/marsh/tidal creek complex is considered part of the coast. The area experiencing regular tidal exchange can serve as a practical landward limit of the coast. The seaward boundary of the coast, the coastline, is the maximum reach of storm waves.

- The shore extends from the low-water line to the normal landward line of storm effects, i.e., the coastline. Where beaches occur, the shore can be divided into two zones: backshore (or berm), above the high-tide shoreline, which is covered with water only during storms, and the foreshore (or beach face). The foreshore extends from the low-water line to the limit of wave uprush at high tide, so it is the portion

exposed at low tide and submerged at high tide. The backshore is nearly horizontal while the foreshore slopes seaward. This distinctive change in slope, which marks the junction of the foreshore and backshore, is called the beach or berm crest.

- The nearshore, also shoreface, is the seaward-dipping zone that extends from the low-water line offshore to a gradual change to a flatter slope, denoting the beginning is the continental shelf. The continental shelf transition is the toe of the shoreface. Its location can only be marked approximately, because of the gradual slope change. The nearshore is never exposed to the atmosphere, but is affected by waves that touch bottom. It is the zone of most frequent and vigorous sediment transport, especially the upper part.

- The continental shelf is the shallow seafloor that borders most continents. The shelf floor extends from the toe of the shoreface to the shelf break where the steeply inclined continental slope begins. It has been common practice to subdivide the shelf into inner-, mid-, and outer zones, although there are no regularly occurring geomorphic features on most shelves that suggest a basis for these subdivisions.

Beaches include both the shore and nearshore subzones. They are composed of the material – sediment – primarily provided by the erosion of beach cliffs and/or by rivers that drain lowland areas. Other sources of materials, like shell fragments and the remains of microscopic organisms that live in the coastal waters, are less common. Beaches on volcanic islands are frequently composed of dark fragments of the basaltic lava that make up islands, or of coarse debris from coral reefs that develop around islands in low latitudes. Thus, around the world, there are beaches composed of crushed coral, beaches made of quartz sand, beaches made of rock fragments, beaches made of black (or even green) volcanic material, beaches composed of shell fragments, and even artificial beaches composed of scrap metal dumped at the beach (Thurman and Trujillo, 1999).

In general sediments consisting of sand and gravel occur on the upper and middle shoreface, muds of fluvial origin occur on the shelf and mixed sands and muds are found in the lower shoreface zone (transition zone to shelf). Bed sediments generally fine in seaward direction, supplied by offshore-directed bottom currents (rip currents and storm-induced currents). Sometimes relatively coarse-grained relict sediments are found on the shoreface.

1.2 COASTAL USES AND VULNERABILITIES

The coastlines of many countries have not only been shaped by natural forces but, over the last few centuries especially, they have also been strongly influenced by people.

Early communities adopted a subsistence way of life which, compared with today's lifestyles, had a low impact on the natural heritage of the coast; these communities lived in relative harmony with their environment.

This is easily explained because in past centuries the littoral was always an area with little attraction, to be avoided at all costs. Apart from fishing communities and ports, there was little to attract people to the coast - quite the contrary, in fact. Climatically it is an area of contrast, hot during the day and cold at night, windy, and without protection against the sun. In terms of resources there was little to exploit except for fisheries and harbours. On the other hand it was a dangerous area. People living there (mostly fishermen) were rude; pirate raids were frequent, killing and looting the local populace. Consequently, the littoral was for a long time a very sparsely populated area (Dias *et al*., 2002).

The awakening interest in the sea and the beaches appears all over Europe from the end of the 19th century. This was when the first bathing beaches started to spring up everywhere, particularly in France and Britain.

From the end of the 19th century to the first half of the 20th century the occupation of the littoral can be said to have been of a therapeutic character, as the objective of bathers when they left their houses carrying their bags and baggage to the beach resorts was to "go to the baths". This consisted of exposing oneself to the waves at the beach. The practice was prescribed medically, being indicated as a treatment for several physical illnesses or states of mind, and applied to adults and children. Baths in the sea were taken "as remedy, not for pleasure" (Colaço and Archer, 1943, in Dias *et al*., 2002).

The 20th century saw changes in the way of looking at the littoral. It became a place for pleasure, where the beach played an important role in leisure, and became a popular holiday destination.

It is a matter of fact that major social and economic changes over the last few hundred years in many countries, including Portugal, have resulted in dramatic changes to the character and natural heritage of the coastline. More intensive farming, coastal development and better access to the coast have all affected the natural coastal processes and led to a loss of habitat and wild coastal land. The bigger cities have grown and spread along the coastline and numerous towns have developed, mostly as fishing ports, on mainland and island coasts alike.

Some indicators are easily stated (Ten Voorde *et al*, 2009):

- 20% and 40% of people live within 30 km and 100 km of the coast, respectively;
- coastal populations are growing more rapidly than global populations, mainly in urban settings;
- global mean sea levels rose 10 to 20 cm in the 20th century;
- in the 21st century, human-induced climate change will contribute to a global rise of 20 to 100 cm, with a mid estimate of 50 cm;
- other climate factors relevant to the coast will also change, although details are unclear.

All around the world, mega-cities (cities with more than 10 million people) are increasing in number as the global human population continues to become more urban. By the end of 2030, three-fifths of the world population will be living in urban areas. Much of this urban growth occurs outside defined city boundaries and the resulting expansion of urban or "built-up" areas can be clearly seen from orbiting satellites. As a consequence, the degradation of coastal ecosystems is to be expected, as well as increased pollution of coastal waters.

Global warming will lead to dramatic coastal changes in the near future. In fact, the greenhouse effect and resulting warming of the earth's temperature may accelerate the mean sea level. A rise in the mean sea level would cause erosion, flooding, and saltwater intrusion in bays and estuaries.

An extensive study of coastal problems has been conducted under the EUROSION project (Eurosion, 2004). This project entailed 60 case studies, considered to be representative of European coastal diversity. The case studies reveal many erosion problems along the European Atlantic coast. The Atlantic Ocean borders Western Europe around the following EU countries: the United Kingdom, Ireland, France, Spain and Portugal. Generally speaking, the coastline around the Atlantic Ocean is made up of hard and soft cliffs interspersed with sandy and shingle beaches and dunes (Eurosion, 2004). The high relief, hard cliffs and rocky coastlines are mostly found in northern Spain, northern Portugal and parts of northern France. The softer coasts may be found in western Ireland (e.g. Donegal and Rosslare) and the southern United Kingdom (Sussex), where soft cliffs with shingle and sand beaches and smaller dunes alternate with small bays and estuaries. Larger, extensive dunes are found on the southwest coast of France (Aquitaine).

Erosion of the Atlantic coastline, as has occurred in Estela, on the coast of Portugal (Figure 1.2), is a consequence of natural and human-induced factors (Gomes and Pinto, 2006). The high-energy, storm generated waves from the Northern Atlantic and the macro-tidal regime (medium range 2-4 m, maximum up to 15 m in the Bay of Mont

Saint-Michel, France), are the dominant erosive forces on the continental European Atlantic coastline. Together they create extreme conditions with strong alongshore tides and/or wave driven currents and cross-shore wave driven currents that can easily erode beaches and undermine cliffs. Climate change is expected to induce accelerated sea level rise (at present 2-4 mm/yr) at some point in the future, as well as a potential increase in storminess. Both will worsen erosion along the Atlantic coast. Human interference, such as the construction of seawalls or groynes, damming of rivers and sand mining, has intensified erosion locally.

Figure 1.2 - Estela golf course, critical erosion zones (Gomes and Pinto, 2006).

In both northern and southern Europe erosion threatens urbanization (the safety of human lives and investments), tourism and nature. Furthermore, in Spain, Portugal and France fishing and aquaculture are of great importance in the coastal zone. In the United Kingdom and Ireland, a lot of agricultural land is found in the coastal zone. The explosive growth of the population in the littoral zone, partly due to tourism, has increased the pressure on the coast, especially in France, Spain and Portugal and the south coast of England. It appears that most of the European Atlantic coastal areas are at high risk due to the low-lying coastal plains that are at risk of flooding (Eurosion, 2004).

The 'hold the line' policy option is often applied when seaside resorts or other recreational facilities are at risk. This is especially true in France, Spain and Portugal but it is often relevant in the south of England and Ireland, too, where tourism plays a leading role in the protected sites. Furthermore, high population densities and economic investments are protected by applying the 'hold the line' policy, as in the United Kingdom, Ireland and Portugal (Eurosion, 2004).

'Managed realignment' is possible at some of the seaside resorts and recreational facilities if the amount of capital at risk is relatively small and the recreational facilities or houses can be moved inland without too many problems. In a flooding area, a new defense line is usually defined (under the principle of 'Managed realignment'). 'Do nothing' is usually applied to cliff coasts where there are no flooding risks and therefore the amount of capital at risk is relatively low.

At many sites along the Atlantic coast, a mixture of hard and soft engineering solutions is adopted to deal with erosion. Various types of hard solutions had been applied in the cases considered. Although applied in nearly all cases, beach nourishments are executed on a much smaller scale (in terms of m^3) than in the North Sea and the Baltic regions. Whereas in the North Sea regions soft measures are often implemented to combat erosion, along the Atlantic coasts the soft solutions are often combined with hard measures. The high energy conditions of the coast and the steep foreshore mean that nourished sediment is quickly transported in an offshore direction, and it might not return by means of the equilibrium movement during the year.

1.3 GENERAL PROTECTION MEASURES

Experience has shown that as yet there is no miracle solution to counteract the adverse effects of coastal erosion (Eurosion, 2004). The best results have been achieved by combining different types of coastal defense including hard and soft solutions, taking advantage of their respective benefits while mitigating their respective drawbacks. Since it can be seen that coastal erosion results from a combination of various natural and human-induced factors it is not surprising that miracle solutions to counteract the adverse effects don't exist. Nevertheless, the general principle of "working with nature" was proposed as a starting point in the search for a cost-effective measure. However, this observation also undeniably takes on board the idea that soft engineering solutions are preferable to hard ones. This is backed by a number of considerations derived from experience (Eurosion, 2004):

- Even tried and tested soft solutions - such as beach nourishment, which aroused tremendous enthusiasm in the 1990's - have suffered serious setbacks. Such setbacks have been caused by inappropriate nourishment scheme design induced by poor understanding of sediment processes (technical setback), difficult access to sand reserves which leads to higher costs (financial setback), or unexpected adverse

effects on the natural system - principally the benthic fauna - (environmental setback). These are well covered by, respectively, the case of Vale do Lobo (Portugal) where 700 000 cubic metres and 3.2 millions euros of investment have been washed away by longshore drift within a few weeks only, the case of Ebro where the amount of sediment needed to recharge the beach sediments had been imported from another region, and the case of Sitges (Spain) where the dredging of sand to be supplied has caused irreversible damage to sea grass communities (Posidonia).

- Soft solutions, due to their particularity of working with nature, are found to be effective only in a medium to long-term perspective, i.e. when coastal erosion does not constitute a risk in the short-term (5 to 10 years). Their impacts do indeed slow down coastline retreat, but they don't stop it. The long term positive effect of soft solutions may be optimized by hard structures which make it possible to tackle an erosion problem efficiently but have a limited lifetime (in general no more than 10 years). This has been particularly well-documented for example in the case of Petite Camargue (France), where the presence of hard structures - condemned anyway – also turned out to provide sufficient visibility for soft defense such as dune restoration wind-screens to operate.

Several technical measures can be taken to combat erosion:

- **Hard measures**

  Hard measures are structures like seawalls, revetment/slope protections, groynes and detached breakwaters. The case studies show that hard measures can work really well if the consequences are accepted. If erosion is predicted for and accepted elsewhere, the overall performance can be good. On several places of the Atlantic coast, strong structures need to be built to resist extreme events that bring very large waves.

- **Soft measures**

  Soft measures are those like beach and dune nourishment, submerged nourishment, vegetation techniques and cliff stabilization. Soft measures can be a short term solution. Erosion can continue at the same rate and soon the action (measure) needs to be repeated. This is especially true in the Atlantic where wave heights and tidal amplitudes can be quite large.

- **Combined measures**

  At many sites along the Atlantic coast, a combination of hard and soft engineering solutions is often adopted for dealing with the erosion issues, probably due to the high energy conditions of the coast.

- **Innovative measures**

These include measures like beach drainage systems. The 'Écoplage' system (applied in Sables-d'Olonne, France) consists of a gravity drain that lowers the water table beneath the beach. As a result, the beach is not saturated with water when waves break on the shore and the infiltration of the water into the sand is improved. The purpose of the system is to reduce swash velocities, sediment transport, and therefore erosion. The water flows by gravity from the drain to a pumping system. The water is then pumped into the sea or is used as (filtered) water in swimming pools or aquariums. The beach drainage system seems successful. It does not block the littoral drift like a groyne does. The treated beach is stabilized and the untreated beach is continuing to be eroded. Figure 1.3 shows a draft scheme of the system installed.

Figure 1.3 – Scheme of the 'Écoplage' system installed in Sables-d'Olonne, France.

A completely different type of measure was tried at El Médano (beach with dunes) on the Canary Islands (Eurosion, 2004). In 1995 an experiment started which aimed at recovering eroded sediments. In this case, it was decided to place small obstacles in a completely bare exposed area. This involved scattering amounts of about 2 m^3 of volcanic gravel around the eastern slope of Bocinegro mountain. The experiment is based on the volcanic gravel's capacity to retain sand, on which plants germinate, beginning the process of soil regeneration and dune formation. The experiment was effective: the retention and accumulation of sand increased, above all on the smaller obstacles.

Another solution was implemented to protect a sand dune system in Leirosa, south of Figueira da Foz, in the centre of the Portuguese West Atlantic coast.

In mid '90's the construction of an underwater effluent emissary was responsible for the disruption of this sand dune system. The use of hard machinery in a fragile area, aggravated by the erosion caused by the breakwater about 1 km north Leirosa, also contributed to the destruction of this system.

The restoration of the Leirosa sand dunes started in 2000. The dunes were reconstructed mechanically according to the AIDS (Artificially Inseminated Dune Systems) method (Reis and Freitas, 2002). This process allowed the damaged dune system to be rebuilt the desired height and slope in a short time. The second part of the rehabilitation process consisted of increasing the stability that had been achieved by revegetation with *Ammophila arenaria*. This beach grass is widely used all over the European coast in the rehabilitation of degraded systems due to its unique capacity for sand stabilization and dune formation.

In February 2001, during a storm that affected the whole of the central region of Portugal, especially on the coast, the ocean front of the Leirosa dune system was destroyed in just one night.

After this event it was decided to try another solution, based on the use of geotextiles. This material can be as effective as any so called "hard engineering protection", with the advantage that it is adaptable to the morphology of the dune system and uses the local available sand (Bleck *et al*., 2003).

In the Leirosa system geotextiles were applied to a dune extension of 120 m along the coast. A defense was created on the front bottom of the dune, at the +2.0 level (hydrographic zero) with sand containers about 6.40 m long, 3.20 m wide and 0.825 m high, in a pyramid arrangement parallel to the coastline (Figure 1.4).

Figure 1.4 – Installation of the sand containers and first layers of geotextiles in the Leirosa sand dune system (Antunes do Carmo, January 2006).

The protective barrier was constructed to a height of 8 m by several layers of sand enveloped in geotextiles, in a so called "wrap around technique", which encapsulates the sand and can be installed quickly.

This technique allows the absorption of the energy of upcoming wave attacks and prevents erosion of the fill material through the tensile forces which are activated by this stress. Furthermore, pore water pressures within the encapsulated sand fill are released thanks to the good drainage capacity of the geotextile.

The upper layer used a geotextile revetment throughout the area, about 8.60 m long, 4.30 m wide and 1.10 m high, followed by a 1.0 m layer of sand where dune vegetation was planted, turning this area into an attractive and safe coastal dune system (Reis *et al.*, 2005).

It is expected that the technique developed to protect the Leirosa sand dunes will become an important model to be used for other dune systems with similar erosion problems.

1.4 NEW CONCEPTS OF COASTAL PROTECTION

Various coastal structures can be used to solve, or at least, to reduce coastal erosion problems. Some of them can provide direct protection, like breakwaters, seawalls and dikes, and others, such as detached breakwaters and artificial reefs, provide indirect protection, reducing the hydraulic load on the coast to the level required to maintain the dynamic equilibrium of the shoreline. To achieve this objective, these structures are designed to allow the transmission of a certain amount of wave energy over the structure by overtopping (and also some transmission through the porous structure, in some types of breakwaters), and/or wave breaking and energy dissipation on a shallow crest (submerged structures) (Pilarczyk, 2003).

Rock walls, breakwaters or groynes usually serve the purpose of protecting land from erosion and/or enabling safe navigation into harbours and marinas, but other commercial value and multi-purpose recreational and amenity enhancement objectives can also be incorporated into coastal protection and coastal development projects. Offshore breakwaters/reefs can be permanently submerged, permanently exposed or inter-tidal. In each case, the depth of the structure, its size and its position relative to the shoreline determine the coastal protection level provided by the structure. Submerged breakwaters could be an interesting and efficient strategy, not only to protect a coastal system, but also to improve the bathing conditions of some coastal zones. Therefore, these so-called multifunctional artificial reefs (MFARs), are one of the new innovative concepts for coastal protection. The actual understanding of the functional design of these structures may still be insufficient for optimum design but it may be just good enough for these structures to be considered as serious alternatives for coastal protection (Pilarczyk, 2003).

The two main purposes of an MFAR (coastal protection and increasing the surfing possibilities in a certain area) are explained in greater detail below.

The construction of an MFAR can play a part in different kinds of coastal protection, like:

- Preventing coastal erosion;
- Increasing, in combination or not with sand nourishment, the stability of beaches.

These sorts of coastal protection are possible because:

- An MFAR can reduce the wave loads on the coast through a series of wave transformation processes occurring on the structure, viz., reflection and energy dissipation due to waves breaking on the structure and to flow circulation inside the porous media;
- An MFAR can create current circulation cells behind the reef which can cause sedimentation at the shoreline;
- An MFAR can be used to regulate wave action by refraction and diffraction.

With one kind of design, waves can break over an MFAR in such a way that surfers can enjoy great sport riding them. Surfing and bodyboarding are growing in popularity, and are practised especially by young people. Surfing means taking a wave board into the sea and waiting for a breaking wave to 'ride' on (Figure 1.5).

Figure 1.5 - Waiting for and surfing a wave (source: www.surfline.come).

Multi-functional reefs are in fact a hard measure for tackling coastal problems, and they have several advantages over soft measures. The most suitable construction material for multi-functional artificial reefs is geotextile, used as a sand container. Sand-filled geotextile containers are becoming increasingly recognized as a tool for coastal defense. Geotextiles are a family of synthetic materials including polyethylene, polyester and polypropylene. In their common form they are flexible, permeable and durable sheet fabrics, resistant to tension and tear. They can be sewn or ultra-sonically welded to produce containers designed to retain sand or mortar for use as a construction

material. Geotextile containers can be filled and placed using many different methods depending on the site location, fill material, container size, available plant, and type of geotextile fabric chosen. The advantages are several:

- **Environmental impact**

  Construction with geotextile containers allows the use of local materials that would otherwise be unsuitable for coastal construction. In many cases permission can be obtained to fill the containers with sandy materials taken from the seabed in the region of the project site itself. This means that the amount of 'foreign' materials introduced to an area is minimized. Unless exposed to high temperatures or pH levels, geotextile materials have been shown to be inert in the marine environment.

- **Durability**

  Modern geotextiles are designed to withstand environmental degradation from abrasion, UV, chemical and biological influences, and as such a life span of the order of 25 years can be expected, notwithstanding vandalism or mechanical damage. Under accelerated testing, life spans of up to 100 years even in challenging marine conditions have been postulated. During the construction of the Narrowneck reef very effective underwater patching techniques were developed to repair damage that had arisen during the construction (Restall *et al.*, 2002). The holes are sealed with a silicone based adhesive and a patch is screwed down over the hole, using nylon wall screws, to provide added protection. Various coatings were trialed for the crest bags, with mixed success. But towards the end of the construction a durable composite (hybrid) material was developed and tested with great success. Initial trials utilized a spray-on polyurethane coating of varying thickness, however this product became rigid once exposed to water and actually made the products more susceptible to impact and wave damage. The composite material, consisting of two layers of non-woven geotextile, used towards the end of the project allows approximately 4 kg/m^2 of sand and shell particles to be retained within it. Once the geotextile is impregnated with these particles its puncture resistance shows significant improvement, while marine growth can protect it from UV degradation.

- **Structure is removable**

  In the unlikely event that the structure has a previously unforeseen negative impact on the surrounding area, geotextile systems allow the reef to be quickly and easily removed. By filling the containers with locally obtained sand, the environmental impact of removal would be insignificant as the material released from the reef would be the same as or very similar to the natural beach sand.

- **Provision of marine habitat**

  Marine ecosystem enhancement is a fourth advantage of the use of geotextile sand containers. These containers have appeared to provide an excellent substrate for marine flora and the development of a diverse ecosystem (Borrero and Nelson, 2003, Jackson *et al*., 2004). Figure 1.6 shows, as an example, short algae and sea grasses on shallower containers in the Narrowneck reef off the Gold Coast of Australia.

Figure 1.6 - Short algae and sea grasses on shallower containers of the Narrowneck reef (Jackson *et al*, 2004).

When the ecosystem on this reef was well developed, a clear zoning between areas of sea grass and kelp could be observed. Visually, the macroalgal communities dominated the reef, covering over 70% of the reef surface. It was also populated by a variety of other benthos, including coralline algae, sub-massive sponges, ascidians, octocorals (soft corals), hydroids and crinoids (feather starfish), echinoids (sea urchin) and abalone. Observations by the National Marine Science Centre indicated that "the biological communities associated with Narrowneck Artificial Reef appear to enhance biodiversity and productivity at a local scale and may also contribute to overall regional productivity" (Edwards, 2003).

- **Soft reef surface**

  The use of sand-filled fabric containers maximizes safety on the reef by providing a relatively soft structure without sharp edges, reducing the risk of injury should a surfer come into contact with the reef.

- **Cost**

  As with any construction method, the cost of a reef project is site dependant, as it relies on the availability of plant, materials, labour and suitable construction conditions. However in many situations, especially with large projects, it has been found that geotextile solutions can have the cost of the equivalent rock structure (ASRLtd, 2008).

However, there are also some limitations:

- **Experience of contractors**

  Coastal engineering contractors around the world are highly experienced in the use of rock and concrete for coastal construction. Experience in the use of sand-filled geotextile systems is less common, although the recent significant growth in the use of geotextiles for coastal projects worldwide is rapidly improving the skill base.

- **Susceptibility to mechanical damage and vandalism**

  Testing has shown modern geotextiles to have good puncture and abrasion resistance; but the resistance of the fabric to mechanical damage and vandalism is clearly lower than that of rock or concrete. As mentioned before, very effective underwater patching techniques were developed to repair damage during the construction of the Narrowneck reef. Notwithstanding this fact, extra care must be taken while handling the units during construction, and in some locations it may be necessary to introduce measures to safeguard against vandalism.

- **Lack of design guidance**

  At present there are relatively few guidelines available for the design of coastal structures using geotextiles. Despite the lack of official design guidance, there has been considerable research in the area of geotextiles and the conclusions of this research along with experience of a wide range of previous projects can be drawn on to allow successful design.

Several reasons may account for the growing interest of MFARs over conventional ways of protecting a local coastline:

- These structures have, by definition, a minimal visual intrusion that especially enhances their value in zones with strong aesthetic constraints;
- The structure becomes known better as a way of boosting surfing possibilities as well as a way to protect the coast;
- The water renewal induced by the high level of transmission is desirable to avoid stagnation and ensure satisfactory quality for recreational waters, especially in tideless seas, and water oxygenation for animals and plants living in the protected area leeward of the breakwater;
- The structure is interesting in economic terms. First, geotextile sand containers tend to be cheaper per unit volume than rubble-mound structures, and second, the surfing aspect can attract the tourism, which is good for the local economy;
- The expansion of the environmental value is a great benefit in these times, in which nature is being destroyed more and more, by the behavior of humans.

1.5 OBJECTIVES AND METHODOLOGY

The main objective of this thesis is to define guidelines for an MFAR. In order to achieve this goal, the research focuses mainly in three activities, which are:

(1) identification and analysis of the influence of key parameters involved in the functionality of an MFAR;

(2) calibration of a numerical model to be used in the study of the MFAR;

(3) definition of the characteristics of the geometry of the MFAR most suitable for the west-coast of Portugal based on physical and numerical modelling.

Throughout these activities, studies will be carried out having in view the following objectives:

- The definition of guidelines for multi-functional artificial reefs on theoretical base;
- The identification of relations between the breaker type, the submergence and the height of an MFAR;
- The calibration of the COULWAVE model (Lynett, 2002) as a reliable tool for the simulation of multi-functional artificial reefs;
- The investigation, using numerical and physical modelling, of the influence of different design parameters of an artificial surfing reef on the hydrodynamics around an artificial surfing reef in order to find the optimal design of an MFAR for the coast of Leirosa in terms of coastal protection and surfability.

To achieve the objectives specified above, the following methodology was adopted. At first an analysis of functionality of a multi-functional artificial reef including the state of art is done. Secondly a theoretical study to achieve preliminary design guidelines for an MFAR is conducted. Thirdly physical experiments in a wave flume and numerical simulations with COBRAS-UC (Garcia *et al*. 2004) to investigate the relation between the breaker type and the length and the submergence of a submerged artificial reef are carried out. In order to be able to use a numerical model to investigate the functionality of a multi-functional reef, a numerical calibration of the COULWAVE model (Lynett, 2002) is done by comparing results with 3D experimental data of Poort (2007). Finally, based on the results found in the methodology followed so far, preliminary numerical simulations with the validated model are executed to define the optimal design of an MFAR for the conditions of the coast in front of Leirosa.

1.6 STRUCTURE OF THE THESIS

The studies conducted to investigate the functionality of multi-functional artificial reefs are described in this thesis along seven chapters, distributed in accordance with what follows.

After this first chapter, which includes the framework of the thesis and presents the main objectives and the methodology adopted in the investigation, chapter 2 describes

the functionality of an MFAR in terms of coastal protection and surfability, together with the state of art. Chapter 3 treats design guidelines for an MFAR according to a theoretical study. In chapter 4, the physical experiments and numerical simulations with COBRAS-UC to investigate the breaker type in relation with the submergence and the length of a submerged reef and its results are described. Chapter 5 gives the description of the mathematical and numerical COULWAVE model and contains also the calibration of this model with data from experimental tests in a wave basin done by M. Poort (2007). In chapter 6, the investigation conducted to obtain the optimal geometry of the reef for the Leirosa coast with numerical simulations is presented. Results from the theoretical study and from the physical and numerical tests constitute the base for the geometry to be investigated with the numerical simulations. Chapter 7 contains the main conclusions and recommendations.

Chapter 2 Functionality of a Multi-Functional Artificial Reef

2. FUNCTIONALITY OF A MULTI-FUNCTIONAL ARTIFICIAL REEF

The viability of an MFAR is related to its functionality regarding the two main goals of the structure: coastal protection and surfing capability. In terms of coastal protection, it is very important to analyze both the hydrodynamics and morphodynamics. Concerning surf characteristics, there are several parameters to be checked, as described below.

This chapter presents a description of the functionality of an MFAR, including the state of art regarding multi-functional artificial reefs, particularly in what concerns coastal protection and surfability. The functionality and the contribution of multi-functional artificial reefs already built and under construction are also described.

2.1 COASTAL PROTECTION

2.1.1 HYDRODYNAMICS IN COASTAL ZONES

Most waves generated in the sea area by storm winds move across the ocean as swell. Generally, they release their energy along the margins of the continents in the surf zone, which is the zone of breaking waves.

According to the physical characteristics of the coastal platform responsible for the wave transformations as they travel cross-shore, wind-generated waves have been described by several different theoretical developments. In deep waters the small amplitude wave theory, which constitutes the first order of approximation of the Strokes theory, performs well. In transitional waters, as the waves become larger, higher orders of approximation to the Stokes theory can be can be used. Other nonlinear theoretical approaches should be used in shallow water conditions, like the cnoidal wave theory derived by Korteweg and De Vries (1895), and others. For very shallow water waves, a solitary wave theory developed by Boussinesq (1872), Serre (1953) and others should be used.

Figure 2.1, adapted from Kamphuis (2000), shows the applicability of the various wave theories. The waves are transformed as they travel into shallower water. Once in shallow waters, a wave undergoes many physical changes before it breaks. The shoaling depths interfere with water particle movement at the base of the wave, so the wave velocity decreases. As one wave slows, the next waveform, which is still moving at unrestricted velocity, comes closer to the wave that is being slowed, thus reducing the wavelength. The energy in the wave, which remains the same, must go somewhere, so wave height increases. The crests become narrow and pointed, and the troughs become wide curves. This increase is called shoaling.

Figure 2.1 - Applicability of various wave theories (Kamphuis, 2000).

The combination of increasing wave height and decreasing wavelength causes an increase in the steepness (H/L) of the waves. In addition, energy is dissipated due to bottom friction.

If sections of a single wave crest are travelling in different water depths, the sections in deeper water will travel further per unit time, and therefore the wave will change direction or refract. Therefore, wave refraction is the gradual reorientation of waves propagating at an angle to the bottom slope or against a current. Figure 2.2 shows a refraction plane for the S. Lourenço fortification – Tagus estuary (Portugal) - corresponding to a wave 3.0 m high (offshore), a 12 sec period, and direction 225º (Antunes do Carmo and Seabra-Santos, 2002). As observed in this figure, refraction patterns are often interpreted by means of orthogonals, or wave rays. The first are lines drawn at right angles to the wave crests, and the second are lines indicating the direction of energy transmission.

Figure 2.2 - Refraction plane for the S. Lourenço fortification – Tagus estuary (Portugal) - corresponding to a wave 3.0 m high (offshore), 12 s period, and direction 225° (Antunes do Carmo and Seabra-Santos, 2002).

In selected situations, like that presented in Figure 2.3, such as when waves pass a small cape, island or even piers and jetties, diffraction occurs; this is a lateral transfer of energy along wave crests.

Incident waves may be reflected from beaches, cliffs, submarine shoals, bars and ridges, jetties, seawalls, etc. The reflected waves may be of the same dimensions as the incident waves, and if the wave travels in exactly the opposite direction then a standing wave can develop. Standing waves are the product of two waves of the same wavelength moving in opposite directions, resulting in no net movement. In confined basins standing waves are known as seiches.

Figure 2.3 – Madeira island and wave crests at Porto Santo island computed by REFDIF (Fortes *et al*., 2006).

2.1.2 *MORPHODYNAMICS IN COASTAL ZONES*

Morphological changes in beaches depend on the nature of beach material, hydrodynamic processes (waves, tides and currents), the original profile and local boundary conditions. This last is related to the existence of headlands and bays, which control the energy acting on the beach and produce spatial variations in beach slope, grain size and sediment transport rates (Rey *et al*., 2002).

Most shorefaces and shelves are underlain by relatively thick marine sedimentary sequences. In general, sediments consisting of sand and gravel occur on the upper and middle shoreface, muds of fluvial origin occur on the shelf, and mixed sands, and muds are found in the lower shoreface zone (transition zone to shelf) (Van Rijn, 2001). Bed sediments are generally fining in a seaward direction, supplied by offshore-directed bottom currents (rip currents and storm-induced currents).

The fluid in the shoreface zone may be homogeneous (well-mixed) or stratified with a surface layer consisting of relatively low fluid density (fresh warmer water) and a

24

bottom layer of relatively high density (saline colder water). Strong horizontal density-related pressure gradients may occur in regions close to river mouths.

The upper shoreface (surf zone) is dominated by wave-driven processes. The surf zone can be seen as a subsystem of the shoreface zone. The shoreface zone influences the surf zone by providing boundary conditions, but the surf zone also affects the shoreface zone by generating strong rip currents that bring sediments to the shoreface. Furthermore, the surf zone is a source of free low-frequency energy propagating into the shoreface zone. The middle and lower shorefaces are affected by tide- and wind-driven currents and by Coriolis effects (Van Rijn, 2001).

Sand can be transported by wind-, wave-, tide- and density-driven currents (current-related transport), or by the oscillatory water motion itself (wave-related transport). The waves generally act as a sediment stirring agent, whereas the sediments are transported by the mean current. Wave-related transport may be caused by the deformation of short waves under the influence of decreasing water depth (wave asymmetry). Low-frequency waves interacting with short waves may also contribute to the sediment transport process (wave-related transport).

Tide- and wind-generated currents with near-bed velocities greater than 0.3 m/s are able, even at great depths, to move the sediments forming the bed surface. Although often rather weak, cross-shore currents combined with the stirring action of the waves are important for the long-term evolution of the shoreface morphology. Big storms are able to move sediments along the bed surface in water at depths of up to 100 m. Thus, the shoreface is an active morphodynamic zone, although the bed evolution processes may proceed rather slowly (Van Rijn, 2001).

While alongshore transport is the primary mechanism for changes in beach plan shape, cross-shore transport is the means by which the beach profile changes. The response time of beaches to variation in cross-shore transport can be as short as one tidal cycle (during storms) or as long as six months (seasonal variations). Predictions of beach response are very important for coastal designers and managers (CIRIA, 1996).

The variation in the processes across the beach results in characteristic beach profiles. The form of the beach profile will then have a feedback role in modifying the subsequent shoaling waves.

Dunes are created by the accumulation of wind-blown sand transported landward from the backshore and the higher portion of the inter-tidal foreshore. To successfully trap and retain this sand, dunes rely on vegetation, especially certain species of grass, which both reduce the wind velocity close to the dune face allowing deposition, and retain moisture, which increases the threshold of motion of sand grains. Figure 2.4 shows a healthy dune system on the central part of Portugal's west coast.

Figure 2.4 – Healthy dune system on the west central Portuguese coast (Lopes *et al.*, 2003).

Dunes located on the backshore of a sandy beach are important in the development of the profile of that beach. They act as a reservoir of material which is available during storms and, if necessary, enables the beach profile to adjust to a flatter profile, and absorb the incoming wave energy (CIRIA, 1996).

2.1.3 SHORELINE RESPONSE ON AN MFAR

Knowledge of the shoreline response on a reef is important for coastal protection purposes. Not only is the published information available on shoreline response to MFARs insufficient, but also relatively little is known about shoreline response to submerged structures in general. Ranasinghe *et al.* (2006a) recently made a compilation and review of reported field, laboratory and numerical modeling investigations and concluded that the key environmental and structural parameters governing shoreline response to submerged structures have not yet been adequately elucidated. The published reports of field experiences with submerged prototype structures mentioned in Ranasinghe *et al.* (2006a) are summarized in Table 2.1. In brief, it was found that 70% of submerged structures constructed for beach protection to date have resulted in net erosion of the shoreline in their lee. It was also concluded that structure length, structure crest level, crest width, nearshore slope, littoral drift rates and the presence or absence of concurrent sand nourishment do not appear to govern the principal mode of shoreline response.

In an innovative study, Black and Andrews (2001) quantified the shape and dimensions of salients and tombolos formed in the lee of natural reefs by visually inspecting aerial photographs of the coastlines of south eastern Australia and New Zealand. By analyzing natural shoreline adjustment, all physical inputs that act to shape salients and tombolos over long time scales are brought together. Results suggested that natural salients are larger than salients created in the lee of breakwaters and in laboratory studies.

Table 2.1 - Features of the sites and the submerged coastal structures reported in the published literature (Ranasinghe *et al.*, 2006a).

Location	Reference	Structure type	Shoreline response	Nourishment	Longshore transport rate (m³/year)	B (m)	Su (m)	W (m)	h (m)	h_c (m)	s
Delaware Bay, USA	Douglass and Weggel (1987)	Single breakwater +2 end groins	Erosion	Y	Negligible	300	75	Not reported	1	At MLW	Not reported
Keino-Matsubara Beach, Japan	Deguchi and Sawaragi (1986)	Single breakwater	Erosion	Y	Not reported	80	85	20	4	2 m below MLW	0.1 nearshore and 0.03 offshore
Niigata, Japan	Funakoshi et al. (1994)	Single breakwater +2 groins	Erosion	N	Exists, but not quantified	540	400	20	8.5	1.5 m below MWL	0.02
Lido di Ostia, Italy (#1)	Tomassicchio (1996)	Single breakwater	Erosion	Y	50,000	3000	100	15	4	1.5 m below MSL	0.05
Lido di Ostia, Italy (#2)	Tomassicchio (1996)	Single breakwater	Accretion	N	50,000	700	50	15	3–4	0.5 m below MSL	0.1
Lido di Dante, Italy	Lamberti and Mancinelli (1996)	Single breakwater	Accretion	Y	Negligible	770	150	12	3	0.5 m below MSL	0.02
Marche, Italy	Lamberti and Mancinelli (1996)	Multiple segmented breakwaters	Erosion	N	Negligible	Not reported	100–200	10–12	3	0.5 m below MSL	Not reported
Palm Beach, FL, USA	Dean et al. (1997)	Single breakwater	Erosion	N	100,000	1260	70	4.6	3	0.7 m below MLLW	0.04
Vero Beach, FL, USA	Stauble et al. (2000)	Segmented breakwater	Erosion	N	30,000	915	85	4.6	2.1–2.7	0.25 m–0.35 m below MLLW	0.03
Gold Coast, Australia	Jackson et al. (2002)	Multi-function surf reef	Accretion	Y	500,000	350	100–600	2	2–10	1 m below MLW	0.02

(B = length of structure, Su = distance from undisturbed shoreline to structure, W = crest width, h = water depth at structure, h_c = water depth at crest of the structure, s = bed slope in the vicinity of the structure)

Analyses produced non-dimensional ratios, enabling the prediction of limiting parameters for salient and tombolo formations, determination of salient apex position with respect to the type of offshore obstacle (islands or reefs), and the length of shoreline affected (salient basal width). One of the suggestions emerging from the analysis was that, if all other parameters (length of reef/structure, B, distance from shoreline to reef/structure, S, wave climate, etc.) are equal, a larger salient would develop in the lee of a submerged reef/structure than in the lee of an emergent structure. However, as mentioned by Ranasinghe *et al.* (2006b), this conclusion is counter-intuitive because wave sheltering will be greater in the lee of emergent structures, leading to more favorable conditions for salient growth in their lee. A subsequent review of the methodology adopted by Black and Andrews (2001), indicated that the approach used to assess the critical length scales of natural reefs from aerial photographs incorporated several shortcomings (Ranasinghe *et al.*, 2006b). The most obvious shortcoming of the predictive empirical relationship proposed by Black and Andrews (2001) is the fact that erosion is not predicted to occur for any combination of B and S. This is highly questionable in view of the fact that a clear majority of submerged structures installed to date have resulted in (unintended) shoreline erosion (see Table 2.1).

In order to gain more insight into the environmental and structural conditions under which shoreline erosion and accretion occur in the lee of submerged structures, and to

gain insight into the nearshore processes governing shoreline erosion and accretion in the lee of submerged structures, Ranasinghe *et al.* (2006b) completed a second study on this subject. The shoreline response to submerged structures, such as MFARs, was investigated. The processes governing this response were found to be different from those associated with emergent offshore breakwaters. This was indicated by the results of a series of 2DH numerical and 3D scaled physical modeling tests. Unlike the case of emergent offshore breakwaters, where shoreline accretion (salient development) is expected under all structural/environmental conditions, the principal mode of shoreline response to submerged structures can vary between erosive and accretive, depending on the offshore distance to the structure. In the case of the left picture of Figure 2.5 erosion was seen, and in the right one accretion.

Figure 2.5 - Distance apex structure-coast 100 m (left) and distance apex structure coast 250 m (right) (Ranasinghe *et al.*, 2006b).

The predominant wave incidence angle and structure crest level also have important implications for the magnitude of shoreline response, but not for the mode of shoreline response (i.e. erosion vs. accretion). With the geometry and the wave conditions tested by Ranasinghe and Turner (2006b) the most significant feature in the structure-induced nearshore circulation patterns under shore normal wave incidence is the 'switch' from a symmetric 2-cell circulation system to a symmetric 4-cell circulation system, as the structure is moved offshore (Figure 2.5). Based on the results obtained in their study, a predictive empirical relationship was proposed as a preliminary engineering tool to assess shoreline response to submerged structures. This relationship is $S_a/SZW > 1.5$, where S_a is the distance between the apex of the structure and the undisturbed shoreline and SZW is the natural surf zone width.

Broad-crested nearshore structures are a relatively new field of research, and a 'standardized' method to describe their geometry has not yet been established in the literature. For more conventional shore-parallel rubble-mound structures it is probably

most usual to define the characteristic length of '*S*' as the distance from the shoreline to the centre-line of the crest. For the broad-crested structures Ranasinghe *et al*. (2006b) modeled, the distance to the apex of the crest (S_a) was chosen as the characteristic length (Figure 2.6).

Figure 2.6 - Characteristic length broad-crested breakwaters.

Much research has been done on currents and waves breaking on and around natural reefs. However, the topography of natural reefs is highly variable, some fringing reefs (reefs which front a continental land mass or island) may have quite flat seaward slopes, for example 1:15, whereas platform reefs (reefs located in open ocean) on the outersections may have very steep seaward slopes, for example 1:2 or steeper (Gourlay, 1993). No publications have been found that deal with the relation between the topography of the reef and the influence on hydrodynamics in general regarding the coastal protection behavior of such natural reefs.

In 2005 the DELOS project finished. The overall objective of this project was to promote the effective and environmentally compatible design of low crested structures (LCSs) to protect European shores against erosion and to preserve the littoral environment and the economic development of the coast. Much experimental and numerical research has been undertaken in this project. In all the experimental studies the LCS were small-crested and designed with a relatively steep slope. This means that the results are not useful for research into the coastal protection aspect of MFARs. Furthermore, no tests were conducted to investigate current velocity in the lee of an LCS in a basin. The focus of the basin tests was stability, hydrodynamics near the structure and wave transmission.

In order to get an idea of the shoreline response on an MFAR, and taking into account all the research described above, the mean current field can be used (Ranasinghe and Turner, 2006b). The numerical model results (current analysis) and the prototype field results (morphodynamic analysis) reported by these researchers showed that:

(a) under shore normal wave incidence, the mode of shoreline response to submerged structures is governed by the structure-induced nearshore circulation; and

(b) under oblique wave incidence, the mode of shoreline response is governed by the interaction between the ambient longshore current and the structure-induced nearshore circulation pattern.

This means that the currents (the ambient longshore and the structure-induced nearshore circulation pattern) can be used as an indication of the shoreline response. Essentially, erosion occurs when the resultant current field contains divergent alongshore currents at the shoreline in the lee of the structure. Conversely, shoreline accretion occurs when convergent alongshore currents are generated at the shoreline in the lee of the structure.

The hydrodynamic processes that govern the development of nearshore circulation patterns around relatively simple delta-form MFARs are explained in Ranasinghe and Turner (2006b) and are partially presented in this section. For reasons of simplicity, just shore normal waves are considered (i.e. no ambient longshore current due to oblique wave incidence at the shoreline). References to 'longshore flow/transport' in this section refer only to structure-induced alongshore flows/currents.

In the two-dimensional case of a submerged structure, such as the case of a submerged reef, longshore flow driven by an alongshore pressure gradient occurs behind the structure to satisfy continuity constraints. The total transport capacity of the longshore flow is determined by the longshore pressure gradient and the cross-sectional area of the longshore flow.

Figure 2.7 shows the cross-shore profile of surface elevation, wave height, and initial bed level at the two cross-sections presented in Figure 2.5 (left) and here when the structure is close to shore (apex at 100 m from the shore).

Figure 2.7 - Wave height and surface elevation along different cross-sections for apex structure-coast distance 100 m (left, Ranasinghe *et al.*, 2006).

One section is across the apex of the structure (Section A) while the other is along the plane bed away from the structure (Section B). Along Section A, the wave height decreases through the surf zone and over the top of the structure producing a higher surface elevation than at Section B. This alongshore gradient in surface elevation drives longshore flows away from the structure in both longshore directions in the lee of the structure. However, in this case, the small gap between the structure and the shoreline and the resulting relatively shallow trough region between the structure and the shoreline constrains the capacity for onshore flow over the structure. Therefore, the longshore flow in the lee of the structure is largely due to the alongshore surface elevation gradients resulting from alongshore gradients in the wave setup in the lee of the structure. However, because of the complex plane shape of the artificial surfing reef structure investigated here, currents are also generated along the two sides of the structure due to waves breaking obliquely on the sides of the structure. These 'along-structure' currents also contribute to the onshore flow over the structure and the alongshore flows in the lee of the structure. The resulting nearshore circulation pattern consists of two cells, symmetric about Section A, with divergent flow at the shoreline in the lee of the structure.

Figure 2.8 shows the cross-shore profile of surface elevation, wave height, and initial bed level at the two cross-sections when the structure is farther away from the shore (apex at 250 m from the shore).

31

Figure 2.8 - Wave height and surface elevation along different cross-sections for the case of distance apex structure-coast 250 m (left, Ranasinghe *et al*., 2006).

Again, one section is across the apex of the structure (Section A) while the other is along the plane bed away from the structure (Section B). In this case, the longshore flow is less constrained by the topography, thereby allowing larger cross-shore flow over the structure. In contrast to the previous case, here wave setup occurs through the surf zone on the structure, reaching a local maximum at the top of the structure slope, and decreases towards mean sea level over the flat top of the structure. Through the surf zone, part of the radiation stress gradient drives the onshore flow over the structure and the setup is reduced relative to the zero-onshore flow case (i.e. adjacent plane bed case). A small amount of wave dissipation occurs across the top of the structure which, together with the hydrostatic pressure gradient due to setup, maintains the onshore flow over the structure. A small positive set-up remains at the back of the structure providing the longshore pressure gradient to drive the longshore flow (directed away from the structure), with the maximum longshore transport occurring in the deepest water immediately behind the structure. As in the previous case, the 'along-structure' currents due to oblique wave breaking on the structure contribute to the onshore flow over the structure and to the alongshore flows in the lee of the structure. However, in contrast to the previous case the substantial distance between the back wall of the structure and the shoreline (i.e. 200 m) allows the waves to re-form to some extent in the lee of the structure. Therefore, wave setup occurs again at the shoreline in the lee of the structure when the re-formed waves break at the shoreline. However, the reformed wave height in the lee of the structure (section A) is lower than the height of the previously unbroken waves at the plane bed away from the structure (section B). Therefore, the wave setup at the shoreline in the lee of the structure is lower than that along the shoreline adjacent to

32

the structure. This longshore gradient in the setup at the shoreline results in a longshore gradient of surface elevation which drives alongshore currents towards the lee area, where they converge before turning offshore, owing to mass conservation requirements. Therefore, in this case, the resulting nearshore circulation pattern consists of four cells, symmetric about Section A, with convergent flow at the shoreline in the lee of the structure.

More complex geometries (for example the presence of a platform) are however more difficult to explain with the theories set forth in the above paragraphs.

2.2 SURFABILITY

Besides coastal protection, the creation of surfing conditions is an important aspect of an MFAR. This section gives a systematic explanation of the key surfing parameters used in the design of an MFAR, viz., the peel angle, the type of breaker, the wave height and the currents. However, due to the importance of waves for surfing, the phenomena of free waves are elucidated first. After the explanation of the key surfing parameters, the state of the art of MFARs will be described.

2.2.1 FREE SURFACE WAVES

Waves form when the water surface is disturbed, by wind, earthquakes or planetary gravitational forces, for instance. Thus, we can identify at sea waves that have very short wave periods (order of 0.10 seconds, known as capillary waves) to tides, tsunamis and seiches (basin oscillations), where the wave periods are expressed in minutes or hours. Wind waves, which account for most of the total available wave energy, have periods from 1 to 30 seconds and wave heights that are seldom greater than 10 m and mostly of the order of 1 m, particularly in deep water conditions. As can be seen in Figure 2.9, most of the energy possessed by ocean waves is in wind-generated waves (Thurman and Trujillo, 1999). During such disturbances energy and momentum are transferred to the water mass and transmitted in the direction of the impelling force. A proportion of the wave energy is dispersed by radial, inertial and convective means, but a large amount is not lost until waves encounter shallow coastal waters.

Figure 2.9 - Distribution of energy in ocean waves (Thurman and Trujillo, 1999).

Wind waves can originate near the shore or offshore. In case of offshore generated waves, storms and depressions cause strong winds to blow over a stretch of ocean surface (fetch) for a certain amount of time. Wind energy is transformed into wave energy by the creation of high frequency waves known as choppy waves. The energy from the higher-frequency waves (lower periods) is in turn transferred to lower-frequency waves (longer periods): the so called **swell waves**. The swell waves travel faster than higher-frequency waves (speed of waves in deep water is $gT/(2\pi)$) and consequently the swell waves will separate from the higher frequency waves as the wave field propagates away from the region of generation. The higher-frequency waves of distant storms have dissipated most of their energy before they reach the coast, and so the wave field gets cleaned up. The swell waves with the longest wave periods can travel thousands of kilometres. The swell energy is distributed over a relatively narrow range of frequencies resulting in a slowly modulated wave field. Therefore, swell waves always arrive in sets. The periods of swell waves vary in general between 8 and 16 seconds. **Local waves** are formed by local winds, which cause the wave climate to be irregular and the waves to have short wave periods (in general between 4 and 7 seconds).

As mentioned, waves with lower frequency (longer wavelengths) travel faster, and thus leave the sea area first. The same is true for wave groups. Waves travel in wave groups. Figure 2.10 shows such a wave group in which L is the wavelength, L_g is the wave-group length, c is the wave celerity and c_g is the wave group celerity.

Figure 2.10 - Wave group (Fredsøe and Deigaard, 1995).

The difference in speed of the single waves is the cause for the principle of wave dispersion, which is a sorting of waves by their wavelength. As a group of waves leaves a sea area and becomes a swell wave train, the group moves across the ocean surface at only half the velocity of an individual wave in the group. Progressively, the leading wave disappears. However, there is always the same number of waves in the group. As the leading wave disappears, a new wave replaces it at the back of the group. Most waves generated in the sea area by storm winds move across the ocean as swell. Generally, they release their energy along the margins of the continents in the surf zone, which is the zone of breaking waves.

2.2.2 PEEL ANGLE

Surfable waves never break all at once along the wave crest. If this does happen, the waves are closing-out and not suitable for surfing purposes. In order for a wave to be surfable, the wave has to break gradually (read peel) along the wave crest. The velocity with which this happens is called the 'peel rate' V_p of the wave (Figure 2.11).

The peel angle is one of the most important surfability parameters (α in Figure 2.11). The peel angle is the angle enclosed by the wave crest and the breaker line (Walker, 1974). Two other vectors that are shown in Figure 2.11 are $\vec{c}$ and $\vec{V}_S$. $\vec{c}$ is the wave celerity and $\vec{V}_S$ (called down-line velocity) is the absolute value of the vector sum of the velocities $\vec{c}$ and $\vec{V}_p$, it is the actual velocity experienced by the surfer. From Figure 2.11 it can be seen that another way to see the peel angle is as the angle enclosed by the velocity vectors of the peel rate $\vec{V}_p$ and the down-line velocity $\vec{V}_S$ (Henriquez, 2004).

Figure 2.11 - Illustration of wave celerity vector $\vec{c}$, peel rate $\vec{V}_p$, down line velocity $\vec{V}_s$ and peel angle α (Source:surfermag.com).

In Figure 2.12 it can also be seen that the peel angle in fact is equal to the wave angle β between the normal on the bathymetry and the wave ray (the conventionally called 'wave angle') if the breaker line is parallel to the bathymetry. The angle θ is the so-called reef angle.

Figure 2.12 - Peel angle on an MFAR.

Whether a wave is surfable depends mainly on the value of the peel angle α, related to the down-line velocity as $\vec{V}_S = \dfrac{\vec{c}}{\sin\alpha}$.

When the peel angle becomes too small, the down-line velocity will become very high and too fast for the surfer. The value of the peel angle, α, needs to be sufficiently large for a wave to be surfable. The velocity that a surfer can reach depends mainly on

the wave height H_b at the breaking point and the skill of the surfer. Hutt *et al.* (2001) investigated what the peel angle α has to be for a given wave height H_b and surfer skill (Figure 2.13). The definition of these surfer skills is shown in Table 2.2.

Table 2.2 - Rating of surfer skill level (Hutt *et al.*, 2001).

Rating	Description of Rating	α (deg)	H_b (m)
1	Beginner surfers not yet able to ride the face of a wave and simply moves forward as the wave advances.	0	0.70 – 1.00
2	Learner surfers able to successfully ride laterally along the crest of a wave.	70	0.65 – 1.50
3	Surfers that have developed the skill to generate speed by 'pumping' on the face of the wave.	60	0.60 – 2.50
4	Surfers beginning to initiate and execute standard surfing manoeuvres on occasion.	55	0.55 – 4.00
5	Surfers able to execute standard manoeuvres consecutively on a single wave.	50	0.50 +
6	Surfers able to execute standard manoeuvres consecutively. Execute advanced manoeuvres on occasion.	40	0.45 +
7	Top amateur surfers able to consecutively execute advanced manoeuvres.	29	0.40 +
8	Professional surfers able to consecutively execute advanced manoeuvres.	27	0.35 +

Figure 2.13 – Peel angle as a function of wave height and surfer skill. The peel angle is on the y-axis, the wave height on the x-axis and the surfer skill is indicated by numbers in the graph (Hutt *et al.*, 2001).

Henriquez *et al.* (2006) proved algebraically that, for an arbitrary peel angle, wave height and offshore depth (in the context of a geometrical optics approximation of linear wave theory), the maximum peel angle occurs at an angle on deep water of *arctan* $\sqrt{5} \approx$ 66°. The algebraic proof means that regardless of wave conditions and offshore depth it will always show the maximum of the peel angle at an angle on deep water of 66º.

In this thesis, the peel angle is studied more deeply. The relation between the peel angle, α, and the angle θ (Figure 2.12) is represented by the graph presented in Figure 2.14. The results shown in this figure are for a 10 s period and a wave height, in deep water conditions, of 1.5 m. The calculations are done for waves travelling over a shelf before reaching the reef (Figure 2.15). However, because linear shoaling is assumed, the results are the same for a wave travelling over a sloping bottom before reaching the reef (Figure 2.16).

Figure 2.14 - Peel angle α as a function of the reef angle θ_s and the shelf depth kh_s or h_s for $T = 10$ s and $H_0 = 1.5$ m.

Figure 2.15 - Peel angle with shelf.

Figure 2.16 - Peel angle without shelf.

Not only does the peel angle have a maximum, but it is clear from Figure 2.14 that it has an exponential growth for the same wave angle θ_s when the reef starts in shallower water. The physical explanations of these two phenomena are described below.

How can the peel angle have a maximum?

When calculating the parameters like wave height, water depth and peel angle at the breaking point, with linear theory, it appears that the larger the wave angle in deep water, the less the water depth at the breaking point. Figure 2.17 shows this phenomenon for different wave angles in deep water. In this figure, the angle of incidence in deep water, θ_0, can be seen as the angle θ in Figure 2.12 and the wave angle in the third column in this figure, at the breaker line position, can be seen as the peel angle α in Figure 2.12. The second 'column' in Figure 2.17 are the values of the wave angles at the line of the breaker line for the angle on deep water of 45 degrees (wave conditions are: a period of 10 seconds and a wave height of 1.5 m in deep water conditions).

From this, it can be seen that the wave angle grows at the same water depth when the wave angle on deep water grows (law of Snellius).

Figure 2.17 – Wave breaking more shorewards for larger wave angle at deep water.

The fact that the wave travels more shoreward, for a larger wave angle on deep water, has to be caused by a stronger decline in the wave height so that the wave can travel on longer before it breaks. For that reason the development of the wave height along the wave ray is investigated. Two processes influence the wave height when a wave travels towards the coast, and these are shoaling and refraction. The variation in the wave height for different water depths is given by Equation 2.1.

$$H_2 = H_1 \times K_s \times K_r \tag{2.1}$$

where $K_s = \dfrac{c_{g1}}{c_{g2}}$ is the shoaling factor and $K_r = \dfrac{\cos\theta_1}{\cos\theta_2}$ is the refraction factor. The wave travels from the location of wave height H_1 towards the location of wave height H_2. Shoaling is independent of the wave angle on deep water; refraction, however, is dependent on that angle. Figure 2.18 shows the factor Ks*Kr when the wave travels from deep to shallow water conditions for angles on deep water of 45 degrees and 75 degrees, considering the same wave conditions shown in Figure 2.14. Figure 2.19 shows the consequence for the wave height of what is demonstrated in Figure 2.16.

Figure 2.18 - Multiplied factor of the shoaling and refraction factor.

Figure 2.19 - Wave height as a function of the shoaling and refraction factor.

Figure 2.19 shows that, for the same water depth, the wave height decreases when the wave angle on deep water increases. Because of this decrease, the wave can travel further towards the coastline before the breaking condition $H_b = 0.78*h$ is met. As a consequence of the law of Snellius, it can be continued longer and the wave angle can

continue to diminish. The maximum peel angle occurs with an angle on deep water of 66 degrees no matter what the wave conditions. So, at an angle of 66 degrees the decrease of the peel angle by the effect of a longer continuation of refraction (law of Snellius) is larger than the increase of the peel angle through the effect of a larger wave angle on deep water.

Why is there exponential growth of the peel angle for the same wave angle θ_s when the reef starts in shallower water?

Another aspect of the peel angle is that it experiences exponential growth with decreasing depth of the start of the reef, for the same wave angle θ_s, as can be seen in Figure 2.14. The only process by which the wave angle changes along the wave ray when a wave travels from deep water towards the shoreline is refraction. The influence of refraction on the wave angle is given by Snellius' law (Equation 2.2).

$$\frac{d}{dx}\left(\frac{sin\,\theta}{c}\right) = 0 \qquad (2.2)$$

where dx is in the direction of the wave ray, θ is the wave angle between the wave ray and the normal to the bathymetry and c is the wave velocity. Equation 2.2 can be re-written as:

$$sin\,\theta_2 = A\,sin\,\theta_1 \; ; \; A = \frac{tanh\,(kh)_2}{tanh\,(kh)_1} \qquad (2.3)$$

where k is the wave number, and the water depth h_1 is greater than the water depth h_2.

The difference in the water depth from point 1 to point 2, $\Delta h = h_1 - h_2$, is assumed to be the same for all water depths. In fact, the value of A in Equation 2.3 gives information about the magnitude of refraction; its value is plotted in Figure 2.20 for different water depths. The period in these calculations is 10 s. It can be seen in Figure 2.20 that refraction for the same Δh is relatively greater in shallower water.

Figure 2.20 - Relative refraction.

In order to show this effect on the exponential growth of the peel angle with decreasing depth, two cases are assumed (Figure 2.21):

- Case 1: two reefs in relatively deep water, starting with a difference of Δh in water depth;

- Case 2: two reefs in relatively shallow water, starting with a difference of Δh in water depth.

Figure 2.21 - Two cases of reefs starting at different depths.

In Case 2, the loss in total refraction of the wave from θ to the wave angle β between the two reefs is larger than in Case 1. Figure 2.22 shows β for the deeper start of the reef in Cases 1 and 2, where Δx is the horizontal distance for the vertical distance Δh. This larger value of loss of refraction in case 2 means that the wave at the breaking point has refracted relatively less in Case 2 than in Case 1 [even though the initial refraction is higher (Figure 2.20)], leading to a stronger growth of the peel angle. This effect appears at every water depth and it is the reason that the peel angle experiences an exponential growth with decreasing depth, for the same wave angle θ. So it can be said that the peel angle grows exponentially for a lower start of the reef depth with the same angle θ because refraction is exponentially greater in shallow water.

Figure 2.22 - Different loss in refraction for the two cases of Figure 2.21.

2.2.3 BREAKER TYPE

The shape of a breaking wave is of great importance for surfing. Battjes (1974) used the surf-similarity parameter, ξ_0 (equation (2.4)), to describe the breaker type on single slopes:

$$\xi_0 = \frac{s}{\sqrt{\dfrac{H_0}{L_0}}}$$

(2.4)

where ξ_0 is the offshore Iribarren number, s is the bottom slope, H_0 is the offshore wave height and L_0 is the deep water wave length. The value of the Iribarren number corresponds with every regime as in

Table 2.3.

Table 2.3 - Breaker type transition values for the offshore Iribarren number.

Regime	Range
Surging/collapsing	$\xi_0 > 3.3$
Plunging	$0.5 > \xi_b > 3.3$
Spilling	$\xi_b < 0.5$

Besides the offshore Iribarren number, also the inshore Iribarren number, ξ_b, has been defined. In the inshore Iribarren parameter the offshore wave height, H_0, has been replaced by the breaker wave height, H_b. All other parameters are equal. In principle, transition values and other wave breaking-related quantities described should be better

predicted in terms of the inshore parameter than the surf-similarity parameter, since the inshore parameter involves the measured breaking wave height rather than the deep-water wave height. However, correlations with measurements using the inshore parameter showed no superiority (Smith and Kraus, 1990). The categorization of the different breaker type regimes of the inshore Iribarren number is presented in Table 2.4.

Table 2.4 - Breaker type transition values for inshore Iribarren number.

Regime	Range
Surging/collapsing	$\xi_b > 2.0$
Plunging	$0.4 > \xi_b > 2.0$
Spilling	$\xi_b > 0.4$

It should be noted that these results are based on experiments on plane slopes where the angle of incidence of the waves was zero. The slope is the slope that the wave experiences, so is along the path of the wave and not along the normal on the reef contours (Figure 2.23).

Figure 2.23 - Path of the wave compared to the normal on the depth contours.

The main breaking types are described as follows [the technical part of terminology is from Galvin (1968), the relation between the breaker types and the Irribaren number from Battjes (1974), and the surfer interpretation from Henriquez (2004)].

1. Spilling breakers

These breaking waves occur if the wave crest becomes unstable and flows down the front face of the wave producing a foamy water surface – surfers would say a 'soft' or 'weak' wave. This regime is considered surfable. Spilling waves are shown in Figure 2.24.

Figure 2.24 - Spilling waves, $\xi_b = 0.2$ (Battjes, 1974).

2. Plunging breakers

These breaking waves occur if the crest curls over the front face and falls into the base of the wave, resulting in a high splash - surfers call this a 'tubing' wave. This regime is preferred by most surfers, and a more spilling plunging wave is preferred over a more collapsing plunging wave. Plunging waves are shown in Figure 2.25 and Figure 2.26 .

Figure 2.25 - Plunging waves $\xi_b = 1.5$ (Battjes, 1974).

Figure 2.26 - Plunging waves, $\xi_b = 0.5$ (Battjes, 1974).

3. Collapsing breakers

These breaking waves occur if the crest remains unbroken and the front face of the wave steepens and then falls, producing an irregular turbulent water surface - surfers often encounter this regime at reef breaks when the tide is too low and the reef is not submerged enough to produce surfable waves, and so it is an unsurfable regime. Collapsing breaking waves are shown in Figure 2.27.

Figure 2.27 - Collapsing waves, $\xi_b = 3$ (Battjes, 1974).

4. Surging breakers

These breaking waves occur if the crest remains unbroken and the front face of the wave advances up the beach with minor breaking. This regime is also unsurfable. Surging breaking waves are shown in Figure 2.28.

Figure 2.28 - Surging waves, $\xi_b = 5$ (Battjes, 1974).

It should be noted that the breaker types mentioned above will only develop as the Iribarren number describes (according to the bottom slope and wave steepness) when the wave experiences the relevant conditions during enough length of the slope. So a wave that should in principle be plunging when it breaks on an MFAR, according to

Equation 2.4, will be more spilling when it breaks if the slope of the reef is relatively too short to reach the Iribarren number for the relevant bottom slope and wave steepness. In other terms, the wave breaks to some extent according to the bottom slope and not just according to the reef slope (Figure 2.29).

Figure 2.29 – Breaker type.

The breaker type is an important parameter in the scope of multi-dimensional artificial reefs. Besides the indication of the energy dissipation it is also an important parameter for the wave shape. It is critical to have a highly-refined definition of the wave breaking intensity and to define the actual shape of the plunging wave profiles, since this type of breaking is preferred by most surfers. Mead and Black (2001a) related wave vortex parameters to seabed slopes at a wide selection of world-class surfing breaks and they have developed a linear equation to predict the vortex length to width ratio. However they didn't take into account the wave height and period in their study. Henriquez (2004) found, in an experimental study in a wave basin, that the depth of the reef crest significantly affects the shape of a breaking wave and that this should be studied by conducting more laboratory experiments.

The conventional method to predict the wave breaking intensity, namely the Iribarren number, was defined for a beach with a constant slope, which is not the case for a wave breaking in an MFAR. The categorization of breaker types defined by Battjes (1974) was based on the Iribarren number on a single, long slope. However, in case of a breakwater the influence of its submergence and the length of the slope on the breaking process is not clear. Even though the Iribarren number could not be the best method to predict breaking waves for surfing, it still is the most appropriate method.

Regarding the breaking behavior on and velocities around artificial reefs with a smooth slope, just one study has been conducted in a wave flume by Corbett and Tomlinson (2002). They performed a physical study for Noosa Main Beach in Australia to investigate the wave breaking behavior and associated safety issues for an artificial reef. The analysis of the results of these tests was especially focused on the breaker type, the breaker wave height and the breaker location as an indication for the safety of the submerged reef. However, no surface elevation and velocity measurements were extensively made. Besides that, even though several submergences were tested, no analysis of the relation between the submergence and the Iribarren number were made.

Furthermore, the influence of the length of the slope on the Iribarren number was not investigated.

Henriquez (2004), Van Ettinger (2005), Over (2006), Trung (2006) and Poort (2007) investigated the breaking behavior on and currents around an artificial reef in a wave basin. However, in these experiments the influence of the length of the slope and the submergence of the reef on the wave shape was not investigated. Several other experimental studies have been conducted in wave basins for projects of artificial reefs as for the Narrowneck reef of which the construction was finished in 2000 and the Dubai reef of which the construction has not started yet. However, the data from design studies are often confidential and not available for science purposes.

2.2.4 WAVE HEIGHTS

By now every possible wave has been surfed. Surfers that surf on a long board are still surfing when waves are 0.15 m high, whereas those that are towed into waves ride the biggest waves they can find, up to 20 m. On the whole, waves between 0.5 m and 10 m are considered surfable (Henriquez, 2004). However, in order to study the viability of an MFAR, wave heights between 1m and 3 m are the most common values, and are adjusted according to the target level of surfers for which the MFAR are being designed.

2.2.5 CURRENTS

Currents around a surf break are of vital importance when considering the surfability of the break. There could be waves in perfect surfing condition but yet unreachable due to strong currents. Usually these cases are rare but it is not ideal to have to be constantly paddling to keep positioning.

Rip currents can destroy good surfable waves. Rip currents are narrow strong currents that move seaward through the surf zone (Bowen, 1969). When the rip-current flows through the breaker zone the wave seems to get a rough surface and breaks in a hesitating manner making the waves unsuitable for surfing. Rip-currents can also be advantageous; the surfer can use the rip-current to get outside the breaker zone more easily (Henriquez, 2004).

2.2.6 WAVE FOCUSING

Wave focusing, like refraction, is another physical process that has a large influence on surfing as it has a large influence on the peel angle. In the study of Mead and Black (2001b) wave focusing is recognized as an important aspect in the design of an MFAR. Besides increasing the wave height and refraction, it has an effect on the peel angle. However, this contribution of the different processes of refraction and wave focusing on the peel angle along the breaker line has not yet been described. It will be threatened in

this section. If wave focusing occurs, the wave rays converge, leading to an increase in wave height and consequently to its earlier breaking. This causes the breaker line to be nearer the intersection of the reef and the sea bottom than if there was no wave focusing, leading to less refraction and thus a higher value of the peel angle.

The influence of wave focusing on the breaker line is part of this thesis and is here presented more deeply. The breaker line in Figure 2.30 and Figure 2.32 and the graph in Figure 2.31can be divided into three parts: part A, where wave focusing occurs; part B, where wave defocusing occurs, and part C, where there is neither wave focusing nor defocusing (α_2 and α_3 are zero, Figure 2.31).

When wave focusing occurs, the value of the peel angle can be divided into several contributions:

- α_1 is the angle θ minus the decrease due to refraction on the reef slope (Figure 2.31 and Figure 2.33);
- α_2 is the difference between the angles for the cases with and without wave focusing, due to less refraction by earlier breaking (see α_2 in Figure 2.31, $\alpha_2 = \alpha_4 - \alpha_1$ inFigure 2.33);
- α_3 is the angle due to deviation of the breaker line from the parallel to the bathymetry of the reef side (Figure 2.31 and Figure 2.34).

Figure 2.30 - Breaker line (Henriquez, 2004).

—————— Peel angle inclusive contribution of wave focusing

— — — Peel angle without contribution of deviation of the breaker line due to wave (de-)focusing

· · · · · · Contribution peel angle due to deviation of the breakerline due to wave (de-)focusing

Figure 2.31 - Contributions to the peel angle along the breaker line (basic Figure: Henriquez, 2004)

Figure 2.32 - Enlargement of part of the breaker line; schematic positions of certain values of the peel angle.

Figure 2.33 - Angles α1 and α4.

Figure 2.34 - Angle α_3.

The transition from wave focusing to wave defocusing occurs at the minimum of angle $\alpha_1+\alpha_2$ on the right side of part A. This can be concluded because at that point the peel angle is equal to α_1, which is the value for the peel angle without no wave focusing.

The peel angle α_1 is different for the areas A and B. In area A, α_1 is the minimum value of $\alpha_1+\alpha_2$, corresponding to a peel angle value when no wave defocusing (after the wave focusing) would occur. For large values of s, the peel angle tends to a certain value. This is the value of α_1 in area B, which would occur if there were no wave focusing and no wave defocusing. α_1 is smaller in area A than in area B. This means that the position of the minimum of $\alpha_1+\alpha_2$ at the right end of area A is nearer the crest level of the reef than the location of the breakerline for large values of s in area C (Figure 2.32).

The angle α_2 is positive in area A and negative in area B (Figure 2.31). It is positive in area A because the breaking occurs further away from the crest level of the reef than it would if there were no wave focusing. The value in area B is negative because the breaking occurs nearer the crest level of the reef than it would if no wave focusing and no wave defocusing occur.

Breaks on natural reefs are used by surfers. A study on 34 world-class surfing breaks lead to a bathymetric classification of these breaks (Mead *et al.*, 2001b). A so-called ramp, platform, focus, pinnacle, wedge, ledge and ridge were identified. All these categories have a different influence on the behavior of the waves. The surfing wave quality at the world-class surfing breaks is provided by a combination of different categories of bathymetry (Mead *et al.* 2001b). Besides Mead *et al.* other researchers also found that a platform can have a positive influence on the creation of surfable waves. Smit and Mocke (2005) found in a numerical study that, in the design evolution of an artificial surfing reef for the coast of Dubai, a reef can create good surfable waves if the reef allows the waves to shoal prior to break without undergoing significant

refraction, and therefore they included a platform in the reef design. However, the influence of the platform on the other surfability parameters besides the peel angle, from a theoretical point of view, has not yet been described and will be done in this thesis.

2.3 MULTI-FUNCTIONAL ARTIFICIAL REEFS

2.3.1 MULTI-FUNCTIONAL ARTIFICIAL REEFS BUILT SO FAR

Until 2007 three artificial reefs have been built either with the purpose of enhancing of surfing possibilities (Artificial Surfing Reef), or jointly with other purposes, like coastal protection (Multi Functional Artificial Reef). Below, the reefs are described in chronological order of building. The description of each reef focuses on the results of environmental and monitoring studies.

Cable station (or Cables), Perth, Australia

The first ASR was built close to Perth in Australia and named Cable Station or Cables (Ranasinghe *et al*., 2001). Construction was completed in December 1999. The purpose of the surf reef was to produce surfable waves regularly. It was not intended as a shore protection structure, as the shoreline at Cable Station consists mainly of rocky outcrops and platforms, and so is naturally stable.

The overall dimensions are 80 m cross-shore by 90 m longshore. The reef (Figure 2.35) was constructed of granite.

Two experimental design studies (one in a wave flume and one in a wave basin) and three numerical surfability studies were undertaken for this reef. In addition, there was a beach response study in the design phase, and an environmental study was also undertaken in which the marine habitats were observed, before and after construction.

The researchers of this last study, Bowman Bishaw Gorham (2000) predicted the recovery of the diversity of marine life that previously inhabited the area. Finally, a post-construction performance study was carried out.

When 90 percent of the reef had been built its performance was studied. During the 6-month study period, 77 surfable days were identified. The researchers concluded that the performance of this reef exceeded expectations (Pattiaratchi, 2000), although this has been disputed by some members of the local surfing population.

Figure 2.35 - Plan view of design reef Cable station (Ranasinghe, 2001).

Narrowneck reef, Gold Coast, Australia

The Narrowneck reef is situated off the Gold Coast, Australia. The construction was finished in December 2000 (Ranasinghe *et al*., 2001). The primary objective of the reef was to widen the beach and mitigate storm erosion, by retaining and protecting the nourished beach (over 1 million cubic metres of nourishment). The secondary objective was to improve surfing.

The overall dimensions are 400 m cross-shore by 200 m longshore. The submergence is 1.5 m below lowest tide (Jackson *et al*., 2005; Corbett *et al*., 2005). The reef (Figure 2.36) was constructed of GSCs that weighed 160-300 tones, being typically 20 m long and up to 5 m diameter (Black, 2000). In all, 332 bags were placed. The total volume of the reef at the end of construction was 110 000 cubic metres. The bags were filled with natural sand in a split-hull hopper dredge. Once filled, the bags were dropped on the seabed using bow and stern satellite positioning to align the dredger.

For this reef one physical study was carried out (Turner *et al*., 2001). Besides the experimental study, four numerical studies were carried out for the reef design (Black and Mead, 2001). The models implemented were a refraction model WBEND, a multi-purpose model 3D, a sediment transport model POL3DD, and a beach circulation and sediment transport model 2DBeach.

A pre-construction study (Ranasinghe *et al*., 2001) had been undertaken to investigate the likely environmental impacts on the area. During and after construction an ARGUS video imaging system was installed to monitor the shoreline response to the reef. This system is capable of providing very accurate quantitative information. Also, a number of hydrographic surveys have been carried out. It appeared from a beach monitoring study (Jackson *et al*., 2005) in the period 2000-2004 that the beach updrift of the reef was of the order of 40 m wider than at the start of monitoring. In the lee of the reef, an additional 30 m had been obtained. However, it has to be mentioned that

before construction a nourishment program of over one million cubic metres of sand was carried out, so it is difficult to analyze the effect of nourishment and the effect of the reef. Another result of four years of monitoring the reef is that, according to the researchers, the size of the reef could have been smaller. Environmental research and analysis have provided a comprehensive list of the diverse marine species found on the reef. It has become evident that since construction the marine habitats created by the reef are of significant value (and much bigger then expected), both environmentally and for recreation in the form of diving and fishing.

The GSCs were predicted to be stable in the 8-10 m amplitude waves that occur during cyclones and up to now they have proved to be so.

Concerning surfing, there use of the Narrowneck area has significantly increased for all types of surfing and a number of competitions are held at Narrowneck because of its more reliable surfing conditions. However, Narrowneck's surfing attraction suffers from its proximity to numerous world class waves and the reef doesn't produce always 'perfect' waves - regardless of wind and wave conditions - as the general surfing public hoped (Jackson *et al*., 2005).

Figure 2.36 - Narrowneck reef, Gold Coast, Australia - Plan view (up) and side view (down) of reef (Black, 2000).

Pratte's reef, El Segundo, America

Pratte's reef near Los Angeles in America was constructed between 2000 and 2001 (Borrero and Nelson, 2003). The purpose of the reef was just to enhance recreational surfing in order to offset the loss of surfing areas due to the construction of a groyne.

The overall dimensions are 30 m cross-shore with 70 m longshore. The submergence of the crest was 0.9 m below lowest tide. The reef (Figure 2.37) was constructed with about 200 GSCs. The bags had a maximum volume of 7.9 cubic metres (the largest bags of the Narrowneck reef were about 400 cubic metres). The total volume was about 1600 cubic metres. The bags were filled in the port of Los Angeles and then loaded onto a barge, to be taken to the site. The bags were placed in the surf zone by a barge-mounted crane.

There is no available information about any design studies that have been carried out for this reef. After construction, however, shoreline monitoring, bathymetric surveys, diving surveys and surf quality surveys were undertaken. As a conclusion of the shoreline and bathymetry surveys it can be said that the reef had no effect on the shoreline and bathymetry. Any noticeable changes are due to natural seasonal changes. One remarkable finding of the diving survey was the rapid biological growth on the bags. Within weeks of the initial bag installation, algae had begun to grow on the bags and schools of small fish were attracted to the site. The diving survey also revealed that several reef bag units were ripped or shredded and were losing their fill material.

The conclusion of the surf quality of the reef is that there is an almost complete absence of surfers. The basic problem is that Pratte's reef is too small to significantly alter wave breaking and near shore coastal processes. The Narrowneck reef is 70 times larger (in terms of dimensions).

Figure 2.37 – Plan view of design of Pratte reef (Henriquez, 2004).

2.3.2 MULTI-FUNCTIONAL ARTIFICIAL REEFS UNDER CONSTRUCTION

In 2008 just two MFAR were under construction, although several studies on the viability of MFAR are underway around the world. As before, the description of this reef concentrates on the results of environmental and monitoring studies.

Mount reef, Mount Maunganui, New Zealand

The reef is located on the east coast of New Zealand's north island. The ASR is designed to have a primary purpose of creating high quality surfing waves. Besides that, the Mount reef will be a research site for sustainable coastal protection and marine ecology. The sand banks, used by surfers, are constantly changing which means there are seldom consistent high-quality surfing waves at any particular spot.

The dimensions of the reef are 70 m cross-shore and 90 m longshore. The reef (Figure 2.38) will be constructed of 24 GSCs. The bags vary from 30 m long with a diameter of 1 m to 50 m long with a diameter of 3.5 m, This is a volume varying from 27 to 660 cubic metres. A smaller geotextile tube ("scour tube") will also be installed behind the reef to prevent sand being scoured from under the two big bags.

The total volume of the reef is 6 000 cubic metres, which is 1/20 of the Narrowneck reef. The reef will be constructed as follows: the empty bags will be tied onto a webbing lattice on dry land before being folded up and towed out to the reef site on a barge. The empty reef will then be offloaded and pulled down into position on the seabed using Ancor Locs. Once secured in place the sand is pumped into the bags to fill them all up and create the shape of the reef.

For this reef one physical study has been carried out and published (Moores *et al.*, 2006). No numerical studies have been published.

Figure 2.38 - Plan view design Mount reef (source: www.mountreef.co.nz).

Bournemouth surf reef, Boscombe, Great Britain

The Bournemouth surf reef is the first artificial surf reef that has been in Europe. The construction started in October 2008. The reef will be located to the east of Boscombe Pier, about 2.5 kilometres from Bournemouth Pier, and takes up approximately one hectare 225 metres from the shoreline. The reef is built from large geo-textile bags pumped hard with sand. The sandbags are up to 70 m long, 2 m high and 6m wide.

The reef will be built in two layers: the bottom layer sitting on the sea bed consists of three sections, on top of which lies the second layer of two sections. The first section is deployed on Boscombe seabed, filled and then the second reef section is laid and filled and so on, until the reef is completed, once the fifth section is laid and filled.

The bottom layer elements consist of three individual sections:

1. a geo-mat to minimize the structure sinking into the sea;
2. overlain by a huge web of specially sewn material that looks like large seat belts;
3. on top of which huge geo-textile empty bags are attached.

These have been tied together to create the first section, which has then been folded into a concertina and placed on a barge, ready for deployment on the seabed. When the weather is good enough for deployment (perfectly calm weather conditions are essential) the barge where it will be transported to the site at Boscombe.

Prior to placing of the first set of bags, 11 temporary anchors have been set around the perimeter of the surf reef site. They will be used for locating and securing the five reef sections elements when they are filled. Each reef element will be placed on a barge, transported to the site, lowered, and the shore end of the reef will be attached to a set of anchors by divers. The barge will then be slowly winched along the reef site allowing the section to gradually unfold and peel off into the water. The section will then be pulled down onto the seabed with winches and secured in place on the anchors ready for filling.

The top layer consists of two larger sets of bags secured to locating webbing without the geo-mat layer, as they will be sitting firmly on top of existing sand bags. The sequence previously described is followed again. When the filling phase has been completed, divers will remove the location straps attached to the anchors, and the contractor will remove the temporary anchors.

No physical or numerical studies of this project have been published.

2.4 CONCLUSION

In this chapter the functionality of an MFAR has been described both in terms of coastal protection and surfability. At one hand the functionality in terms of hydrodynamics and morphodynamics has been treated and at the other hand the state of art of the functionality of an MFAR has been presented. From the state of the art it can be concluded that until 2007 three artificial reefs have been built in the world and that in 2008 two other reefs were in construction. Another conclusion is that there is a significant lack of design guidelines for an MFAR and that the optimal design of a MFAR is site specific.

Chapter 3 Designing an Optimal Geometry

3. DESIGNING AN OPTIMAL GEOMETRY

Due to several reasons it would be unrealistic to present one optimal design of an MFAR for all locations in the world. These reasons have to do with local circumstances, like tidal range, wave climate, bathymetry, currents and sediment transport and the budget.

However, for the design of any artificial reef that will be built to both protect the local coastline and to create surfing conditions, several design parameters have to be considered. What should be taken into account for these parameters in terms of hydrodynamics is described below. This chapter concentrates on hydrodynamics, but once an optimal geometry in relation to hydrodynamics has been determined, a thorough morphodynamic study (physical and/or numerical) is necessary to investigate the capacity of an MFAR to protect a local coastline.

3.1 MFAR-ANGLE

The choice of the MFAR-angle, θ, (Figure 3.1) is mainly related to the peel angle. As described in chapter 2, section 2.2.2, the peel angle has its maximum for $\theta = 66°$ and consequently this is the first option for this value. However, this maximum is found with linear refraction and without wave focusing. In order to get the proper form for the design peel angle, numerical simulations, that take irregular waves and wave focusing into account, ought to be performed.

Figure 3.1 - Reef angle (reef in plane view).

3.2 THE HEIGHT OF THE REEF

The height of the reef depends on: its horizontal dimensions, its distance from the shore, its submergence and its slopes. However, the height needs a minimum value in relation to the breaker type. For a certain reef slope, the height determines the length of the reef side. This should be long enough for the wave to feel the reef, otherwise the

wave does not have enough space, and that it will also break in accordance with the slope of the bottom (see Figure 2.29).

It is not yet known how long a reef needs to be to get the desired breaker type under certain wave conditions and slope of the reef (according to Equation (2.4)). The research of Smith and Kraus (1991) is closely related to the influence of the length of the reef slope on the breaker type. They conducted a laboratory study of a wave breaking over bars and artificial reefs and used the results to categorize the offshore breaker type differently from Battjes (1974) when the bottom has a barred profile. However, this categorization is general, for varying reef slopes and wave conditions, and the length of the reef slope is not taken into account, so it is not appropriate for this study.

To determine the exact length of the reef side required for the proper breaker type, as a function of the wave length, and thus the value of the reef height, numerical simulations should be performed. In order to choose the initial geometry for the numerical simulations, a fraction of the local wave length can be taken as the minimum length of the reef; take, for example, 1/4 times the local wave length. Thus, for a relatively long wave period of 14 seconds and a reef start at a depth of 4 m, the minimum length is 22 m. Assuming 1:10 slope, the minimum height is then 2.2 m for waves breaking on the crest of the reef. For the design, an extra value can be added, so waves can also break a little before reaching the crest, for example, 0.3 m. In this example, the minimum height that should be taken is 2.5 m. For shorter wave periods (or shorter wave lengths) a lower reef height should achieve the design breaker type.

3.3 THE GEOMETRY OF THE REEF

The choice of the form of the geometry is, like the choice of the MFAR-angle, mainly related to the peel angle. An initial design choice for the initial geometry shape for the numerical simulations can be a delta form composed of two rides (a left and a right ride) with a constant MFAR-angle $\theta = 66°$, as described previously.

Such a delta structure, which will be designed to create surfable waves, could be placed on the sea bottom or on a platform. A platform is, in theory, positive for the coastal protection aspect of the reef, because it makes the (large) waves break over it across its whole width (Smit and Mocke, 2005). But the effect of the presence or absence of a platform on the current cells that will be formed needs to be studied with numerical simulations. Regarding the surfer parameters of peel angle, α, breaker type, here related to the corresponding inshore Iribarren number, ξ_b, and wave height at the breaking point, H_b, it has to be determined if the platform has a positive influence.

The peel angle should be taken between 40 and 60 degrees for the waves to be surfable for most surfers (see Table 2.2 and Figure 2.13), and the peel angle has a maximum for an MFAR angle of 66 degrees.

Some calculations have been made to gain more insight into peel angle values. To estimate the peel angle we have to know what the design wave height is. The larger the design wave height the smaller the peel angle will be (the wave breaks sooner, and so refracts less).

Calculations were performed for a reef consisting of a platform with a delta structure on top, having an MFAR-angle of 66 degrees and where the submergence of the reef is 1.5 m, for safety reasons (see section 3.4 in this chapter).

The wave conditions were wave periods of 6, 10 and 14 s and wave heights of 1, 2, 3 and 4 m and the breaker criterion was chosen to be $H_b = 1.1h_b$ (Table 3.1). Over gentle slopes, waves are expected to break when $H_b = \gamma*h_b$, where H_b is the breaker height and h_b is the breaking depth, and γ is equal to 0.78 (Sverdrup and Munk, 1946). As the beach slope increases, as though over a reef, the value of γ increases for the same wave steepness in deep water. The chosen value of γ of 1.1 is based on the work of Kaminsky and Kraus (1993). These researchers derived an empirical formula in a review of seventeen data sets obtained by various investigators in laboratory experiments. The formula is:

$$\gamma_b = 1.20\,\xi_\infty^{\,0.27} \tag{3.1}$$

where γ_b is the breaker condition and ξ_∞ is the deep water breaker parameter. ξ_∞ is equal to ξ_b with the exception that the breaker wave height has to be replaced by the wave height in deep water, H_0. Assuming a reef slope of 1:10, the mean value of γ_b is 1.1 for the tested wave conditions, and the maximum is 1.3.

The peel angle was computed for two depths for the platform: 4.0 m, which is the minimum depth of the platform in the example cited in the part about the height of the reef (1.5 m submergence + 2.5 m minimum height of the delta structure), and 5.0 m (Table 3.1). Waves that break before they have traveled a length equal to 1.0 m height of the delta are not taken into account, because they are not expected to result in plunging waves. Although the calculations use linear theory and the wave focusing is not taken into account, they give an indication about the values of the peel angle.

Table 3.1 - Peel angles for a reef with a submergence of 1.5 m and reef start depths of 4.0 m (left) and 5.0 m (right).

a) Reef starts at 4.0 m depth.

T\H	1 m	2 m	3 m	4 m
6 s	*	**35.7**	**44.6**	-
10 s	*	**38.6**	**49.5**	X
14 s	-	**41.8**	X	X

b) Reef starts at 5.0 m depth.

T\H	1 m	2 m	3 m	4 m
6 s	*	**31.9**	**39.1**	-
10 s	*	**33.8**	**41.8**	X
14 s	-	**36.0**	**45.3**	X

Bold values	= wave breaks on the reef
*	= waves go over the reef
x	= wave has already broken or breaks at the beginning of the reef
-	= rarely existing wave conditions at west coast of Portugal

Results from Table 3.1 show that for wave heights in the range of 1-2 m the case with a platform at the minimum depth of 4.0 m offers more peel angle conditions within the range of amateurs, i.e. between 40 and 60 degrees. For cases with a platform lower than 5.0 m under the still water level the peel angles will be even lower than the values shown in Table 3.1b.

As the peel angle values are better for a start depth of the delta structure as small as possible, taking the example minimum height of the reef, it can be concluded that a platform at the seaward end of the structure definitely has a positive influence on the peel angle.

However, if the platform is under the whole delta structure, it probably has a relatively negative influence on the peel angle at the shoreward end compared with the case without a platform, because the delta structure can be higher at this point.

Moreover, the influence of a platform on the other two surfer parameters, i.e., the breaker type and the wave height at the breaking point, has not yet been investigated. In order to analyze this, the qualitative development of the peel angle, α, the inshore Iribarren number, ξ_b, and the wave height at the breaking point, H_b, along the breaker line are presented for both cases presented before: with and without a platform under the delta structure. The development of α, $1/\xi_b$ and H_b is presented in Figure 3.2 and shows that, for the case without a platform, α, $1/\xi_b$ and H_b are smaller at the beginning of the reef and larger at the end. These differences are caused by more refraction at the beginning of the reef (by longer slope) and less refraction at its end (by shorter slope) in the case without a platform. When wave focusing no longer plays a role, α, ξ_b and H_b increase towards the end of the reef without a platform and stay constant in the case with a platform.

Figure 3.2 - Relative development of the peel angle, wave height and Iribarren number along the breaker line.

From this analysis, it can be concluded that the choice of a platform does have an influence on the three surfer parameters: peel angle, breaker type and wave height at the breaking point. Wave defocusing is not taken into account in this analysis, for two reasons. First, because the area over which the wave focusing occurs is relatively small and second because the contributions to the peel angle of wave defocusing are relatively small compared with the area where wave focusing occurs, as described in the theoretical background.

Regarding the peel angle, the choice of a platform is not straightforward. A small variation in the peel angle along the ride does not represent a problem since surfers actually like some variation. However, the peel angle should be between 40 and 60 degrees, as mentioned before. Calculations have shown that these values of the peel angle are reached with the platform at the minimum depth for most wave conditions. So in terms of the peel angle, a platform in the first part of the reef is a better option. However, if the height at the last part of the reef is smaller in the case without a platform, the option of no platform would be better because refraction will be less.

Regarding the breaker type, the use of a platform is again a better option, because ξ_b is smaller at the beginning and stays constant along the ride.

Regarding to the wave height at the breaker point, the preferred wave height depends on the skill of the surfer. However, it is easier to start surfing when the wave is somewhat higher, at the beginning, especially when the peel angle is small. So, it can be concluded that, for the wave height at the breaker point, a platform is a good option, since for this case the wave is higher at the beginning of the reef.

In conclusion, the use of a platform has a positive influence on the most important surfer parameters: the peel angle, the breaker type and the wave height at the breaker point. However, not using a platform is better for the peel angle if the reef is less high,

even though it should be higher than the minimum, as stated in the part about the height of the reef.

Moreover, constructing a platform only at the seaward part of the delta structure would give a maximum peel angle along the entire ride. In some cases this is actually the only possibility, because the platform intersects with the bottom (Figure 3.3). Positioning the reef more seawards in order to construct a platform under the whole delta is often not an option since, as will be explained in the part of about the horizontal dimensions, the distance between the shoreline and the structure is established with the objective of preventing coastline erosion.

reef

platform

Intersection platform and bottom

Figure 3.3 - Intersection of platform and bottom.

Even though, in theory, a platform has a positive influence on the main surfer parameters, it still has to be taken into account that the exact influence can vary considerably with different geometries, and especially the reef angle is expected to be of much influence. One way to investigate this influence is to perform numerical simulations.

Another important factor that should be taken into account is that the form of the platform in the horizontal plane should be chosen so that its volume is as small as possible.

3.4 THE SUBMERGENCE OF THE REEF

The submergence of the reef is determined by two factors. Firstly it should be shallow enough for the design waves to break on the reef. Secondly it should be deep enough to ensure the safety of surfers.

With regard to the first factor, the submergence is dependent on the design breaking wave height and the breaking condition. Assuming a critical breaking condition of $H_b = 1.3 \cdot h$, which gives the smallest breaking depth, the submergence of the reef with, for example, a 2.0 m design breaking wave height is 1.5 m.

Concerning the second factor, it is a known fact that the water depth during backflow under the wave trough can be very shallow and the reef may even become emerged ('suck dry'). However, surfing is a sport that involves risks. Surfers know that and most of them develop their own way to see if they can surf a certain section safely.

Nonetheless, safety should be considered in the design. For diving in pools, FINA (International Federation of Swimming) regulations suggest 1.8 m as an acceptable depth for submergence (Corbett *et al.*, 2005). But surfers tend to fall off their boards rather than dive vertically, reducing both the depth of the dive and the risk of serious injury (e.g. damage to the neck and spine). This fact and the physical experiments conducted by Corbett and Tomlinson (2002), in which the water depth above a reef with certain submergence was investigated for different wave heights, led to the design choice that submergence should be deeper than the design wave height in deep water. As an example, if the design wave height is 1.5 m, the minimum submergence for safety would be 1.5 m. The sucking dry phenomenon is probably hard to prevent completely, especially with high waves at low tide. Experience with the Narrowneck reef has indicated that, with a submergence of 1.5 m, the crest containers 'sucked dry' during larger wave conditions (>2 m) at low tide (Jackson *et al.*, 2005). In specific design studies numerical simulations will be needed to verify if and for what wave heights this phenomenon occurs.

It should be noted that the design wave height and the corresponding design submergence mentioned above are for low tide, because this tidal level gives the critical submergence. But many coastal zones have tidal conditions, so the influence of the tide on the peel angle should not be neglected. To investigate this influence on the peel angle, calculations assume a tidal level 1.5 m higher than that in Table 3.1a) and b), so the submergence is now 3.0 m and the depths of the platform are 5.5 and 6.5 m. Table 3.2 show the values of the peel angle obtained.

Table 3.2 - Peel angles for a reef with a submergence of 3.0 m and reef start at depths of 5.5 m (a) and 6.5 m (b).

a) Reef starts at 5.5 m depth.

T\H	1 m	2 m	3 m	4 m
6 s	*	*	*	-
10 s	*	*	*	**46.5**
14 s	-	*	**42.3**	**51.1**

b) Reef starts at 6.5 m depth.

T\H	1 m	2 m	3 m	4 m
6 s	*	*	*	-
10 s	*	*	*	**41.4**
14 s	-	*	*	**44.5**

Bold values	= wave breaks on the reef
*	= waves go over the reef
x	= wave has already broken or breaks on the beginning of the platform
-	= rarely existing wave conditions at west coast of Portugal

From Table 3.2 it can be seen that in both cases the peel angles are high enough for both amateur and professional surfers, but the waves that break over the delta have an H_0 of 3-4 m. However, by refraction and shoaling, the H_b on the reef will be even higher

than 4 m. These wave heights cannot be surfed by surfers with skill levels 3 and 4. In conclusion, it can be said that higher tidal levels make surfing impossible for most amateurs. The tide also influences the breaker type by affecting the breaker wave height over the delta. Consequently, a guideline would be to pay attention to the fact that just one tidal level can be the 'design' level if the reef is designed for a certain category of surfers.

The minimum submergence and the minimum needed height of the reef for surfing, together with the distance offshore of the reef, and the slope of the sea bottom have a large influence on the effectiveness of a reef in terms of creating surfable waves. The slope of the sea bottom, the minimum submergence and the distance from the base of the delta to the shoreline will determine the height at the shore side of the reef. In order to verify achievement of the minimum height needed for surfing, some calculations have been performed.

Table 3.3 shows the values of the reef heights at the shore side for a reef with a submergence of 1.5 m, a distance from the base of the delta to the shoreline of 175 m, a distance from the apex of the delta to the shoreline of 250 m (see section 3.5 in this chapter) and different slopes of the sea bottom. In this case the cross-shore length of the delta is 75 m.

Table 3.3 - Reef heights for different bottom slopes.

Distance from shoreline (m)	1:25	1:50	1:75	1:100
175 (base delta)	5.5 m	2.0 m	0.8 m	0.3 m
250 (apex delta)	8.5 m	3.5 m	1.8 m	1.0 m

A height of 2.0 m at the base of the reef is here accepted as the minimum value for surfing. This is less than the value of the example presented in section 3.2 in this chapter, where the minimum height was 2.5 m, because the reef will be higher further seawards where the wave rays that reach the end of the reef start.

Table 3.3 shows that the minimum slope value for building a multifunctional artificial surfing reef that functions properly is 1:50, because then the minimum height of 2.0 m is reached at the base of the delta. If a platform is chosen in the design, the intersection of the platform with the bottom, as a consequence of the chosen minimum height, gives a figure of 50 m under the seaward part of the delta. It is preferable for surfers to make the ride from the seaward crest of the delta up to the base of the delta. Some simple refraction calculations can give an indication as to whether the wave rays at the shoreward intersection of the platform and the reef still reach the crest of the delta

(Figure 3.4). Numerical simulations have to be performed to confirm these simple calculations.

Figure 3.4 - Wave rays reaching the crest delta.

3.5 THE HORIZONTAL DIMENSIONS

The horizontal alongshore dimension depends on the length of the local coastline to be protected. The cross-shore dimension of the reef depends on the design length of the ride, which is the length of the breaker line at one of the sides of the reef (Figure 2.30). This dimension is limited, however. As mentioned in the state of art, Ranasinghe and Turner (2006b) found that the principal mode of shoreline response to submerged structures can vary from erosive to accretive, depending on the offshore distance to the structure (Figure 2.5). Based on these results, a predictive empirical relationship is proposed as a preliminary engineering tool to assess the shoreline response to submerged structures. This relationship is $S_a/SZW > 1.5$, where S_a is the distance from the apex of the structure to the undisturbed shoreline and SZW is the natural surf zone width. The distance S_a should clearly not be too large, because the effect of the structure on the morphodynamic processes adjacent to the shoreline will start to decline with increasing values.

3.6 THE SLOPE OF THE REEF STRUCTURE

A surfable wave for amateurs should be plunging, almost spilling. Based on experimental results with a 1 m wave height, Henriquez (2004) found that the inshore Iribarren number, ξ_b, should be between 0.6 and 0.9 to get surfable waves. These are plunging waves with relatively small inshore Iribarren numbers (see Table 2.4). Some calculations using linear theory have been performed for different wave heights to

analyze which slopes will cause waves to break as a plunging breaker type. Figure 3.5 shows the inshore Iribarren numbers for a slope (that the wave meets) varying from 1:6 to 1:18, a wave height at breakpoint varying from 1 to 4 m and a wave period of 10 s. As can be seen, only a few combinations of slope and wave height give a plunging breaking wave in the surf range.

Figure 3.5 - Surf range.

The values of ξ_b that lie in the surf range (given by Henriquez, 2004) are for slopes between 1:8 and 1:18, as can be seen in Table 3.4. It should be pointed out that the theory used is linear and that the surf range of 0.6 m to 0.9 m was found in experiments for a wave height of 1 m (prototype) at the wave maker, and here it is applied to a wave height range of 1 to 4 m at the breakpoint. However, it does give an indication as to what combination of reef slopes and breaking wave heights give surfable waves. Based on this indication an initial slope of the reef can be chosen to start with in numerical simulations.

Table 3.4 - Inshore Iribarren number for different slopes and wave heights in the surf range.

Tan α	H_b (m)	ξ_b
1:8	4	0.79
1:10	2	0.89
	3	0.73
	4	0.63
1:12	2	0.74
	3	0.61
1:14	2	0.64
1:16	1	0.79
1:18	1	0.70

If for example the breaking wave height is 2 m, the design choice of the side slope of the delta structure could be 1:10 because with this slope it can be expected that the design breaking wave height, H_b, of 2 m experiences slopes between 1:10 and 1:14 and that, consequently, the breaker type lies in the surf range. This will have to be confirmed with numerical simulations for each specific set of geometry and wave conditions.

The design choice for the slope at the shoreward end of the delta structure and for the slope of the platform at all sides should be as low as possible, in order to keep its volume smaller.

3.7 CONCLUSION

As a result of a theoretical study, a preliminary design, achieved step by step, is proposed for a multi-functional artificial reef making use of the theory and the state of the art. The proposed reef geometry is used as initial design in the numerical and physical tests, which are executed to analyze the capacity of a multi-functional reef breakwater to protect a stretch of the northern coast of Portugal and increase the local surfing possibilities. Wave focusing is not taking into account in the formation of the preliminary design. The main design parameters for a MFAR are the reef angle, the height of the reef, the geometry of the reef, the submergence of the reef, the horizontal dimensions and the slope of the reef structure. Taking into account the condition that the proposed geometry will only function properly on a sea slope bottom of less than 1:50, the main preliminary choices are as follows: the upper part of the structure is delta shaped with an angle of 66º and a side slope of 1:10, and the lower part consists of a platform whose slopes are as steep as possible. The position of the reef should be such that the distance from the apex of the structure to the undisturbed shoreline is greater than 1.5 the natural surf zone width.

Chapter 4 Investigation of Multi-Functional Artificial Reef Cross-Section Design Parameters

4. INVESTIGATION OF MULTI-FUNCTIONAL ARTIFICIAL REEF CROSS-SECTION DESIGN PARAMETERS

4.1 INTRODUCTION

The optimal geometry for a multi-functional artificial reef is the geometry that protects the local coastline and offers surfing possibilities in the best possible way according to the local conditions. This investigation concerns an optimal geometry of a multi-functional artificial reef to be applied in the west coast of Portugal. Six parameters have to be defined for an optimal geometry, as mentioned before (see chapter 3, the theoretical study):

- the height of the reef;
- the side slope of the reef;
- the submergence of the reef;
- the reef angle;
- the geometry of the reef (with or without a platform);
- the horizontal dimensions.

Three of them have mainly a 2DV behavior (x, z): the height, the submergence and the slope of the reef. For these parameters, some values were suggested, namely:

- the height of the reef, h_reef, to be equal to $0.25*L_w$, being L_w the local wave length at the start of the reef;
- the submergence of the reef, S, to be equal to the design wave height;
- the seaward slope of the reef, s_reef to be 1:10.

This chapter treats the confirmation of those values for the wave and bathymetric conditions at the west coast of Portugal, where the case study, the coast of Leirosa, is located. For that, a 2DV physical and numerical study was done focusing on the breaker type regarding surfing.

The situation in Leirosa is currently especially vulnerable. A frontal dune that runs from the groin of Leirosa till almost the mouth of Extremal stream is totally destructed. This has caused a retreat of the coastline and has put at risk (Lopes *et al*., 2003):

a) the agglomerate of Leirosa, which situation is not yet critical, but it has to be kept an eye on;

b) the emissary of urban wastewater of the agglomerate van Leirosa, which extends parallel to the coast, to the south, and that is connected to the emissary of cellulose factories;

c) the pressure chamber of submarine emissary of cellulose located about 1 km south of Leirosa.

A fragment of the dune in front of the pressure chamber of the emissary was partly strengthened in 2005, using bags of geotextile filled with sand on a length of about 120

m as described in Chapter 1. This has been done after storms that occurred in February 2001 which affected especially this zone and that will lead to a gradual and dangerous weakening in the next years. Although the resolution of the large vulnerability of this zone by the construction of a groin south of the cellulose emissary is considered, such a heavy protection structure is not planned in the POOC (legally development plan of the coast). The research of this thesis is a contribution to the implementation of a solution for Leirosa, along a very sensitive coastal fragment that is shown in Figure 4.1.

Figure 4.1 - View from the air with Leirosa at the top, pressure chamber of the emissary in the middle and the part of the dune in front of the pressure chamber that was partly repaired in January 2006 (Antunes do Carmo).

The bottom slope of 1:50 is used, since it is a reasonable value for the centre of the west coast of Portugal. The design wave condition for surfing is chosen in order to have a good surfable wave and to be a common wave condition at the Portuguese west coast. For that, the wave regime near by Figueira da Foz (Capitão *et al.*, 1999) was analyzed, Figure 4.2. Figueira da Foz is situated near by Leirosa, the case study place, for which the optimal geometry will be defined. In the future bathymetric and wave data at Leirosa itself will be gathered.

From Figure 4.2, it can be seen that the wave height, H_s, of 1.5 to 2.5 m and the mean zero up-crossing period, T_z, of 6 to 8 s are the most frequent. Based on these values for the regular design wave condition, a wave height, H, of 1.5 m is chosen and a period, T, of 9 s. The period T is chosen to be higher than 6 to 8 s, because the T_p is used here as the characteristic value for T. Assuming a Jonswap spectrum, T_p is 1.25 times T_z (Goda, 1987).

Figure 4.2 - Wave regime near by Figueira da Foz (Capitão *et al.*, 1999).

In section 4.2 the physical study conducted to investigate the height of the reef and the submergence is described. The physical tests show clearly the breaker shape, however the parameters can not be varied thoroughly. Besides that no data about the exact position of wave breaking and the height at the breaking point were available from the physical experiments. In order to fill this gap, complementary studies were made using a numerical model that solves the Reynolds average Navier-Stokes (RANS) equations, called COBRAS-UC (Garcia *et al*., 2004), (COBRAS = Cornell Breaking Waves and Structures, UC = University of Cantabria). The investigation on the height, the submergence and on the slope of the reef with the COBRAS-UC model is presented in section 4.3.

4.2 PHYSICAL STUDY

4.2.1 INTRODUCTION

The objective of the experiments is two-fold: to record the breaker type over an artificial reef with a smooth slope and to measure surface level elevations over a reef constructed with an impermeable broad-crested submerged structure.

These measurements provide a unique set of data, allowing one to estimate the breaker type on submerged broad-crested breakwaters with a smooth slope. Besides that the data provides the possibility to calibrate and validate numerical models. Particularly, it will be possible to verify, for a submerged reef with a smooth slope, the categorization of the Iribarren number presented in the literature (Battjes, 1974), that was made for a single slope beach.

4.2.2 THEORETICAL FRAMEWORK

The term 'breaker type' refers to the form of a depth-limited wave at breaking and influences other breaking-wave properties. Although there are several classifications of breaker type, it is generally accepted that waves break by spilling, plunging, collapsing, and surging (Galvin, 1968; 1972). Section 2.2.3 in Chapter 2 gives more information about the breaker types.

Smith and Kraus (1991) performed a laboratory study for waves breaking over bars and artificial reefs. They constructed the bar of marine plywood and tested six different design seaward angles and four design shoreward angles. They tested several combinations of shoreward and seaward angles of the bar, five regular wave conditions and three random wave conditions. They found for barred profiles the following transition values:

- surging or collapsing if $\xi_0 > 1.2$;
- plunging if $0.4 < \xi_0 < 1.2$;
- spilling if $\xi_0 < 0.4$.

However, their results are for narrow crested artificial reefs and the influences of the structure submergence, of the length of the slope and of the depth at the start of the structure on the breaker type and on the Iribarren number were not studied.

Regarding the breaking behavior on artificial reefs with a smooth slope, just one study has been conducted in a wave flume by Corbett and Tomlinson (2002). They performed a physical study for Noosa Main Beach in Australia on a permeable reef built from geotextile sand containers to investigate the wave breaking behavior and associated safety issues for an artificial reef. The analysis of the results of these tests was especially focused on the breaker type, on the breaker wave height and on the breaker location as an indication for the safety of the submerged reef. However, even though several submergences were tested, no analysis of the relation between the

breaker type and the corresponding Iribarren number were made. Furthermore, the influence of the length of the slope on the breaker type and the corresponding values of the Iribarren number was not investigated.

In the present work, the transition values for submerged broad-crested artificial reefs will be determined taking into account the following structure characteristics:

- submergence;
- length of the seaward slope.

4.2.3 *JUSTIFICATION OF EXPERIMENTS*

The purpose of these experiments is, as referred, to investigate the relation between the breaker type and the submergence and the length of the slope of a broad-crested reef.

Based on the Iribarren number, the breaker type has to be the same for the same slope, the same offshore wave height (or breaker wave height) and the same period. However, as indicated by the physical experiments conducted by Henriquez (2004), the submergence has also an influence on the breaker type. Besides the submergence, it is expected that the length of the slope of the reef will also have an influence on the breaker type. This expectation is based on the fact that the wave will develop differently when the slope has a difference in length due to difference in shoaling.

To investigate the influence of the length of the reef and the submergence on the breaker-type, different tests were made with:

a. the same wave conditions, the same submergence and different lengths of the slope;

b. the same wave conditions, the same length of the slope and several submergences.

4.2.4 *EXPERIMENTAL SET UP*

Physical model tests were made in one of the LNEC's flume with the following dimensions: 73.0 m long, 3.0 m wide and 2.0 m deep. The model was operating according to Froude's similarity law, with a geometric scale of 1:10.

Two geometries (low and high geometry), with a structure built on concrete, were tested with two different values for the length of the seaward slope. Figure 4.3 shows the flume: the left picture is in the direction of the wave maker and the right one in a direction contrary to the wave-maker.
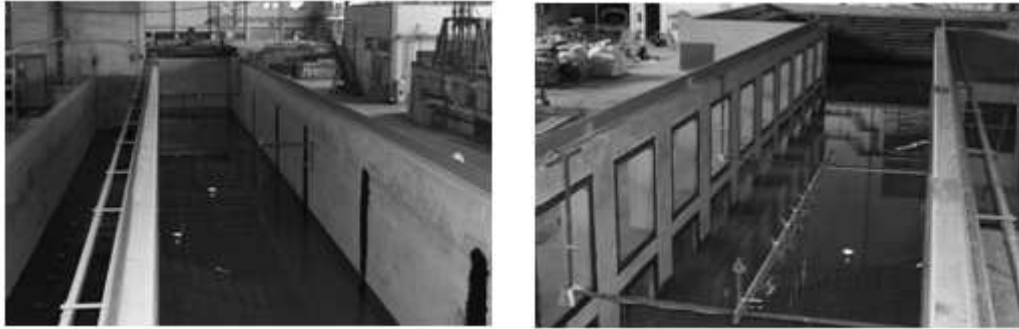
Figure 4.3 - LNEC's flume used for the tests.

The seaward slope of the reef, *s_reef*, was constant and equal to 1:10. This is a regular value for the side slope of a multi-functional artificial reef. The shoreward slope should be as steep as possible, 1:2 or 1:3.

In chapter 3 is mentioned that the minimum length of the reef, in order to get a good surfable wave, is 1/4 times the local wavelength. Based on this assumption the length of the low geometry, L_s, was chosen to be 19 m in prototype scale. For the high geometry the length of the reef, L_s, was twice the value for the lower geometry: 36 m in prototype scale. As a consequence the height of the reef, *h_reef*, is for the low geometry 1.9 m and for the high geometry 3.6 m in prototype scale.

The length from the wavemaker till the start of the foreshore is 18.2 m in prototype scale. The slope of the foreshore, *s*, is 1:50. The length of the foreshore, *L_init*, for the low geometry is 240 m and for the high geometry is 155 m, all in prototype scale; this is at least 1.5 times the wavelength at the wave maker for each depth tested. The height of the foreshore, *h_fore*, is for the low geometry 4.80 m and for the high geometry 3.10 m in prototype scale. Based on that and on the reef submergences, the water depth at the wave maker was defined and varies from 9.1 m and 7.5 m, in prototype scale. The width of the reef, L_c, is 75 m, in prototype scale. This value is at least one time the wavelength. Consequently, it was determined for all periods tested and for the water depth at the start of the deepest reef (larger submergence) tested for the high geometry. Figure 4.4 shows the geometry parameters of the reef. Table 4.1 and Table 4.2 show the values of the geometric parameters in the model and in prototype scales.

Figure 4.4 - Geometry parameters (not scaled).

80

Table 4.1 - Values of the structure parameters in the model scale.

Case	Material	h_reef (m)	s_reef	s	L_s (m)	L_c (m)	h_fore (m)	h (m)	L_init (m)	L_fore (m)
1	Concrete	0.19	1:10	1:50	1.90	7.5	0.48	0.75 - 0.91	18.2	24.2
2		0.36			3.60		0.31			15.5

Table 4.2 - Values of the structure parameters in prototype scale.

Case	Material	h_reef (m)	L_s (m)	L_c (m)	h_fore (m)	h (m)	L_init (m)	L_fore (m)
1	Concrete	1.90	19.0	75	4.80	75-91	182	242
2		3.60	36.0		3.10			155

The low geometry is shown in Figure 4.5 and Figure 4.6. The high geometry is shown in Figure 4.7 and Figure 4.8. Figure 4.6 and Figure 4.8 show the slope of the structure in black.

Figure 4.5 - Low geometry.

Figure 4.6 - Low geometry (slope of the structure is in black).

Figure 4.7 - High geometry.

Figure 4.8 - High geometry (slope of the structure is in black).

4.2.5 TEST CONDITIONS

For each tested reef geometry 51 experiments were executed, corresponding to 17 combinations of different values of the wave height and the submergence. Each wave height was tested for three different periods. Each test lasted 320 seconds, which corresponds to, at least, 100 waves.

The selection of the submergence values was based on the following. In order to guarantee breaking, a depth smaller than $0.8*H_b$ was assumed to be necessary (Kaminsky and Kraus, 1993), where the height of the wave at breaking H_b was chosen to be at minimum $1.0*H_{wm}$. H_{wm} is the wave height at the wave maker. For most wave heights a submergence of $0.8*H_b$ was tested. However, in order to see if waves with larger submergences than that will also break, some wave heights have been tested with submergences of $(0.8*H_b + 0.04)$ m and $(0.8*H_b + 2*0.04)$ m. Table 4.3 shows the test conditions.

Table 4.3 - Test conditions (model scale).

H_{wm}(m)	S (m)	h (m)	T (s)
0.10	0.08	0.75	2.52, 2.84, 3.16
	0.12	0.79	
	0.16	0.83	
0.15	0.08	0.75	
	0.12	0.79	
	0.16	0.83	
	0.20	0.87	
0.20	0.12	0.79	
	0.16	0.83	
	0.20	0.87	
	0.24	0.91	
0.25	0.16	0.83	
	0.20	0.87	
	0.24	0.91	
0.30	0.20	0.87	
	0.24	0.91	
0.35	0.24	0.91	

4.2.6 INSTRUMENTATION

It was the primary purpose of this experimental research to obtain accurate images of the breaker type. In each test the breaker type was captured by video techniques. A video camera recorded the breaker type of the breaking wave. On the windows a grid of 10 cm by 10 cm was made to help the measurements made from the videos.

Also 8 wave resistive type gauges were mounted in order to measure surface elevation at several positions along the wave flume, mostly positioned in the breaker zone. The data collected will provide mainly wave height records, but it can also be used to obtain mean surface displacement (setup/setdown). Two sensors, gauge 1 and gauge 2, remained throughout the experiment at a seaward location close to the wave paddle, for control and repeatability tests. Another gauge was located in the beginning of the foreshore slope and another in the beginning of the reef. The remained 4 gauges were mounted in the breaking zone. All tests were repeated with these 4 gauges, 0.5 m moved in the direction of the end of the channel. In that way at eight positions, 0.25 m from each other, in the breaking zone the time series of the surface elevation were acquired (Figure 4.9).
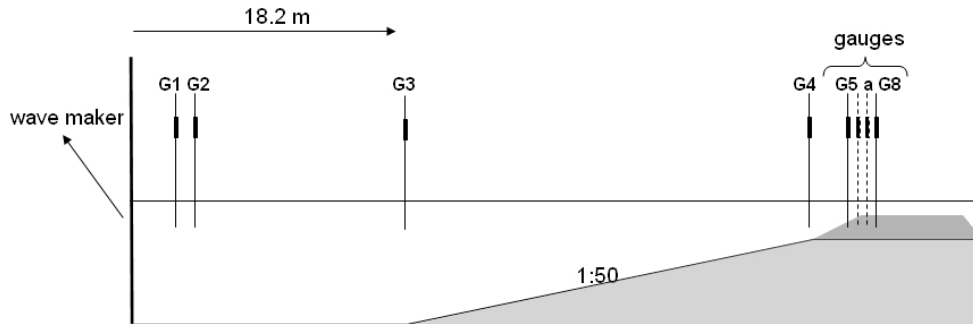
Figure 4.9 – Schematic representation of the gauges along the channel.

4.2.7 RESULTS

The results, in what concerns to the mean wave height in front of the paddle, obtained in the tests with the high and low geometry were not the same. However, since the goal of the experiments was to see the influence of the length of the reef and the influence of the submergence, comparison of the breaker types was made by comparing the results of the breaker types with the same Iribarren number ranges. From all videos in which the wave breaks in the window, a picture of the breaker type was made after around 2 min of tests, which is about 30-40 waves, depending on the period used in the test. These pictures were selected into 5 categories of the Iribarren number: smaller than 0.6, from 0.6 to 0.8, from 0.8 to 1.0, from 1.0 to 1.2 and larger than 1.2. These categories were made to analyze the breaker type more conveniently. All pictures of the breaking waves are presented in annex I according to the Iribarren number in such a way that different lengths of the reef and different submergences can be compared easily. If there are pictures of a wave in the window with almost equal Iribarren numbers for the same submergence and different lengths of the reef they are put besides each other. If no equal Iribarren number could be found for the other tested length, the spot besides the picture is kept empty in Annex I. In the pictures, H_m is the mean wave height, T_m is the mean wave period in the wave gauge at 5.1 m from the wave maker (gauge 1), S is the submergence and Ir is the Iribarren number.

Based on the test results, some conclusions for each category can be made and are presented hereafter, together with two comparing pictures for different reef geometries with the same submergences that illustrate the results. All breaking waves analyzed here, are plunging. Due to the fact that all wave shapes are plunging it is not possible to draw a conclusion regarding the influence of the length of the reef and the submergence on the wave shape according to the categorization of Battjes (1974). However, within each mentioned category of smaller than 0.6, from 0.6 to 0.8, from 0.8 to 1.0, from 1.0 to 1.2 and larger than 1.2 differences can be notified.

For Iribarren values larger than 1.2 no comparison can be made because there is just one picture of a breaking wave for the low geometry.

84

Iribarren number < 0.6

For $Ir < 0.6$, no comparison can be made for difference in submergence on the wave shape. However, for the difference in the length of the reef, the wave for a low reef geometry, *h_reef* is 0.19 m, is better for surfing due to the larger space in the tube. Regarding the breaker position is, in case of the high geometry and for the same submergence, about 30 to 40 cm more towards the end of the seaward slope of the reef compared to the low geometry. Figure 4.10 shows the breaker type for the low and high geometries, and a submergence of 0.24 m.
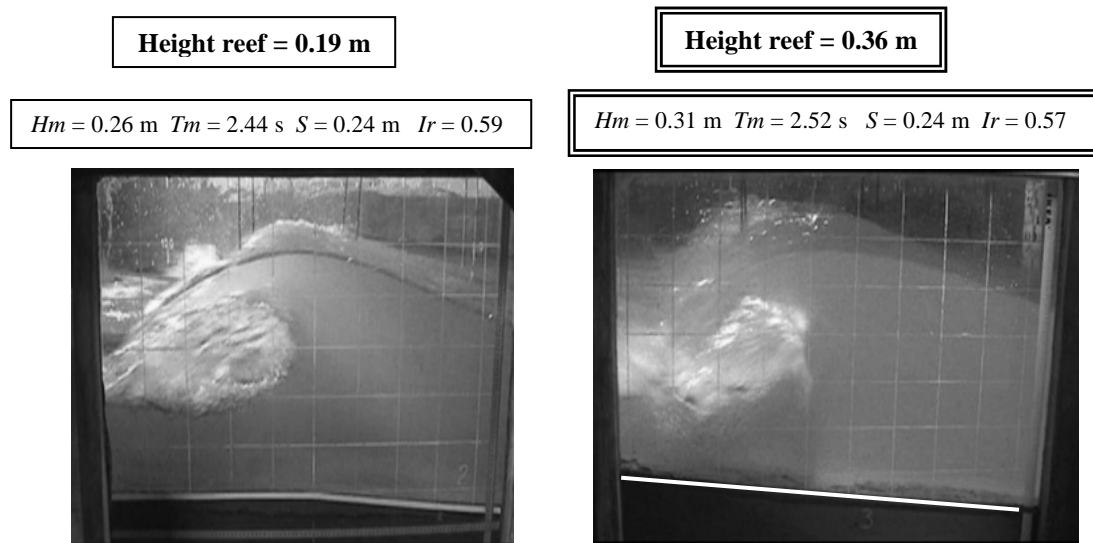
Height reef = 0.19 m	**Height reef = 0.36 m**
$Hm = 0.26$ m $Tm = 2.44$ s $S = 0.24$ m $Ir = 0.59$	$Hm = 0.31$ m $Tm = 2.52$ s $S = 0.24$ m $Ir = 0.57$

Figure 4.10 - Breaker type for low and high geometries, and for an Iribarren number smaller than 0.6.

0.6 < Iribarren number < 0.8

For $0.6 < Ir < 0.8$, the higher the submergence and the wave height, the better the tube is for surfing. No significant difference could be notified in the wave shape comparing the low and high geometry. It could be notified that in case of the low geometry the most waves with a large wave height, that are tested with a large submergence of 0.20 and 0.24 m, break already before the reef starts. Regarding the breaker position is in case of the high geometry for the same submergence about 30 to 40 cm more towards the end of the seaward slope of the reef, compared with the low geometry. Figure 4.11 shows the breaker type for the low and high geometries, and for the submergence of 0.16 m.
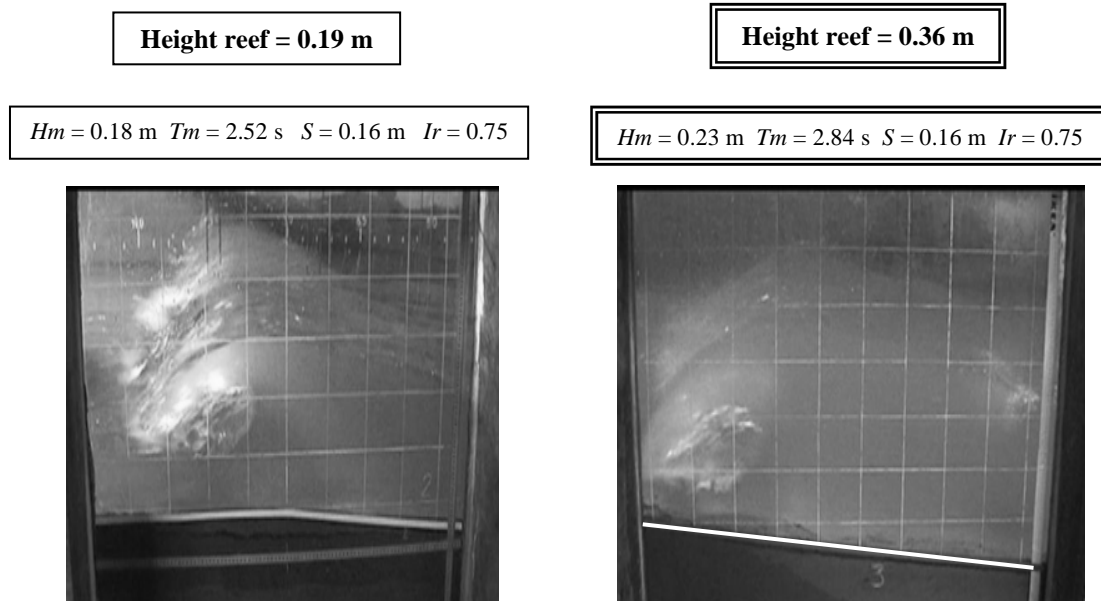
Height reef = 0.19 m	Height reef = 0.36 m
Hm = 0.18 m Tm = 2.52 s S = 0.16 m Ir = 0.75	Hm = 0.23 m Tm = 2.84 s S = 0.16 m Ir = 0.75

Figure 4.11 - Breaker type for low and high geometries, and for the Iribarren number between 0.6 and 0.8.

0.8 < Iribarren number < 1.0

For $0.8 < Ir < 1.0$, the breaking wave with a submergence of 0.08 do not seem to be good for surfing due to the small space in the tube. However, a submergence of 0.12 m and higher do give a good tube for surfing, also for wave heights of 0.15 m. This means that the safety submergence of 1.50 m gives still good breaking waves for surfing. No significant difference could be notified in the wave shape comparing the low and high geometry. Regarding the breaker position, again in case of the high geometry for the same submergence more towards the end of the seaward slope of the reef compared with the low geometry, about 20-30 cm. Figure 4.12 shows the breaker type for the low and high geometries for a submergence of 0.20 m.

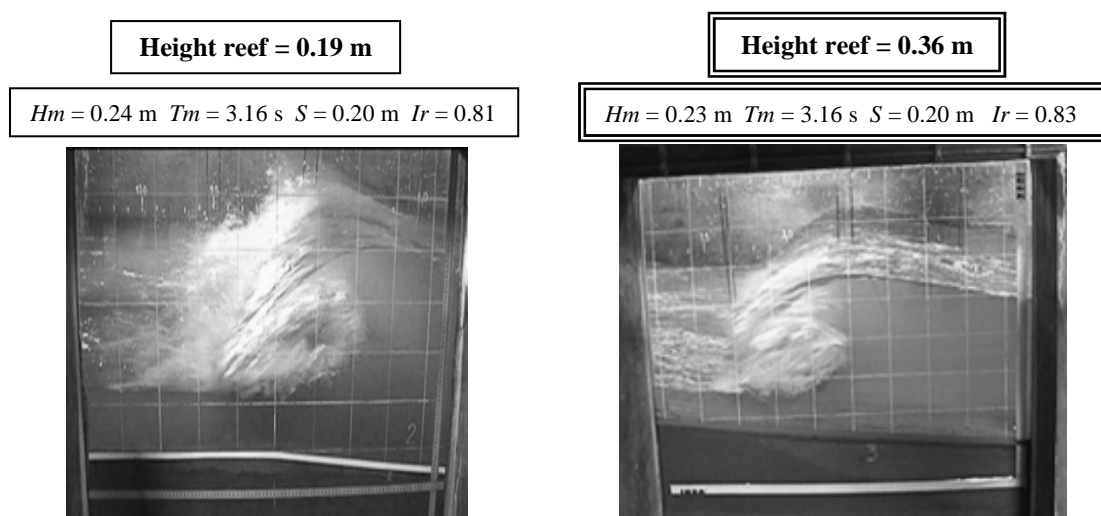| Height reef = 0.19 m	Height reef = 0.36 m
Hm = 0.24 m Tm = 3.16 s S = 0.20 m Ir = 0.81	Hm = 0.23 m Tm = 3.16 s S = 0.20 m Ir = 0.83

Figure 4.12 - Breaker type for low and high geometries, and for the Iribarren number between 0.8 and 1.0.

1.0 < Iribarren number < 1.2

For $1.0 < Ir < 1.2$, like the previous category, again the breaking wave for a submergence of 0.08 does not seem to be good for surfing due to the small space in the tube. About the higher values of the submergences not much can be concluded. Regarding the breaker position, for the high geometry it is more towards the end of the seaward slope of the reef, compared with the low geometry. Figure 4.13 shows the breaker type for the low and high geometries, and for a submergence of 0.12 m.
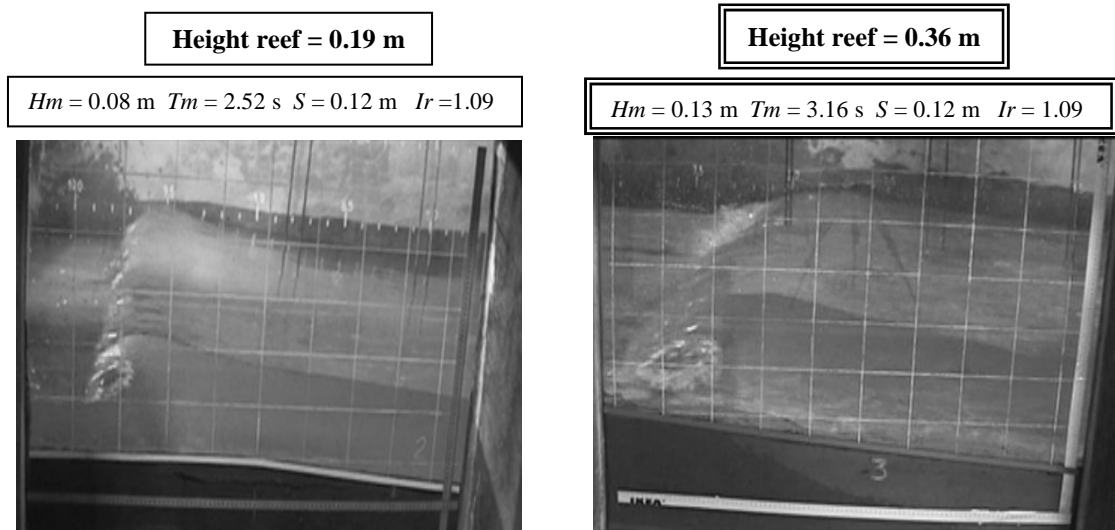
Height reef = 0.19 m	Height reef = 0.36 m
$Hm = 0.08$ m $Tm = 2.52$ s $S = 0.12$ m $Ir = 1.09$	$Hm = 0.13$ m $Tm = 3.16$ s $S = 0.12$ m $Ir = 1.09$

Figure 4.13 - Breaker type for low and high geometries, and for the Iribarren number between 1.0 and 1.2.

4.2.8 PRELIMINARY CONCLUSION

From the physical experiments, it can be concluded that the wave breaks in a plunging way in most of the cases. The length of the reef does not have an influence at all in the cases that were tested. However, the submergence has an influence. Most shapes are good to surf, however for a submergences of 0.08 m the tube of the breaking wave is not very good for surfing due to a lack of space in the tube. Furthermore it can be concluded that a submergence of 1.60 m (prototype scale) gives, in most cases, still a good breaking wave for the design wave height of 1.50 m, which means that the safety submergence of 1.50 can give good shape of the breaking waves for surfing.

4.3 NUMERICAL SIMULATIONS

To get more insight in the breaker type and in the position of breaking simulations for the prototype scales and for several heights of the reef, numerical simulations with COBRAS-UC (Garcia *et al*. 2004) were made for several submergences and several slopes.

The physical study treated in section 4.2 has shown that the breaker type gets better when the submergence is larger than 0.12 m and when the wave height is larger than

0.10 m; it also shows that a submergence of 1.60 m (prototype scale) gives, in most cases, still a good breaking wave for the design wave height of 1.50 m.

To confirm these results, numerical simulations in prototype scale were made for three different wave heights and, to confirm the slope of 1:10, several slopes were also tested with COBRAS-UC. The design wave has a 1.5 m wave height and a period of 9 s, as referred before. These conditions provide the input values for the geometry that is tested in the 2DH simulations. Numerical simulations were conducted and results are shown in chapter 6.

4.3.1 NUMERICAL MODEL

By taking the RANS equations, Liu *et al*. (1999) presented a two-dimensional, in the vertical plane, numerical model COBRAS, to describe the flow inside and outside coastal structures. Hsu *et al*. (2002) extended the preliminary model by including a set of volume-averaged k-ε turbulence balance equations. The movement of free surface is tracked by the Volume of Fluid (VOF) method. COBRAS-UC is a new version of the model developed at the University of Cantabria in order to overcome some of the initial limitations and especially to convert it into a tool for practical application. Most of these modifications in the new version COBRAS-UC have been founded on the extensive validation work carried out for low-crested structures (Garcia *et al*., 2004; Losada *et al*., 2005, and Lara *et al*., 2006a) and wave breaking on permeable slopes (Lara *et al*., 2006b) carried out with the model. The improvements cover the wave generation process; code updating and refactoring; optimization and improvement of the main subroutines; improvement of input and output data definition and the development of a graphical user interface and output data processing programs, Losada *et al*. (2008).

4.3.2 SIMULATIONS

4.3.2.1 THE HEIGHT OF THE REEF

The height of the reef is the first parameter to be investigated because the first thing that has to be known is the length of the reef in order to guarantee that it is enough to get the wished breaker type. Two reef heights, *h_reef* (Figure 4.14) have been tested at first:

- *h_reef* = 1.90 m, like in the physical experiments,
- *h_reef* = 3.90 m, a little higher than in the physical experiments in order to have a broader range of heights.

As referred before, the submergence is 1.50 m and the slope of the reef has been chosen 1:10. Figure 4.14 shows the geometry tested and Table 4.4 presents the geometry parameters and the wave conditions. $L_{initial}$ is the wavelength at the source.
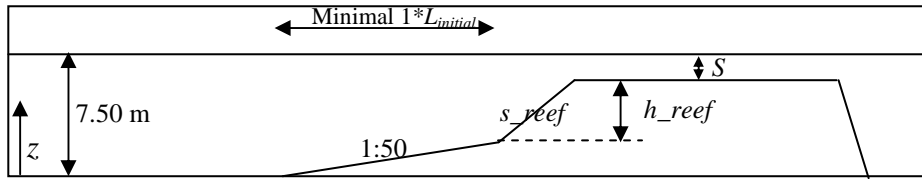
Figure 4.14 - Height of the reef: Geometry tested.

Table 4.4 - Height of the reef: Geometry parameters and wave conditions.

h_reef (m)	s_reef	S (m)	H (m)	T (s)
1.90				
	1:10	1.50	1.50	9
3.90				

From Figure 4.15 and Figure 4.16, it can be seen that with h_reef 1.90 m a spilling break is formed and with a reef height of 3.90 m a plunging break is formed. Since for surfing a plunging break is preferred, a third simulation is conducted in order to be able to see if a plunging break can be got with a smaller height, namely 3.20 m. The results of the breaker shape are shown in Figure 4.17.

Figure 4.17 shows that still a plunging break is formed with a height of the reef of 3.20 m. Because of that, a height of 3.20 m is chosen as the value for the height of the reef to use in the 2DH simulations in chapter 6. A height of 3.20 m means a length of the reef of 32 m; this value is about half the wavelength at the start of the reef, L_{begin_reef} (59 m). So a length of the reef of 0.5*L_{begin_reef} is assumed to be the minimal value that is necessary to form a surfable wave.

Figure 4.15 - Wave shape on the reef with a height of 1.90 m (after 62 s, wave 3).

Figure 4.16 - Wave shape on the reef with a height of 3.90 m (after 62 s, wave 3).

Figure 4.17 - Wave shape on the reef with a height of 3.20 m (after 62 s, wave 3).

Figure 4.18 shows the calculated wave height, H_m, in several points on the reef for all three tested reef heights, in prototype scale. Figure 4.19 shows the corresponding values of the breaker height (H_b), the breaker height divided by the offshore wave height (H_b/H_0) and the breaker parameter H_b/h_b. From these two figures, it can be seen that all breaker heights H_b and all relations H_b/H_0 are almost the same. The breaking point is like in the physical experiments more seawards in case of the lower reef.

It was expected that the higher the reef would be the higher the parameter H_b/h_b would be, as this value is higher for a relatively large slope than for a relatively small slope (Komar, 1998), and the large slope is longer experienced when the height of the reef is larger. Figure 4.19 shows that H_b/h_b is significantly larger for the reef with a height of 3.20 m than the one with a height of 1.90 m. The value for a reef with a height of 3.90 m is again somewhat smaller, but not much.
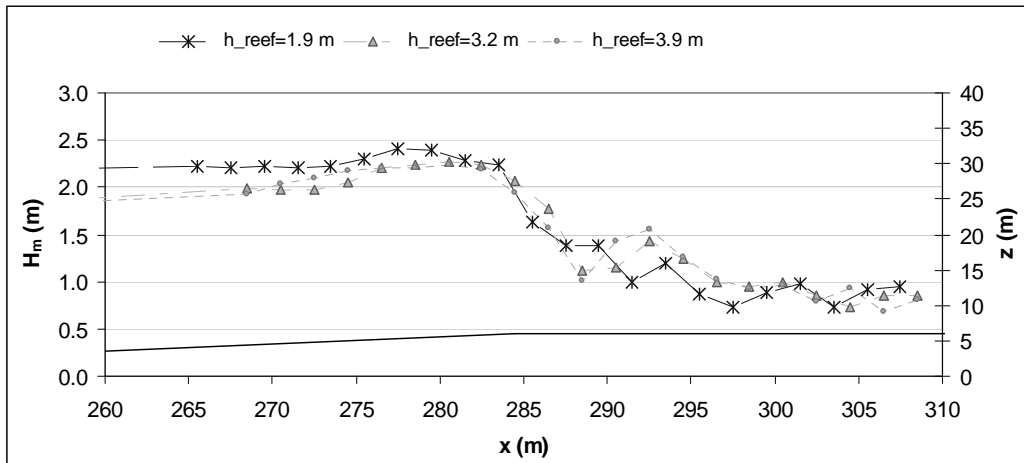
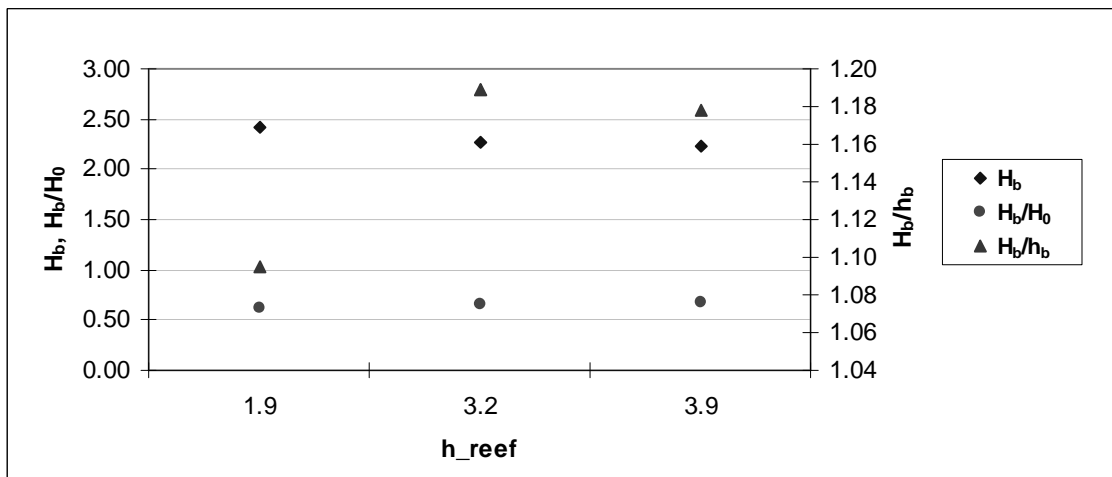Figure 4.18 - Height of the reef: Wave height development on the reef.

Figure 4.19 - Influence of *h_reef* on the values of H_b, H_b/H_0 and H_b/h_b.

4.3.2.2 THE SLOPE OF THE REEF

The slope of the reef, *s_reef*, is the second parameter that will be investigated, because, by safety reasons, the submergence of the reef is restricted to certain values. The geometry and the wave conditions are shown in Figure 4.20 and Table 4.5. Figure 4.21 to Figure 4.24 show the shape of the breaking wave for these four cases.
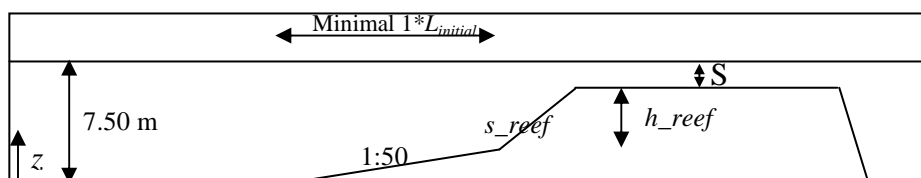

Figure 4.20 - Slope of the reef: Geometry tested.

Table 4.5 - Slope of the reef: Geometry parameters and wave conditions.

s_reef	h_reef (m)	S (m)	H (m)	T (s)
1:6				
1:10	3.20	1.50	1.50	9
1:14				
1:18				

Figure 4.21 - Wave shape on the reef with a slope of 1:6 (after 62 s, wave 3).

Figure 4.22 - Wave shape on the reef with a slope of 1:10 (after 62 s, wave 3).

Figure 4.23 - Wave shape on the reef with a slope of 1:14 (after 91 s, wave 6).

Figure 4.24 - Wave shape on the reef with a slope of 1:18 (after 62 s, wave 3).

Figure 4.21 shows that a breaker shape close to surging is formed with a slope of 1:6. Figure 4.22 and Figure 4.23 show that a plunging, surfable wave is formed with both slope of 1:10 and 1:14. Figure 4.24 shows that a spilling break is formed and tries to break like plunging at first but is not able to. From the results that are shown in Figure 4.21 to Figure 4.24 it can be drawn the conclusion that indeed the wave should experience a slope between 1:10 and 1:14, like found in chapter 3. Because of that, a slope of the three-dimensional reef that will be tested in 2DH (Chapter 6) is 1:10. Figure 4.25 shows the wave height in several points on the reef for all four tested slopes. Figure 4.26 shows the values of the breaker height (H_b), the breaker height divided by the offshore wave height (H_b/H_0) and the breaker parameter H_b/h_b. From these two figures it can be seen that all breaker heights H_b and all relation values of H_b/H_0 are almost the same. However, the breaking point goes away from the top of the reef the

larger the slope gets. The breaker parameter H_b/h_b decreases when the slope of the reef gets smaller. So these data confirm the results of Komar (1998) that the factor H_b/h_b grows when the slope gets relatively larger.
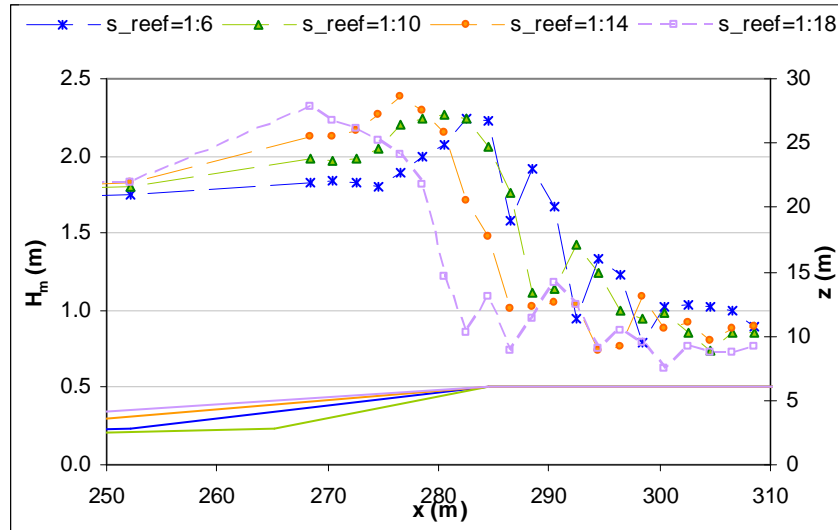

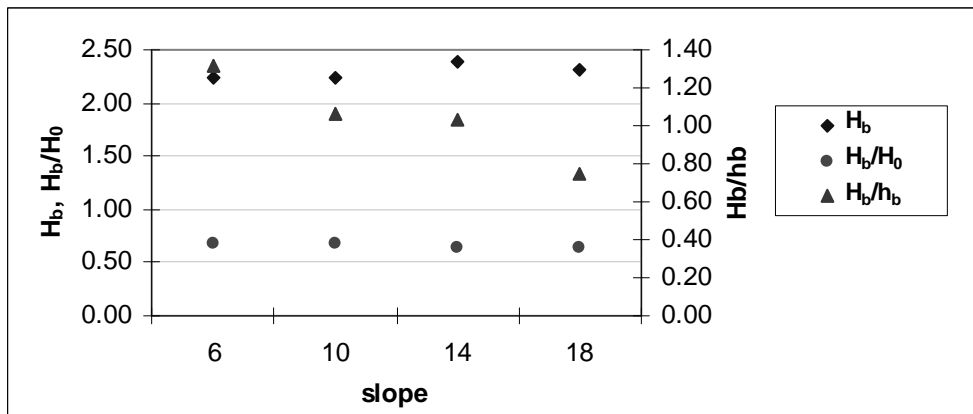Figure 4.25 - Slope of the reef: Wave height development on the reef.

Figure 4.26 - Influence of *s_reef* on the values of H_b, H_b/H_0 and H_b/h_b.

4.3.2.3 THE SUBMERGENCE OF THE REEF

The submergence of the reef, *S*, is the third parameter that is investigated. In contradiction to the previous two cases, the initial height, *h_init*, varies in these simulations. The geometry and the wave conditions are shown in Figure 4.27 and Table 4.6. Figure 4.28 to Figure 4.31 show the shape of the breaking wave for these four cases.
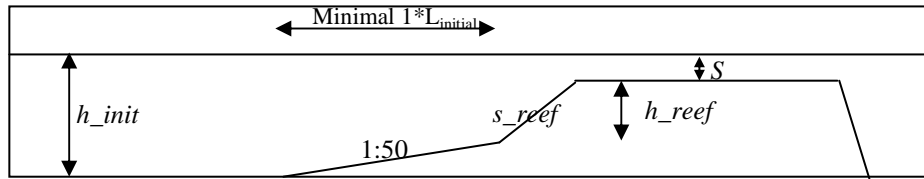
Figure 4.27 - Submergence of the reef: Geometry tested.

Table 4.6 - Submergence of the reef: Geometry parameters and wave conditions.

S (m)	h_init (m)	h_reef (m)	s_reef	H (m)	T (s)
0.8	6.8				
1.2	7.2				
1.5	7.5	3.20	1:10	1.50	9
2.0	8.0				

Figure 4.28 - Wave shape on the reef with a submergence of 0.8 m (after 63 s, wave 3).

Figure 4.29 - Wave shape on the reef with a submergence of 1.2 m (after 63 s, wave 3).

Figure 4.30 - Wave shape on the reef with a submergence of 1.5 m (after 63 s, wave 3).

Figure 4.31 - Wave shape on the reef with a submergence of 2.0 m (after 63 s, wave 3).

The wave shape with a submergence of 1.50 m still seems very good; so concerning both the wave shape and the safety, a submergence equal to the design wave height is chosen. Figure 4.32 shows the wave height in several points on the reef for all four tested submergences. Figure 4.33 shows the values of the breaker height (H_b), the breaker height divided by the initial wave height (H_b/H_0) and the breaker parameter H_b/h_b. Figure 4.32 shows clearly that the breaking point goes more towards the end of the shore as the submergence gets smaller. This is exactly like expected. Figure 4.33 shows that the factor H_b/h_b is almost the same for all tested submergences.
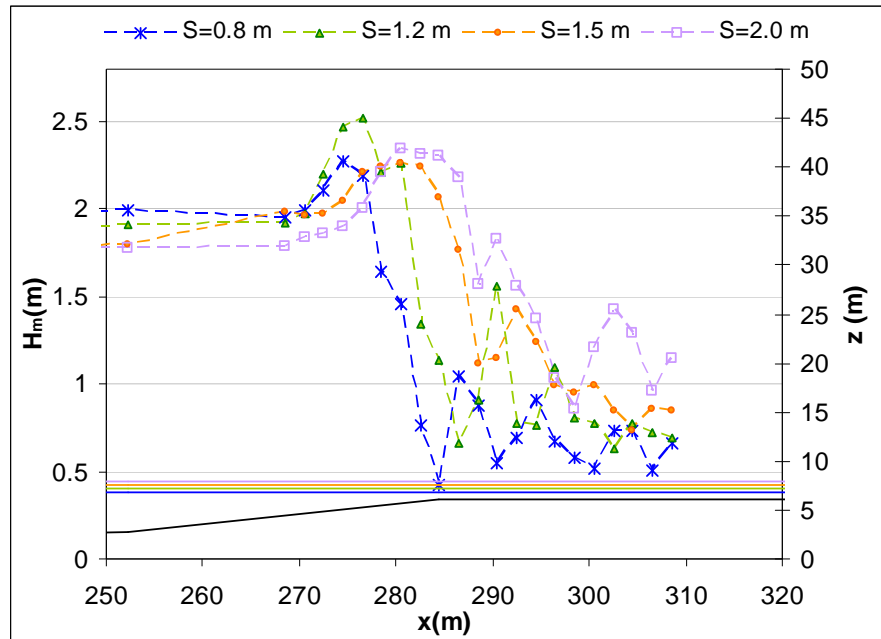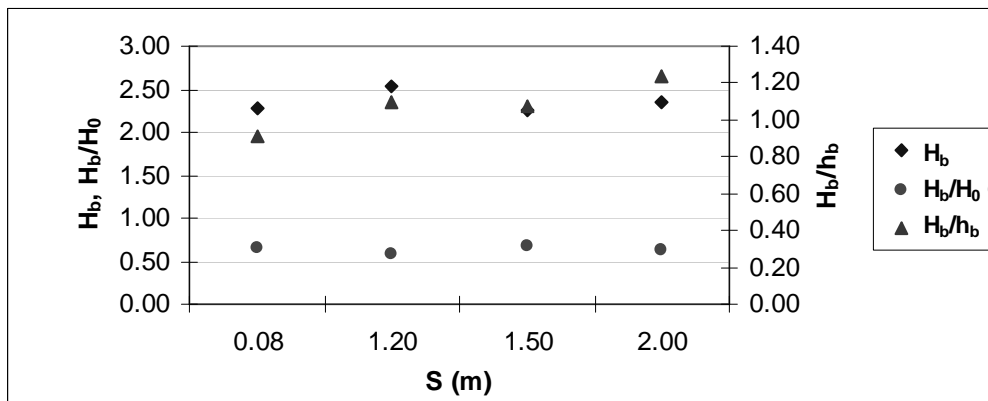
Figure 4.32 - Submergence of the reef: Wave height development on the reef.

Figure 4.33 - Influence of S on the values of H_b, H_b/H_0 and H_b/h_b.

4.4 CONCLUSION

From both physical and numerical 2DV simulations related to the breaker type, it can be concluded that, for the wave condition tested, the design wave height of 1.50 m will give a good surfing wave for a submergence of 1.50 m. From the numerical tests, initial values of several parameters for the simulations in 2DH, carried out in chapter 6 'Optimal geometry of the multi-functional artificial reef', were determined: the height of the reef will be 3.20 m, the seaward slope will be 1:10 and the submergence will be equal to the design wave height of 1.50 m.

Chapter 5 Numerical Model COULWAVE

5. NUMERICAL MODEL COULWAVE

5.1 INTRODUCTION

The knowledge of the characteristics of the flow associated with currents and surface waves, as well as its dependence to the bathymetry and the geometry of the coast, is important in the design of coastal protection structures like groins, breakwaters and artificial reefs.

Until around 1980 linear models were used to simulate the effect of refraction produced by the variation of the depth in the direction of the propagation of the wave and to simulate the effect of diffraction produced by the gradient of the amplitude along the crest of the wave. However, as they are based on the linear theory, those models should not be used in shallow water.

Several factors have contributed to the possibility of using more complete and complex mathematical models nowadays. Not only did our theoretical knowledge of the involved physical phenomena evolved, but also the numerical methods are used more efficiently nowadays. Above all, since the beginning of the 1980s, a significant growth of the processing capacities and storage of great volumes of information took place.

In the first phase the models of the Saint-Venant type were mostly used. However, in shallow water conditions and for certain types of waves, models based on non-dispersive theories, of which the model of the Saint-Venant is an example, are limited. They do, in general, not give good results for long periods of analysis. Besides that in real applications, it is important to have in consideration the effects of the gravity waves, inclusive the processes of refraction, diffraction, reflection, swelling and breaking of the waves, as well as the wave-wave and wave-current interaction processes. The models of the Saint-Venant are limited and are not usually able to compute satisfactory results over long periods of analysis.

Only models of order μ^2 (μ = wavenumber times depth (kh), in which h is the water depth and $k = 2\pi/L$, is the wavenumber, being L the wavelength) or greater, of the Boussinesq or Serre types, are capable to reproduce the nonlinear and dispersive effects resultanting from the propagation of waves in shallow water conditions with enough accuracy. The conventional Boussinesq equations (Peregrine, 1967), which make use of a quadratic polynomial approximation for the vertical flow distribution, have two major constraints: (1) The depth-averaged model poorly describes the frequency dispersion of wave propagation in intermediate depths, and (2) the weakly nonlinear assumption limits the largest wave height that can accurately be modeled. These constraints are consistent with the fundamental assumption of the Boussinesq equations, which states that leading order dispersion and nonlinear effects are of the same order and are weak, i.e., $O(\mu_0)^2 = O(\varepsilon_0) \ll 1$, with ε_0 = amplitude over depth (a/h). The dispersive properties of the conventional Boussinesq equations have been improved by modifying

the dispersive terms (Madsen *et al.*,1992) or using a reference velocity at a specified depth (Nwogu, 1993). These techniques yield a set of equations whose linear dispersion relation can be adjusted such that the resulting intermediate-depth dispersion characteristics are close to those of linear wave theory. Liu (1994) and Wei *et al*. (1995) extended Nwogu's approach to highly nonlinear waves, developing models that not only can be applied to intermediate water depth but also are capable of simulating wave propagation with strong nonlinear interaction, i.e. $\varepsilon_0 = O(1)$. In general, these mathematical model contain accurate linear dispersion properties to $kh \approx 3$. In intermediate depths, nonlinear properties tend to exhibit larger relative errors than linear properties (Madsen *et al.*, 1998), although additional enhancements can indeed create accurate nonlinear characteristics to near the linear accuracy limit, $kh \approx 3$ (Kennedy *et al.*, 2000). Further enhancing the deep water accuracy of the depth-integrated approach is the so-called high-order Boussinesq-type equations. These high-order models use fourth, and higher, order polynomial approximations. Gobbi *et al.* (2000) used a fourth-order polynomial and developed a model with excellent linear dispersive properties up to $kh \approx 6$. Nonlinear behavior was faithfully captured to $kh \approx 3$. With the drastic improvement in accuracy over previous model equations comes a significant computational increase as well. The fourth-order polynomial employed results in fifth-order spatial derivatives in an extremely complex equation system, requiring an equally complex numerical scheme. Madsen *et al.* (1998) and Agnon *et al.* (1999) derived model equations with even higher order polynomial approximations. The highest order of spatial differentiation in these model equations increases linearly with the order of the polynomial approximation. Additionally, the complexity increases again for a two-horizontal dimension (2HD) problem, for which no high-order modeling attempts have yet been made.

All these developments have the objective to extend the application of classical Boussinesq type models to the propagation of waves from intermediate waters till the breaking zone. In this thesis, the Boussinesq-type model COULWAVE is used. This model uses, for relative high *kh* numbers, a different approach to obtain a high-order spatial approximation for the vertical distribution of the flow field; two quadratic polynomials are used, matched at an interface that divides the water column in two layers.

The model consists of a set of equations, derived by piecewise integration of the primitive equations of motion through an arbitrary number, N, of layers. Within each layer, an independent velocity profile is determined. With N separate velocity profiles, matched at the arbitrary interface of the layers, the resulting set of equations will have 2N-1 free parameters, allowing for an optimization with known analytical properties of water waves. The one-layer model is equivalent to the well-studied "extended"

Boussinesq model, which is accurate up to $kh = 3$. The optimized two-layer model shows good linear behavior up to a kh of 8, while second-order nonlinear behavior is well-captured to kh values near 6.

The multi-layer concept has been attempted previously by Kanayama *et al.* (1998), although the derivation and final model equations are quite different from those used in COULWAVE. Green & Naghdi's (1976) approach is often termed "directed fluid sheets", however there is also little similarity to the method used in COULWAVE. Their approach employs an arbitrary number of vertical shape functions to describe the vertical profile of the flow field. All of the shape functions exist throughout the entire water column, which is different from the piecemeal matching of vertical profile segments done in COULWAVE. Internal and stratified flow modelers often employ a multi-layering concept, although the layers are always layers of different density and thus represent a different physical problem than the one used in COULWAVE. See Lynett *et al.* (2002) about details of the multi-layer used in the model..

A high-order, predictor-corrector, finite-difference numerical algorithm is developed for the one- and two-layer models. Included in the numerical code is a parameterization of bottom friction and wave breaking (see section 5.4.1 and 5.4.2), as well as a moving boundary scheme to simulate wave runup and rundown (see section 5.4.3).

Considering one layer only, the corresponding mathematical and numerical models that are the base of the model COULWAVE are presented in section 5.2 and 5.3. See Lynett *et al.* (2002) for details about the two-layer mathematical model.

5.2 MATHEMATICAL MODEL FOR ONE-LAYER

Defining the parameters $S_1 = \nabla . u_1$ and $T_1 = \nabla . (h\,u_1) + (1/\varepsilon)(\partial h/\partial t)$, the model uses the following approach for the continuity equation (calculation of the values of ς), in non-dimensional variables (Lynett and Liu, 2002):

$$\frac{1}{\varepsilon}\frac{\partial h}{\partial t} + \frac{\partial \varsigma}{\partial t} + \nabla . \left[(\varepsilon\varsigma + h)u_1\right]$$

$$- \mu^2 \nabla . \left\{ \left[\frac{\varepsilon^3\varsigma^3 + h^3}{6} - \frac{(\varepsilon\varsigma + h)k_1^2}{2}\right]\nabla S_1 + \left[\frac{\varepsilon^2\varsigma^2 - h^2}{2} - (\varepsilon\varsigma + h)k_1\right]\nabla T_1 \right\} \quad (1)$$

$$= O(\mu^4)$$

where $\nabla = (\partial/\partial x, \partial/\partial y)$ the horizontal gradient vector , $h =$ water depth, $\varsigma =$ surface elevation, $t =$ time, $u_1 =$ horizontal velocity vector, $\varepsilon =$ wave number times depth and $\mu =$ amplitude divided by depth, $k_1 = \alpha_1 h + \beta_1 \varsigma$, α_1 and β_1 are the coefficients to be defined by the user. The index 1 means one-layer model.

For the equation of conservation of momentum, also in non-dimensional variables, the following approach is decided (calculation of the components of the velocity).

$$\frac{\partial u_1}{\partial t} + \varepsilon u_1.\nabla u_1 + \nabla\varsigma + \mu^2\frac{\partial}{\partial t}\left\{\frac{k_1^2}{2}\nabla S_1 + k_1\nabla T_1\right\}$$
$$+ \varepsilon\mu^2\left[(u_1.\nabla k_1)\nabla T_1 + k_1\nabla(u_1.\nabla T_1) + k_1(u_1.\nabla k_1)\nabla S_1 + \frac{k_1^2}{2}\nabla(u_1.\nabla S_1)\right]$$
$$+ \varepsilon\mu^2\left[T_1\nabla T_1 - \nabla\left(\varsigma\frac{\partial T_1}{\partial t}\right)\right] + \varepsilon^2\mu^2\nabla\left(\varsigma S_1 T_1 - \frac{\varsigma^2}{2}\frac{\partial S_1}{\partial t} - \varsigma u_1.\nabla T_1\right) \tag{2}$$
$$+ \varepsilon^2\mu^2\nabla\left[\frac{\varsigma^2}{2}\left(S_1^2 - u_1.\nabla S_1\right)\right] = O(\mu^4)$$

The horizontal velocity is given by:

$$U_1 = u_1 - \mu^2\left\{\frac{z_1^2 - k_1^2}{2}\nabla S_1 + (z_1 - k_1)\nabla T_1\right\} + O(\mu^4)$$

with $z_1 = -0.531h$.

This one-layer model, often referred to as the "fully nonlinear, extended Boussinesq equations" in the literature (e.g. Wei & Kirby, 1995), has been examined and applied to a significant extent. The weakly nonlinear version of (1) and (2) (i.e. assuming $O(\varepsilon) = O(\mu^2)$, thereby neglecting all nonlinear dispersive terms) was first derived by Nwogu (1993).

Nwogu, through linear and first-order nonlinear analysis of the equation model, recommended that $z_1 = -0.531h$, and that value has been adopted by other researchers using these equations. Nwogu's model was extended to "full nonlinearity" by Liu (1994) and Wei *et al.* (1995). There are some discrepancies between Liu's and Wei & Kirby's derived equations, which can be attributed to a neglect of some nonlinear dispersive terms in Wei & Kirby (Hsaio & Liu, 2002). The above one-layer equations (1) and (2) are identical to those derived by Liu (1994).

5.3 NUMERICAL MODEL FOR ONE-LAYER

A finite difference algorithm is used for the general one- and two-layer model equations. The structure of the present numerical model is similar to those of Wei & Kirby (1995) and Wei *et al.* (1995). Differences between the model presented here, for the one-layer system, and that of Wei *et al.* exist in the added terms due to a time-dependant water depth and the numerical treatment of some nonlinear dispersive terms. The equations are solved utilizing a high-order predictor-corrector scheme, employing a

third order in time explicit Adams-Bashforth predictor step, and a fourth order in time Adams-Moulton implicit corrector step (Press *et al.*, 1989). The implicit corrector step must be iterated until a convergence criterion is satisfied. The equations (1) and (2) are dimensionalised for the numerical model, the dimensional equations are equivalent to the non-dimensional ones with $\varepsilon = \mu = 1$ and the addition of gravity, g, to the coefficient of the leading order free surface derivative in the momentum equation.

To simplify the predictor-corrector equations, the velocity time derivatives in the momentum equations are grouped into the dimensional form:

$$U = u + \frac{k^2 - \varsigma^2}{2} u_{xx} + (k - \varsigma)(hu)_{xx} - \varsigma_x\left[\varsigma u_x + (hu)_x\right] \tag{3}$$

$$V = v + \frac{k^2 - \varsigma^2}{2} v_{yy} + (k - \varsigma)(hv)_{yy} - \varsigma_y\left[\varsigma v_y + (hv)_y\right] \tag{4}$$

where subscripts denote partial derivatives. For reasons of stability and less iterations required in the process of convergence, the nonlinear time derivatives, arisen from the nonlinear dispersion terms $\nabla\left[\varsigma(\nabla.(hu_\alpha)_t + h_{tt}/\varepsilon)\right]$ and $\nabla\left[(\varsigma^2/2)\nabla.u_{\alpha t}\right]$, can be reformulated using the relation:

$$\nabla\left[\varsigma\left(\nabla.(hu_\alpha)_t + \frac{h_{tt}}{\varepsilon}\right)\right] = \nabla\left[\varsigma\left(\nabla.(hu_\alpha) + \frac{h_t}{\varepsilon}\right)\right]_t - \nabla\left[\varsigma_t\left(\nabla.(hu_\alpha) + \frac{h_t}{\varepsilon}\right)\right]$$

$$\nabla\left(\frac{\varsigma^2}{2}\nabla.u_{\alpha t}\right) = \nabla\left(\frac{\varsigma^2}{2}\nabla.u_\alpha\right)_t - \nabla(\varsigma\varsigma_t\nabla.u_\alpha) \tag{5}$$

The predictor equations are:

$$\varsigma_{i,j}^{n+1} = \varsigma_{i,j}^n + \frac{\Delta t}{12}\left(23E_{i,j}^n - 16E_{i,j}^{n-1} + 5E_{i,j}^{n-2}\right) \tag{6}$$

$$U_{i,j}^{n+1} = U_{i,j}^n + \frac{\Delta t}{12}\left(23F_{i,j}^n - 16F_{i,j}^{n-1} + 5F_{i,j}^{n-2}\right) + 2\left(F_1\right)_{i,j}^n - 3\left(F_1\right)_{i,j}^{n-1} + \left(F_1\right)_{i,j}^{n-2} \tag{7}$$

$$V_{i,j}^{n+1} = V_{i,j}^n + \frac{\Delta t}{12}\left(23G_{i,j}^n - 16G_{i,j}^{n-1} + 5G_{i,j}^{n-2}\right) + 2\left(G_1\right)_{i,j}^n - 3\left(G_1\right)_{i,j}^{n-1} + \left(G_1\right)_{i,j}^{n-2} \tag{8}$$

where

$$E = -h_t - \left[(\varsigma + h)u\right]_x - \left[(\varsigma + h)v\right]_y$$
$$+ \left\{(\varsigma + h)\left[\left(\frac{1}{6}(\varsigma^2 - \varsigma h + h^2) - \frac{1}{2}k^2\right)S_x + \left(\frac{1}{2}(\varsigma - h) - k\right)T_x\right]\right\}_x$$
$$+ \left\{(\varsigma + h)\left[\left(\frac{1}{6}(\varsigma^2 - \varsigma h + h^2) - \frac{1}{2}k^2\right)S_y + \left(\frac{1}{2}(\varsigma - h) - k\right)T_y\right]\right\}_y$$

$$F = -\frac{1}{2}\left[\left(u^2\right)_x + \left(v^2\right)_x\right] - g\varsigma_x - kh_{xtt} - k_t h_{xt}$$
$$+ \left(Eh_t + \varsigma\, h_{tt}\right)_x - \left[E\left(\varsigma\, S + T\right)\right]_x - \left[\frac{1}{2}\left(k^2 - \varsigma^2\right)\left(uS_x + vS_y\right)\right]_x$$
$$- \left[\left(k - \varsigma\right)\left(u\, T_x + v\, T_y\right)\right]_x - \frac{1}{2}\left[\left(T + \varsigma\, S\right)^2\right]_x$$

$$F_1 = \frac{\varsigma^2 - k^2}{2} v_{xy} - \left(k - \varsigma\right)\left(hv\right)_{xy} + \varsigma_x\left[\varsigma\, v_y + \left(hv\right)_y\right]$$

$$G = -\frac{1}{2}\left[\left(u^2\right)_y + \left(v^2\right)_y\right] - g\varsigma_y - kh_{ytt} - k_t h_{yt}$$
$$+ \left(Eh_t + \varsigma\, h_{tt}\right)_y - \left[E\left(\varsigma\, S + T\right)\right]_y - \left[\frac{1}{2}\left(k^2 - \varsigma^2\right)\left(uS_x + vS_y\right)\right]_y$$
$$- \left[\left(k - \varsigma\right)\left(u\, T_x + v\, T_y\right)\right]_y - \frac{1}{2}\left[\left(T + \varsigma\, S\right)^2\right]_y$$

$$G_1 = \frac{\varsigma^2 - k^2}{2} u_{xy} - \left(k - \varsigma\right)\left(h\, u\right)_{xy} + \varsigma_y\left[\varsigma\, u_x + \left(h\, u\right)_x\right]$$

and

$$S = u_x + v_y \qquad T = h_t + \left(hu\right)_x + \left(hv\right)_y$$

All first order spatial derivatives are differenced with fourth order ($\Delta x^4 = \Delta y^4$) accurate equations, which are five-point differences. Second order spatial derivatives are approximated with three-point centered finite difference equations, which are second order accurate.

The fourth-order implicit corrector expressions for the free surface elevation, ς, and horizontal velocities, u and v, are:

$$\varsigma_{i,j}^{n+1} = \varsigma_{i,j}^{n} + \frac{\Delta t}{24}\left(9E_{i,j}^{n+1} + 19E_{i,j}^{n} - 5E_{i,j}^{n-1} + E_{i,j}^{n-2}\right) \tag{9}$$

$$U_{i,j}^{n+1} = U_{i,j}^{n} + \frac{\Delta t}{24}\left(9F_{i,j}^{n+1} + 19F_{i,j}^{n} - 5F_{i,j}^{n-1} + F_{i,j}^{n-2}\right) + \left(F_1\right)_{i,j}^{n+1} - \left(F_1\right)_{i,j}^{n} \tag{10}$$

$$V_{i,j}^{n+1} = V_{i,j}^{n} + \frac{\Delta t}{24}\left(9G_{i,j}^{n+1} + 19G_{i,j}^{n} - 5G_{i,j}^{n-1} + G_{i,j}^{n-2}\right) + \left(G_1\right)_{i,j}^{n+1} - \left(G_1\right)_{i,j}^{n} \tag{11}$$

The system is solved by first evaluating the predictor equations, then u and v are solved via (3) and (4), respectively. Both (3) and (4) yield a diagonal matrix after finite differencing. The matrices are diagonal, with a bandwidth of three (due to three-point finite differencing), and the efficient Thomas algorithm can be utilized. At this point in the numerical system, we have predictors for ς, u and v. Next, the corrector expressions are evaluated, and again u and v are determined from (3) and (4). The error

is calculated, in order to determine if the implicit correctors need to be reiterated. The error criteria employed is a dual calculation, and requires that either

$$max \left| \frac{w^{n+1} - w_*^{n+1}}{w^{n+1}} \right| < \frac{\varepsilon}{100} \quad \text{or} \quad \frac{\sum \left| w^{n+1} - w_*^{n+1} \right|}{\sum \left| w^{n+1} \right|} < \varepsilon \tag{12}$$

In these expressions w represents any of the variables ς, u and v., and w_* is the previous iterations value. The value of the error is set to 10^{-6}.

Linear stability analysis performed by Wei (1995), Hsiao (2000) and Woo (2002) show that $\Delta t < \Delta x / (2c)$ to ensure stability, where c is the celerity.

5.4 ENERGY DISSIPATION MECHANISMS

Two forms of physical dissipation are considered in the numerical model, wave breaking and bottom friction. These mechanisms modify the momentum equation:

$$\frac{\partial u_1}{\partial t} + ... + \boldsymbol{R}_f - \boldsymbol{R}_b = 0 \tag{13}$$

where $\boldsymbol{R}_f$ accounts for bottom friction dissipation and $\boldsymbol{R}_b$ for wave breaking. The evaluation of these two additional terms are discussed in 5.4.1 and 5.4.2.

5.4.1 BOTTOM FRICTION

Bottom friction is described in the quadratic form:

$$\boldsymbol{R}_f = \frac{f}{H} \boldsymbol{u}_b / \boldsymbol{u}_b / \tag{14}$$

where f is a bottom friction coefficient, typically in the range of 10^{-3} to 10^{-2} (e.g. Whitfor and Thorton, 1996; Kobayashi *et al.*, 1997), depending on the Reynolds number and seafloor condition, $H = h + \zeta$ is the total water depth, and $\boldsymbol{u}_b$ is the horizontal velocity at the seafloor.

The above expression (14) has been utilized in similar models (e.g. Chen *et al.*, 1999) and has a direct correlation to the Chezy coefficient, C. This relationship is:

$$f = \frac{g}{C^2} \tag{15}$$

where g is gravity.

5.4.2 WAVE BREAKING MODEL

One of the most significant obstacles in the way of developing a practical numerical model with depth-integrated equations is wave breaking. There exist three reasons that constitute major problems with wave breaking in depth-integrated models (Lynett, 2002):

- A depth-integrated model, by definition, can only have a single elevation value of the water-air interface at any horizontal coordinate, and thus phenomena such as wave overturning cannot be simulated.

- Along the same lines, very strong horizontal vorticity typically accompanies breaking, which an irrotational or weakly rotational model will not capture.

- Most depth-integrated derivations use as an initial assumption inviscid flow (those in this thesis included), and therefore do not have any means to dissipate energy.

The first reason given, that of the impossibility of simulating wave-overturning, is the only unapproachable one of the three. Thus, it will always be necessary to parameterize the large-scale features of wave breaking when using depth-integrated equations. Two distinct approaches to simulating the effects of wave breaking with depth integrated models exist: numerical dissipation and ad-hoc addition of dissipative terms to the momentum equation. Numerical dissipative approaches most notably include shock capturing schemes. In these schemes, energy dissipation is related to the local smoothness of the solution, which is of course strongly related to the gridlength near the shock. Most recently, Li and Raichlen (2002) used the weighted essentially non-oscillatory shock capturing scheme, adapted from gas dynamics research, to model solitary wave run-up. The results presented in Li and Raichlen are excellent, among the best numerical-experimental comparisons to date. With shock capturing methods, the numerical results tend to be very smooth. However, the dissipation is entirely numerical, and although the general form of the dissipative terms may be of the proper physical form, the dissipation will inevitable be related to the grid length and time step. Utilizing post-derivation-added dissipation terms to the momentum equation removes this dissipative dependence on numerical parameters. However, these added terms are ad-hoc terms, and will contain coefficients that must be obtained based on comparison with experiment. Whether the numerical or ad-hoc approach is more desirable will depend entirely on the individual preference of the researcher. In this thesis, the addition of ad-hoc dissipation terms is employed, as it is of simple implementation and efficient to avoid numerical dissipative and dispersive enhancements/errors whenever possible.

Breaking Scheme and Validation

The breaking scheme employed in this work closely follows the scheme presented in Kennedy *et al*. (2000). Description of this particular breaking scheme can also be found in Chen *et al*. (2000), which is a companion paper to Kennedy *et al*. The scheme is developed from an "eddy viscosity" approach, where a user defined formulation for an eddy viscosity is developed based on agreement with experimental data. The eddy viscosity is part of a momentum conserving ad-hoc dissipative term $\boldsymbol{R}_b = R_{bx}\boldsymbol{i} + R_{by}\boldsymbol{j}$. R_{bx} and R_{by} are computed by (see also Lynett, 2002):

$$R_{bx} = \frac{1}{H}\left\{\left[\nu(Hu_1)_x\right]_x + \frac{1}{2}\left[\nu(Hu_1)_y + \nu(Hv_1)_x\right]_y\right\} \tag{16}$$

$$R_{by} = \frac{1}{H}\left\{\left[\nu(Hv_1)_y\right]_y + \frac{1}{2}\left[\nu(Hv_1)_x + \nu(Hu_1)_y\right]_x\right\} \tag{17}$$

where $\nu = BH\varsigma_t$ is the viscosity, being B a variable that ensures a smooth transition between breaking and non-breaking states, and $H = h + \zeta$, is the total water depth.

For the few differences between the breaking model of Kennedy *et al*. (2000) and the model used in COULWAVE, see Lynett (2002).

5.4.3 SIMULATING WAVE RUNUP & RUNDOWN

Wave propagation using depth-integrated equations is now well simulated and understood, but the process of runup and rundown is not. Shoreline boundaries may move significantly under the temporal influence of incident waves. A numerical model should be able to take into account such variations correctly in order to obtain realistic flow patterns. Researchers generally use a fixed grid, finite differences or finite elements methods to solve depth-integrated equations. Using a fixed grid numerical model to solve a moving boundary problem can lead to difficulties related to the loss of mass conservation and instabilities in the computations (Leendertse, 1987) as a result of imposing discrete fixed increments to the extent of wetting and drying areas (Balzano, 1998). To reduce the computational instabilities near the wet-dry interface, some researchers added bottom friction into the momentum equations. However, a numerical model should be stable even without using bottom friction dissipation. Zelt (1991) used a Lagrangian form of the Boussinesq equations to simulate shoreline movement. This model produced maximum runup values that compared well with experimental values, but the shape of the wave as it traveled up the slope did not compare as favorably. A handful of others have utilized Lagragian techniques with depth-integrated equation models to simulate a moving shoreline (e.g., Petera and Nassehi, 1996; Gopalakrishnan, 1989). Another treatment of moving boundary problem is employing a slot or permeable-seabed technique (Tao, 1983). The first application of the permeable slot

with a Boussinesq-type model (Madsen *et al*., 1997) yielded runup errors on the order of ten percent of the maximum. Modifications have been made to this permeable slot technique (Kennedy *et al*., 2000), increasing the accuracy, but it was also shown that the empirical coefficients that govern the technique can not be universally determined, due to numerical stability problems (Chen *et al*., 2000). In this section, a new moving boundary treatment for wave propagation models is presented. The moving boundary algorithm is conceptually simple, easy to implement, and can be employed by different numerical schemes (i.e., finite differences and finite elements) utilizing depth-integrated equations. The moving boundary technique utilizes linear extrapolation near the wet-dry boundary, thereby allowing the real boundary location to exist in-between nodal points. See further Lynett (2002).

Moving Boundary Algorithm

The development of the moving boundary algorithm presented began with a search for a scheme that allows for the wet-dry boundary to exist at any location, not restrictively at a node on a fixed grid (Lynett, 2002). One method of achieving this is through dynamic regridding, using a Lagrangian approach. Methods such as this have been used in finite difference and finite element nonlinear shallow water (NLSW) and Boussinesq equation models (e.g., Petera and Nasshei, 1996; Zelt, 1991). Lagrangian moving boundary techniques require numerical flexibility, in terms of utilizing constantly changing space and time steps, to be implemented in conjunction with a Eulerian-type model. This flexibility is not present in the current numerical scheme, and is difficult to achieve due to the nature of the required high-order derivatives, and so a different approach is developed. Owing to the significant number of derivatives calculated by the one-layer numerical model (~50 in 2DH), it would be advantageous if the moving boundary scheme did not require any sort of special treatment of the derivatives near the wet-dry boundary (i.e., forward, backward, or low order finite differences). To require, for example, directional differences at the boundary leads to abundant conditional statements, making the programming tedious and the runtime longer. Therefore, the five-point centered finite differences that are employed in the numerical model are desired to be used at all locations, including those points near the shoreline, where neighboring nodes may be dry. With this in mind, the moving boundary scheme will employ a linear extrapolation of free surface displacement, ζ, and velocity components, u_1 and v_1, from the fluid domain, through the wet-dry boundary and into the dry region. Kowalik and Bang (1987) presented a similar approach of employing a linear extrapolation into the dry region, based on Sielecki and Wurtele's (1970) earlier developments. Their model uses a leap-frog scheme to approximate the Nonlinear Shallow-Water Wave (NLSW) equations, and is limited to one-dimensional,

non-breaking problems. Lynett (2002) extended this idea to two horizontal dimension breaking problems, using a high-order numerical model. An extrapolation through the wet-dry boundary permits this boundary to exist in-between nodal points. Figure 5.1 gives a numerical example of how the extrapolation is performed in a one-dimensional problem, showing a solitary wave interacting with a 1:20 slope.

Figure 5.1 - Runup and rundown of a solitary wave, where extrapolated nodes are shown by the dots (Lynett, 2002).

The free surface locations that are determined using the one-layer governing equations, (1) and (2), are shown by the solid line, whereas the linearly extrapolated points are shown by the dots. With extrapolated values of ζ and velocity components in the dry region, solving the model equations at wet nodes can proceed. When solving the model equations, five-point centered differences are employed to approximate the spatial derivatives. Although no derivatives are calculated at dry (extrapolated) points, the physical values of free surface and velocity at these points are used to evaluate derivatives at neighboring wet-points. The determination of the location of the wet-dry boundary is performed once per time step, immediately after the predictor step. The moving boundary technique is numerically stable, and does not require any additional dissipative mechanisms. See further Lynett (2002).

5.5 LABORATORY DATA

For both section 5.6, the comparison between the serial and the parallel version, and section 5.7, the calibration, the experimental results of Poort (2007) are used. In this work detailed laboratory measurements of surface elevation and velocities around the reef were conducted. The used bathymetry is shown in Figure 5.2.

Figure 5.2 - Bathymetry of the experimental setup.

All tests were done with bichromatic waves, 1 and 2, and the following wave conditions:

- Water level: 0.40 m;
- Wave height: $H_1 = H_2 = 0.04$ m;
- Frequency of wave 1: $f_1 = 0.4714$ Hz;
- Frequency of wave 2: $f_2 = 0.4086$ Hz.

With a water depth of 0.40 m and the used frequencies, the wavelength of the first wave is 3.95 m and of the second wave is 4.64 m.

5.6 SERIAL AND PARALLEL VERSIONS

5.6.1 INTRODUCTION

Implementations of COULWAVE model to calculate free surface wave evolution in large basins are, in general, computationally very expensive, requiring large amounts of CPU time and memory. For large scale problems, it is either not affordable or practical to run on a single PC. To facilitate such extensive computations, a parallel COULWAVE model was developed by Sitanggang and Lynett (2005) using the domain decomposition technique in conjunction with the message passing interface (MPI). The published and well-tested numerical scheme used by the serial model, a high-order finite difference method, is identical to that employed in the parallel model. Parallelization of the three-diagonal matrix systems included in the serial scheme is the

most challenging aspect of the work, and is accomplished using a parallel matrix solver combined with an efficient data transfer scheme. Numerical tests on a distributed-memory supercomputer showed that the performance of the current parallel model in simulating wave evolution is very satisfactory. A linear speedup is gained as the number of processors increases. The tests showed that the CPU time efficiency of the model is about 75-90% (Sitanggang and Lynett, 2005). COULWAVE is parallelized using the domain decomposition method, where each processor performs the same operations. The parallel algorithm is identical to its serial counterpart, based on an iterative predictor-corrector scheme also requiring a three-diagonal solution for each iteration. The model test indicates that both the validity and the performance of the model are excellent. However, the performance of the model may be further improved if a more efficient parallel three-diagonal solver is employed. Success at parallelizing COULWAVE will allow for large domain simulation which is not possible to run on a single PC due to limited memory size and large computation time. This parallel model provides the future opportunity for large wave-resolving simulations in the nearshore, with global domains of many million of grid points, covering O (100 km^2) and greater basins. Additionally, real-time simulation with Boussinesq equations becomes a possibility.

5.6.2 *APPLICATION OF BOTH THE SERIAL AND PARALLEL VERSIONS*

The input that one has to give to the program is in both the serial and the parallel versions almost the same. In both versions the input grid is interpolated by the program depending of the number of grid points per wavelength that is given as an input. The grid that the program uses is always regular, in the whole domain. The time step is calculated by the value given for the Courant number as an input. The Courant number C_r should always be smaller than 0.5, which is given by:

$$C_r = \frac{dt}{dx}\sqrt{gh}$$
(5.1)

When the option of inserting an internal source is used, the location of the source should be given from the right boundary of the sponge layer. Regarding the wave gauges that record the surface elevation and the velocities in x and y directions at every time step, the position that has to be given is different in the serial and the parallel version. In the parallel version the position of the wave gauges has to be given as the distance from the right boundary of the sponge layer, where, the left boundary of the sponge layer is the left boundary of the grid. In the serial version the position of the wave gauges have also to be given from the right boundary of the sponge layer, however in this version this is the left boundary of the input grid.

In order to compare these two versions regarding the needed CPU time simulations for the geometry in a basin, which will be used for the calibration of COULWAVE in this chapter, have been made. The bathymetries for the serial version and for the parallel version are not exactly the same, because in the serial version the sponge layers are added by the model to the input grid and in the parallel version the sponge layers are put in the input grid by the model. The bathymetry for the parallel version is schematically shown in Figure 5.3 and the bathymetry for the serial version in Figure 5.4. The bathymetry for the parallel version is wider, namely 2 times the width of the sponge layer, one layer at the right and one at the left side. Besides that, the grid for the parallel version is five cells larger around all boundaries, because the five last grid cells at all boundaries of the grid that one uses as input in the program are used as ghost boundary cells to enforce the boundary conditions. The physical wall is put inside these ghost boundary cells. In the serial version this is not the case. More information about the formation of the grid is given in section 5.7.2.

Figure 5.3 - Cross-section A-A in Figure 5.2 for parallel version.

Figure 5.4 - Cross-section A-A in for serial version.

The conditions in the simulations are the same as in the laboratory data of M. Poort (2007), section 5.4). The sponge layer has a width of 1.25 times the smallest wavelength, so this is 4.93 m. The grid size is 0.1975 m, so the 5 ghost cells are together 0.9875 m.

For this thesis a workstation has been used for the simulations. The characteristics of the workstation are CPU – Dual Core AMD Opteron 265 (4 processors), memory – 8 Gb, SPECfp_rate2000 = 54.7. Simulations have been made with both the serial and the

parallel model to investigate the differences in CPU time (see Table 5.1). It has appeared that in the workstation no division in the x-direction could be made (Figure 5.5). Therefore only divisions in the y-direction have been made, like demonstrated in Figure 5.5 (right).

Figure 5.5 - Division in *x*-direction (left), in both directions (middle) and in in y-direction (right), Pr = processor.

Table 5.1 - CPU time needed with both the serial and parallel versions.

	CPU time needed
Serial version	4 hours, 37 min
Parallel version – 1 processor	4 hours, 55 min
Parallel version – 2 processors	2 hours, 33 min
Parallel version – 3 processors	1 hour, 55 min

As can be seen in Table 5.1 the serial version and the parallel version with one processor need around the same amount of CPU time, and it can also be seen that the more the grid is divided in the parallel version the less CPU time is needed. Due to the fact that the parallel version is the most recent version of the code of COULWAVE, it was decided to use the parallel version. Mostly 2 to 3 processors were available to run simulations in the workstation. Table 5.1 shows that it is more interesting to run 3 different simulations at the same time, each one using 1 processor (total time 5 hours), than to run 3 simulations in sequence with 3 processors (total time 6 hours). Because of that, the choice was made to use for the simulations the parallel version without division.

5.7 CALIBRATION

The influence of relevant parameters on wave propagation and breaking will be investigated for the significant wave height. The wave height in different points of the domain for several values of the relevant parameters will be compared with the wave height obtained in the laboratory. As significant wave height is not totally appropriate to analyze a bi-chromatic wave, the spectra will be also compared.
In the parameterizations of the model several parameters can be varied:

I. Bottom friction (see section 5.4.1). Even thought that is written in section 5.4.1 that this parameter typically ranges between 10^{-3} and 10^{-2}, in the model the parameter can be varied between 10^{-4} and 10^{-2}.

II. Fraction of upwinded differences composing convective terms. Value 0 means no upwinding and 1 means fully upwinding. Upwind schemes use an adaptive or solution-sensitive finite difference stencil to numerically simulate more properly the direction of propagation of information in a flow field. The upwind schemes attempt to discretize hyperbolic partial differential equations by using differencing biased in the direction determined by the sign of the characteristic speeds.

III. Yes or no implementing of a wave breaking model (see section 5.4.2). When the wave breaking model is implemented, five parameters in the code of the model can be changed. These parameters are treated in section 5.7.3.

Besides that, an analysis will be done on the influence of the input bathymetry and of the grid on the model results.

5.7.1 BATHYMETRY

A comparison of the bathymetry has been made before and after running the program. Both options smoothing and not smoothing have been selected in two different simulations. Figure 5.6 shows the bathymetry before and after running the program for two values of *y* (see also Figure 5.2 for the location of this *y*-value). The changes in the bathymetry are considered to be unacceptable, as the wave height is 0.04 m and the difference in submergence at the offshore side of the reef is about 0.02 m. Because of that the option 'not smoothing' is chosen. It appeared no stability problems were created due to this choice.

Figure 5.6 - Bathymetry comparisons with and without smoothing option.

5.7.2 GRID MODEL

In the physical experiments (Poort, 2007), the *x*-dimension of the basin is 25 m (see Figure 5.2) and at x = 0 in the basin three piston wave makers, generating uni-

directional shore normal incident waves, were placed in one line and were linked to operate synchronously. For the wave maker there was a second-order wave paddle steering system with no reflection compensation. Behind the wave maker porous rocks were present to diminish reflection of the generated waves.

For the numerical simulations a grid was created with the source at x = 10 m, so the total *x*-dimension of the grid is 35 m (Figure 5.7). The source was situated at x = 10 m in order to have space at the left side of the source for the sponge layer ($1.25 \times L$) and for the wave generation ($1.0 \times L$).

For this calibration it is important to simulate the exact dimensions of the basin as the reef was positioned at one side of the basin against the wall. In order to obtain the simulations with the exact dimensions, the input bathymetry domain was made artificially 5 cells larger at the side boundaries due to the five ghost cells. One grid cell has a dimension of 0.1975 m, so at both sides about 1.0 m was added in the input grid.

Figure 5.7 - Bathymetry for simulations with COULWAVE.

The greater the number of points per wavelength more stable the simulation is. The grid size is determined by dividing the minimum wavelength to the number of grid points. The width of the boundary layer is calculated by 1.25 times the wavelength of the first wavelength that is given as input. In Table 5.2 the estimated CPU time needed is given for several numbers of grid points per wavelengths. The time is rounded to whole hours. The other parameters are all the same.

Table 5.2 - Comparison of CPU time needed for several numbers of grid points per wavelength.

Number of gridpoints per wavelength	CPU time needed
20	5 hours
30	17 hours
40	39 hours
50	80 hours
60	190 hours
70	Program doesn't run

Table 5.2 shows the characteristics of the simulation. For the calibration, a minimum of 20 points per wavelength was chosen to spare simulation time. The grid size is 0.1975. This means that the maximum error in location of a certain gauge for comparison is less than 0.10 m; this value is found acceptable for comparison of the time series.

Table 5.3 - Characteristics of the simulation.

Simulation time	600 s
CPU time needed	4.5 hours
Number of gridpoints per wavelength	20
Courant number	0.10
Grid size	0.1975 m
Time step	0.01 s
Total number of gridpoints	12616

5.7.3 INFLUENCE OF THE PARAMETERS

For the study of the influence of the parameters bottom friction and fraction of upwind differences, one wave gauge from the laboratory data of Poort (2007) shown in Figure 5.8 is selected (coordinates x, y of 21.79, 3.72, respectively). This gauge was chosen, due to its good position to study the influence of the several wave propagation parameters. The acquisition of the surface elevation in the laboratory was done with a frequency of 100 Hz. The value of the significant wave height obtained in the laboratory in this gauge is 0.074 m for the gauge shown in Figure 5.8. For this investigation on the influence of the parameters the one-layer option of the model was selected.

Figure 5.8 - Wave gauge location to investigate the parameters influence.

Preliminary results

Before starting with the investigation of the influence of the parameters, time series and spectrums of the surface elevation and of the velocity in the x-direction measured in laboratory are compared with results of COULWAVE. As a first approximation, simulations were conducted with an eddy viscosity of 0.5, a bottom friction coefficient of 0.01 and an upwind fraction coefficient of 1. In laboratory, the velocity was measured at 0.5 times the water depth; in the model, the velocity is obtained at $z = -0.531*h$. Figure 5.9 compares time series of the surface elevation simulated by COULWAVE with laboratory data. As can be seen, the time series are very close. Figure 5.10 compares the spectrum of these time series. This figure shows that the spectrum is very close. A small difference is that the peaks at both periods are more narrow and higher in the laboratory measurements. However, the position and the energy of the superharmonics is almost the same.

Figure 5.9 - Laboratory and Coulwave time series of surface elevation.

Figure 5.10 - Spectrum of time series shown in Figure 5.9.

Figure 5.11 shows time series comparisons between velocity results of COULWAVE and laboratory data in the x-direction. Aside a small difference between the groups velocity in this gauge, which seem to be greater in the laboratory than in COULWAVE, the general results are acceptable.

Figure 5.11- Time series of the velocity in x-direction for the gauge presented in Figure 5.8.

I. Bottom friction

To investigate the influence of the bottom friction, the values of *f* are varied between 0.0001 and 0.01. The calculated significant wave heights can be seen in Figure 5.12.

Figure 5.12 - Influence bottom friction on the significant wave height.

Figure 5.13 to Figure 5.16 show the energy spectra for the different values of the bottom friction coefficient *f*. From Figure 5.12 it can be seen that the significant wave heights for the several values of the bottom friction in COULWAVE are very close. Figure 5.13 to Figure 5.16 can be seen that the energy spectra of COULWAVE are also almost the same. As can be seen, the energy spectra from the laboratory and from COULWAVE model are similar for all values of the bottom friction with the energy peaks exist at the same frequencies. The only difference is that the energy peak of the smallest frequency is little narrower and higher than as in the laboratory. Because the results are so close, the default value of 0.01 is chosen for the bottom friction for further simulations.

Figure 5.13 - Energy spectrum for bottom friction 0.0001.

Figure 5.14 - Energy spectrum for bottom friction 0.001.

Figure 5.15 - Energy spectrum for bottom friction 0.005.

Figure 5.16 - Energy spectrum for bottom friction 0.01.

II. Fraction upwind differences

To investigate the influence of the fraction upwind differences, the values are varied between 0 and 1. The calculated significant wave heights can be seen in Figure 5.17. Figure 5.18 to Figure 5.22 show the spectra for the different values for the fraction upwind differences.

Figure 5.17 - Influence upwind fraction on the significant wave height.

Figure 5.18 - Energy spectrum for upwind fraction 0.

Figure 5.19 - Energy spectrum for upwind fraction 0.25.

Figure 5.20 - Energy spectrum for upwind fraction 0.5.

Figure 5.21 - Energy spectrum for upwind fraction 0.75.

Figure 5.22 - Energy spectrum for upwind fraction 1.0.

Figure 5.17 shows that the significant wave heights for the several values of the upwind fraction are also very close with a maximum difference of 10%. As in the variation of the bottom friction, also energy spectra of COULWAVE for the different values of the upwind fraction are very close to the spectra obtained for the laboratory results. The same pattern in the energy spectrum of COULWAVE compared with the laboratory can be seen as with the bottom friction. As the results are so close, the most stable option for the upwind fraction and the one that presented the closest agreement with the experimental data, namely 1, is chosen for further simulations.

III.   Breaking model

In the breaking module of the code four parameters can be changed; dzdt_I, dzdt_F, T_star and delta_breaking. The default values for the different parameters are shown in Table 5.4. Nine cases were run to see the influence of these parameters, see Table 5.5.

Table 5.4 – Default values of the breaking parameters, *co_c* is sqrt(9.81*H_total*), *H_total* is $h+\varsigma$

	Formula	Default value
Dzdt_I	0.65*co_c	0.65
Dzdt_F	0.08*co_c	0.08
T_star	7*sqrt(abs(H_total/9.81))	7
Delta_breaking	-	6.5

Table 5.5 – Tested values of the breaking parameters.

	Parameter changed	Value
Case 1	No	Default values
Case 2	Dzdt_I	0.25
Case 3	Dzdt_I	1.05
Case 4	Dzdt_F	0.04
Case 5	Dzdt_F	1.12
Case 6	Delta_breaking	2.5
Case 7	Delta_breaking	10.5
Case 8	T_star	3
Case 9	T_star	11

The results of the selected gauges of the model, compared with results from the laboratory data of Poort (2007), are shown in Figure 5.23. Figure 5.24 shows the wave heights of the laboratory data and the results of the cases run with COULWAVE. There appeared no differences in case 1 and cases 3 to 9. Only case 2 gave slightly different results. As can be seen, the results of cases 1 and 2 are very close till 27 m; after this distance the gauges from the laboratory give slightly higher wave heights. The breaking point however is in the same position.

Figure 5.23 - Wave gauges on the experimental setup.

Figure 5.24 shows the wave heights obtained in laboratory data and 9 cases run with COULWAVE. There appeared no differences in cases 1 and 3 to 9. Only case 2 gave slightly different results. This leads to the conclusion that the most important parameter is dzdt_I. As can be seen, the results of cases 1 and 2 are close till 27 m, after this distance the wave heights in case 1 decrease more than in case 2. The values of the wave height in cases 1 to 9 are higher than in the laboratory till 25 m. However the breaking point is almost in the same position. The values of the wave height in cases 1 and 3 to 9 after breaking are closer to the experimental results than case 2.

Figure 5.24 - Wave heights in gauges from Figure 5.23.

As the default values give the best results in comparison with the laboratory wave heights, there is chosen to set the breaking parameters on the default values.

5.8 CONCLUSION

In this chapter, the influences of the bathymetry, grid definition, bottom friction and the upwind fraction differences on the model results regarding the wave height around the domain were investigated. The energy spectrum and the influences of the breaking parameters on the significant wave height were also studied. It can be concluded that the default values of all investigated parameters give very similar results with the laboratory data of a flow around a submerged reef in a wave basin (Poort, 2007). Because of that, it was chosen to set all investigated parameters on the default values for the simulations carried out to investigate the design parameters of the MFAR.

Chapter 6 Optimal Geometry of the Multi-Functional Artificial Reef

6. OPTIMAL GEOMETRY OF THE MULTI-FUNCTIONAL ARTIFICIAL REEF

6.1 INTRODUCTION

In this chapter the optimal geometry will be designed for the conditions at the west coast of Portugal, especially the local coastline in front of Leirosa. The optimal geometry is investigated for a reef that will be good for amateur surfers (skill 3-6, see chapter 2), but that will be as interesting as possible for professionals too, so that championships may eventually be an option. Because of that the peel angle is between 40 and 60 degrees and the breaker type is at the transition of spilling and plunging (with relatively low values of ξ_b).

In chapter 3 six parameters of an MFAR have been mentioned that have to be defined for an optimal geometry:

- reef angle;
- height of the reef;
- geometry of the reef (with or without a platform);
- submergence of the reef;
- horizontal dimensions;
- side slope of the reef.

In chapter 5 three parameters, namely the height of the reef, the submergence of the reef and the seaward slope of the reef have been investigated and determined; the values are summarized in Table 6.1.

Table 6.1- Geometry parameters defined previously (see chapter 5).

Height of the reef	3.20 m
Side slope of the reef	1:10
Submergence of the reef	1.50 m

This chapter treats the investigation of the parameters mentioned before (see chapter 4 that have a behavior in 2DH (x,y), namely:

- the reef angle;
- the geometry of the reef (with or without a platform);
- horizontal dimensions.

In order to investigate these parameters, simulations are executed with the calibrated COULWAVE model (see chapter 5). The simulations are executed with regular waves and the incident angle of the waves is chosen to be zero degrees, since the point of the crest will be directed toward the most common wave direction, giving the best surfing

conditions. As the reef will be designed with two goals, namely coastal protection and the increase of surfing possibilities, two wave conditions will be tested:

- Design condition for coastal protection (storm condition): $H = 4.0$ m, $T = 15$ s.
- Design condition for surfing (common condition): $H = 1.5$ m, $T = 9$ s.

As it is expected that the reef angle, the eventual presence of a platform and the horizontal dimensions interact with each other, it is decided to make the simulations with variations of the reef angle considering a reef with a platform and without a platform. The horizontal dimensions vary automatically with the variation of the reef angle and the use or not use of a platform.

Like mentioned in chapter 4, the reef angle gives highest peel angles for 66 degrees. However, in the determination of 66 degrees 2DH effects of wave focusing are not taken into account. Besides that, with a lower reef angle more local shoreline is protected. Consequently, in this section, two reef angles are tested for both mentioned wave conditions, namely 45 and 66 degrees.

6.2 SIMULATIONS

The numerical simulations to study the 2DH behavior of the hydrodynamics around an MFAR have been done for eight cases, varying the reef angle (45° and 66°) and the use or not use of a platform, for the two mentioned wave conditions. Table 6.2 gives an overview of the values of the parameters in these simulations.

Table 6.2 - Tested values of the parameters.

Case	Reef angle (°)	Form of the reef	H (m)	T (s)
1	45	Triangle	4.0	15
2	45	Triangle	1.5	9
3	45	Triangle plus platform	4.0	15
4	45	Triangle plus platform	1.5	9
5	66	Triangle	4.0	15
6	66	Triangle	1.5	9
7	66	Triangle plus platform	4.0	15
8	66	Triangle plus platform	1.5	9

Figure 6.1 shows the reef parameters in the simulations for a reef without platform and for a reef with platform.

Figure 6.1 - Geometry simulations (left: without platform, right: with platform).

Table 6.3 gives the characteristics of the simulations for the different cases described in Table 6.2. Cases 1, 3, 5 and 7 have a larger grid than the cases 2, 4, 6 and 8 due to the larger wave length. Due to this larger wave length both the plane bottom in the beginning of the reef and the sponge layers are longer, since the sponge layer is 1.25 times the wave length at the wave maker.

Table 6.3 - Characteristics of the simulations.

	Cases 1,3,5,7	Cases 2,4,6,8
Simulation time (s)	600	600
CPU time needed (hours)	33	23
Number of gridpoints per wavelength	58	32
Courant number	0.10	0.10
Grid size (m)	2.99	2.99
Time step (s)	0.025	0.025
Total number of gridpoints	196645	148740

6.3 METHODOLOGY

6.3.1 COASTAL PROTECTION

For the analysis concerning coastal protection, the velocities around the reef are analyzed. The output velocities of the model correspond to values at a depth $0.531h$ under the water surface. The velocity at this depth is, by several authors, as Nwogu (1993), taken as the depth representative of the flow and was adopted by the authors of the COULWAVE model. However, the mean current is a better parameter as an indication for the sediment transport than the mean velocity. For this purpose, i.e., to obtain the mean current value, the numerical code of the model has to be changed. The velocity has to be integrated in the vertical and subsequently divided by the depth at each point; this is a future task. In this work, even for the preliminary analysis of the flow that could give an indication of the sediment transport, the output velocity at a depth $0.531h$ under the water surface is used. In each gridpoint the time series of the velocities in both the x and y directions are averaged in time. The two vectors, of u in x direction and v in y direction, are summed to get the velocity vector in each gridpoint, in the x,y field. This velocity field gives an indication about the direction of the movement that the sediment will have in the simulated cases.

6.3.2 SURFABILITY

In chapter 3 the theoretical study of surfability has been described. Three surfability parameters were investigated, namely the breaker height, the Iribarren number and the peel angle. In this chapter the same parameters will be analyzed. Furthermore the results of the 2DH simulations with COULWAVE give the possibility to study the position of the breaker line and the wave height around the reef. Below the parameters that will be studied are named:

- Position of the breaker line and wave heights around the reef, which shows the wave focusing;
- Peel angle;
- Breaker height;
- Iribarren number, which indicates the type of the breaking wave.

The steps for the computed analysis of the surfability parameters are as follows:

1. A selection of a simulating area is made around the reef. And the model is run with the incident wave characteristics presented in Table 6.2. The offshore boundary is at least two times the wave length at the wave maker and the side boundaries are at least one time the wave length (Figure 6.2).

Figure 6.2 - Simulation area.

2. In order to spare calculation time a small area where the reef is situated, is selected for the analysis. This area is represented as the striped rectangle in Figure 6.3.

Figure 6.3 - Selected area around the reef.

Based on model results, for the selected area shown in Figure 6.3 and for each grid point, the maximum wave height, H_{max}, is calculated based on the time series of the surface elevation that is an output of the model and presented in a figure where the wave focusing and defocusing can be analyzed. The wave height has to be calculated because the model doesn't give the wave height as an output.

3. To find the point of breaking at the edges of the reef the criteria adopted is that the breaker height divided by breaker depth is 0.8, according to Sverdrup and Munk, 1946. For the tests to achieve preliminary guidelines (see chapter 3) a value of 1.1 was used, according to the results presented in Kaminsky and Kraus, 1993. However, as the breaker height and the slope that the wave experiences on the reef vary along the breaker line, it is chosen to use in this 2DH analysis the original value of the breaker parameter of 0.8.

4. Through the breaking point, a polynomial function is created to get smooth breaker line, see Figure 6.4.

Figure 6.4 - Polynomial function for breaker line.

5. For every found breaking point, it is defined:

- The breaker wave height. Defined by the wave height in the found breaking points under point 3.

- The inshore Iribarren number. The value of the slope is taken 1:10. The value of the breaker wave height is taken like the one calculated in the concerning grid point and the value of the wave length offshore is calculated according to the initial wave period.

- The peel angle. The peel angle (α) is calculated as the angle φ minus ϕ (see Figure 6.5). Below is described how angles ϕ and φ are calculated:

  o Angle φ is the angle between the breaker line and the line parallel to the base of the delta;

  o Angle ϕ is equal to $90° - \theta - \sigma$, where θ is the wave angle, which is calculated with linear refraction on the reef and σ is the reef crest angle.

Figure 6.5 - Peel angle calculation.

6.4 RESULTS

6.4.1 COASTAL PROTECTION

As referred before, for coastal protection the velocity cells near by the shoreline gives an indication of the sediment transport. The results of the velocity field for the eight cases are presented in Figure 6.6 to Figure 6.9.

Figure 6.6 - Velocity pattern of cases 1 and 3, for storm condition $H = 4$ m, $T = 15$ s.

Figure 6.7 - Velocity pattern of cases 5 and 7, for storm condition $H = 4$ m, $T = 15$ s.

Case 2

Case 4

Figure 6.8 – Velocity pattern of cases 2 and 4, for common condition $H = 1.5$ m, $T = 9$ s.

Figure 6.9 - Velocity pattern of cases 6 and 8, for common condition H = 1.5 m, T = 9 s.

Divergent cells indicate erosion near by the shoreline and convergent cells indicate sedimentation. When cells can be identified in the velocity fields, in Figure 6.6 to Figure 6.9, they are shown with striped lines. For each case below is written what kind of velocity cells appear near by the shoreline:

For storm condition, H = 4.0 m, T = 9 s:
Case 1: divergent cells were found, which means that there is an indication for erosion near by the shoreline;

Case 3: not convergent/not divergent cells were found, which means that there is no indication for erosion neither for sedimentation near by the shoreline;

Case 5: divergent cells appear, which means that there is an indication for erosion near by the shoreline;

Case 7: divergent cells appear, which means that there is an indication for erosion near by the shoreline. Anyway, it is not very clear.

For common condition, *H* = 1.5 m, *T* = 9 s:

Cases 2, 4, 6 and 8: not convergent/divergent cells, this means there is no clear indication neither for erosion nor for sedimentation near by the shoreline.

From Figure 6.6 to Figure 6.9 and according to with what was described above the following can be concluded:

- For the storm condition, it can be said that the case of a reef angle 45° without platform and the cases with a reef angle of 66° with and without a platform (cases 1, 5 and 7) give an indication to erosion at the shoreline. These cases will need large attention in the morphological study to see if this indication is correct, because if erosion will really take place in storm conditions these are not good geometries to choose;

- For all other cases (cases 2, 3, 4, 6 and 8) no clear indication is found for erosion or sedimentation at the shoreline. A morphological study will be needed to get more information about the mode of sedimentation occur or not near by the shoreline behind the reef.

6.4.2 SURFABILITY

As mentioned in section 6.2.2 five parameters will be analyzed here to get insight in the surfability capacities obtained with the several geometries of the reef shown in Table 6.2. Below these parameters, namely (I) the breaker line and wave focusing, (II) the breaker height, (III) the peel angle and (IV) the Iribarren number, will be treated in sequence.

I. Breaker line and wave focusing

For all cases studied, the breaker line on the reef is shown in Figure 6.10 to Figure 6.14. In order to show the effect of wave focusing on the breaker line for cases 2, 4, 6 and 8 the wave heights around the reef are also presented in Figure 6.10 to Figure 6.14. These figures show clearly that the more presence of wave focusing, the earlier the wave breaks on the reef. For cases 1, 3, 5 and 7 there is almost no wave focusing on the reef. This is due to the fact that the high waves have already broken before the reef. The figures with the wave heights around the reef for cases 1, 3, 5 and 7 can be found in Figure II.1 to Figure II.4, in Annex II.

Common condition, H = 1.5 m, T = 9 s:

Figure 6.10 - Breaker line for case 2, wave heights for case 2 and breaker line for case 4.

Figure 6.11 – Wave heights for case 4, and wave heights and breaker line for case 6.

Figure 6.12 – Breaker line and wave heights for case 8.

Storm condition, H = 4.0 m, T =15 s:

Figure 6.13 – Breaker line for case 1.

Figure 6.14 - Breaker line for cases 1, 3, 5 and 7.

Regarding to the breaker line contours, the longer the breaker line the better for surfers. From Figure 6.10 to Figure 6.14 it can be concluded that in all tested cases a breaker line will be created on the reef. About the variation in the wave angle with and without platform for both wave conditions, it can be concluded that the breaker line is longer for the reef angle of 45° than for the angle of 66°. This makes the reef with a reef angle of 45° more interesting for surfers than the reef with a reef angle of 66°.

II. Breaker wave height

For all eight cases analyzed here, the wave breaker height along the breaker line is given in Figure 6.15 to Figure 6.18. The figures were separated in cases with storm condition (cases 1, 3, 5 and 7) and cases with common condition (cases 2, 4, 6 and 8). Due to this reason the graphs of cases 1 and 3, cases 5 and 7, cases 2 and 4 and cases 6 and 8 are combined in separate figures.

Figure 6.15 - Breaker wave height for cases 1 and 3.

Figure 6.16 - Breaker wave height for cases 5 and 7.

Figure 6.17 - Breaker wave height for cases 2 and 4.

Figure 6.18 - Breaker wave height for cases 6 and 8.

Regarding Figure 6.15 to Figure 6.18, below is described, for all cases, what is the development of the breaker wave height along the breaker line from the apex of the structure and in the direction of the shoreline. The beginning of the breaker line is at the apex of the delta, at x = 500 m.

For the storm condition, *H* = 4.0 m and *T* = 15 s:

Case 1: H_b gets a bit larger in the beginning (during the first 50 m each side) and gets smaller at the end; varying from 3.0 to 2.5 m;

Case 3: H_b is quite constant in the beginning (during the first 50 m each side) and gets smaller at the end, the maximum is 2.6 m; varying from 2.6 to 2.2 m;

Case 5: H_b gets a bit larger and constant during the first 30 m and much smaller at the end; varying from 3.0 to 2.3 m;

Case 7: H_b gets higher in the beginning and decreases constantly along the breaker line; varying from 2.3 to 2.0 m.

For the common condition, *H* = 1.5 m *T* = 9 s:

Case 2: H_b gets higher in the beginning and decreases constantly along the breaker line; varying from 2.7 to 1.7 m;

Case 4: H_b gets higher in the beginning and stays approximately constant at the end (after 40 m each side); varying from 2.4 to 1.9 m;

Case 6: H_b gets higher in the beginning, decreases suddenly reaching the minimum at about 15 m each side, then grows and gets smaller again; varying from 2.8 to 1.5 m;

Case 8: H_b is gets a bit smaller in the beginning and gets a bit larger in the end; varying from 2.5 to 2.3 m.

Concerning the wave height at the breaker point, the preferred wave height depends on the skill of the surfer. The higher the skill of the surfer, the higher wave is preferred. However, it is easier to start surfing for every surfer when the wave is somewhat higher, at the beginning, especially when the peel angle is small. From Figure 6.15 to Figure 6.18 and from what is described above the following can be concluded:

For the storm condition, $H = 4.0$ m and $T = 15$ s:

- Concerning the reef angle variation without platform (cases 1 and 5), its development along the breaker line case 5, with a reef angle of 66°, is better than case 1, with a reef angle of 45°, because the wave height are higher at the apex in that case;
- Regarding the reef angle variation with platform (cases 3 and 7), its development along the breaker line case 3, with a reef angle of 45°, is more interesting for more professional surfers, because the wave height is larger;
- For the option of yes or no for a platform for the reef angle of 45° (cases 1 and 3), it can be concluded that case 1, without platform, is more interesting for more professional surfers;
- For the option of yes or no for a platform for the reef angle of 66° (cases 5 and 7), it can be concluded that case 5, without platform, is more interesting for more professional surfers.

Case 7 is the best case for the storm condition tested, as the wave height is best for amateur surfers along the ride and the wave height is larger at the apex, which makes starting easier.

For the common condition, $H = 1.5$ m and $T = 9$ s:

- Concerning the reef angle without platform (cases 2 and 6), its development along the breaker line case 6, with a reef angle of 66°, is better, because the wave height is smaller along the ride;
- Regarding the reef angle with platform for the common condition (cases 4 and 8), neither case 4, with a reef angle of 45°, nor case 8, with a reef angle of 66°, show a significant advantage;

- For the option of yes or no for a platform for the reef angle of 45° (cases 2 and 4), case 2, without platform, is more interesting for more professional surfers, although there is not much difference;
- For the option of yes or no for a platform for the reef angle of 66° (cases 6 and 8), case 8, with platform, is more interesting for better surfers, because the wave height has a constant higher value.

Case 6 is the best for the surf condition tested, because the wave height is best for amateur surfers along the ride and larger at the apex.

III. Peel angle

For all cases analyzed in this chapter, the peel angle along the breaker line is given in Figure 6.19 to Figure 6.22. For all cases the peel angle at the apex, at $x = 500$ m, is the smallest one.

Figure 6.19 - Peel angle for cases 1 and 3.

Figure 6.20 - Peel angle for cases 5 and 7.

Figure 6.21 - Peel angle for cases 2 and 4.

Figure 6.22 - Peel angle for cases 6 and 8.

Regarding Figure 6.19 to Figure 6.22, below is described, for all cases, what is the development of the peel angle along the breaker line from the apex of the structure and in the direction of the shoreline.

For the storm condition, *H* = 4.0 m and *T* = 15 s:

Case 1: The peel angle is quite constant over most part of the breaker line (during about 40 m each side), varying between 33° and 39°. At the apex there is a low value of 7° due to the rounding of the breaker line; at the ends there is a high value of more than 60° due to the larger angle of the breaker line.

Case 3: The development of the peel angle is almost the same as in case 1, just in this case the constant part varies between 33° and 38°, the low value at the apex is 10°.

Case 5: The peel angle grows from 40° near by the apex till 55° at the end. At the apex there is a minimum value of 5°.

Case 7: The peel angle varies from 30° to 38°. At the apex there is a minimum value of 21°.

For the common condition, *H* = 1.5 m and *T* = 9 s:

Case 2: The peel angle has a minimum value of 10° at the apex and goes up and down towards the end, varying from 38° near by the apex to 28° in the middle and 42° near by the end. At the end the value decreases to 12° and increases again to 50°.

Case 4: The peel angle has a minimum value of 15° at the apex and goes down from the apex toward the end, varying from 42° near by the apex to 15º-20° near by the end. At the end the value increases again to 50°.

Case 6: The peel angle has a minimum value of 23° at the apex. The value varies from 50° near by the apex to 33° in the middle and 67° at the end.

Case 8: The peel angle has an equal development as in case 6, just in this case the minimum value is 10° and the values vary from 33° near by the apex to 18° in the middle and 33° at the end.

Regarding the peel angle, the preferred peel angle is not straightforward. A small variation in the peel angle along the ride does not represent a problem since surfers actually like some variation. However, the peel angle should be between 40° and 60° for amateur surfers, as mentioned before. More professional surfers can also surf peel angles between 30° and 40°. From Figure 6.19 to Figure 6.22 and also from what is described above the following can be concluded:

For the storm condition, *H* = 4.0 m and *T* = 15 s:
- Concerning the reef angle without platform (cases 1 and 5), both cases can be surfed, however case 5 with a reef angle of 66° is better for amateur surfers;
- Regarding the reef angle with platform (cases 3 and 7), both cases can be surfed. The difference is minimal;
- For the option of yes or no for a platform for the reef angle of 45° (cases 1 and 3), both cases can be surfed. The difference is minimal;
- For the option of yes or no for a platform for the reef angle of 66° (cases 5 and 7), both cases can be surfed, however case 5 without platform is better for amateur surfers.

For the common condition, *H* = 1.5 m and *T* = 9 s:
- Concerning the reef angle without platform (cases 2 and 6), case 6 with a reef angle of 66° is surfable for amateur surfers. Case 2 with a reef angle of 45° can only be surfed by more professional surfers;
- Regarding the reef angle with platform for the common condition (cases 4 and 8), both cases are not able to be surfed by amateurs. Case 4 with a reef angle of 66° could be surfed in the beginning by professional surfers, but gets difficult to surf towards the end;
- For the option of yes or no for a platform for the reef angle of 45° (cases 2 and 4), both cases can only be surfed by more professional surfers. However, surfing gets difficult towards the end of the breaker line in case 4 with platform;

- For the option of yes or no for a platform for the reef angle of 66° (cases 6 and 8), case 6 without platform is surfable for both amateur and professional surfers. Case 8 with platform is not surfable.

IV. Iribarren number

For all cases analyzed in this chapter, the development of the Iribarren number along the breaker line is given in Figure 6.23 to Figure 6.26.
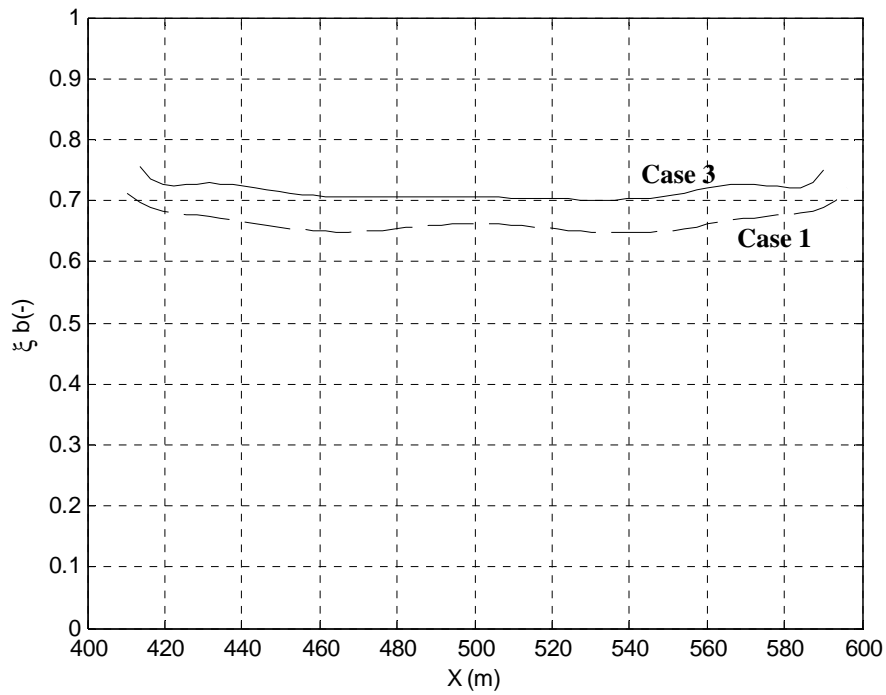

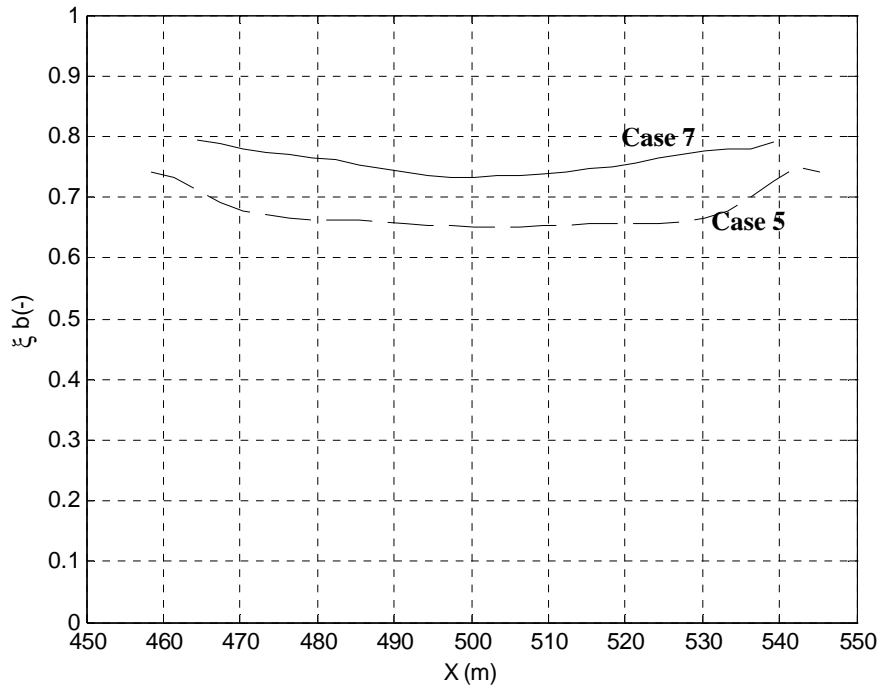Figure 6.23 – Iribarren number for cases 1 and 3.
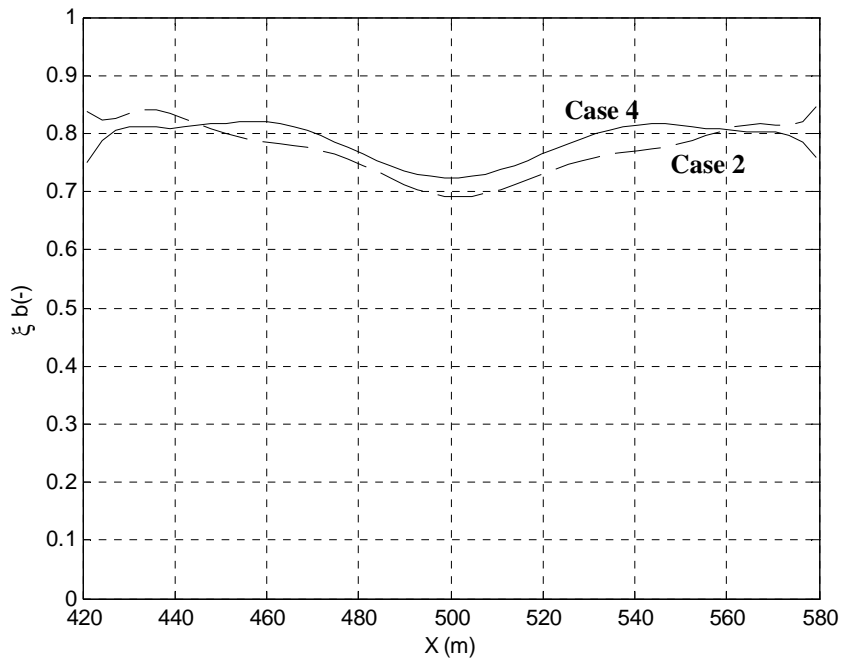
Figure 6.24 – Iribarren number for cases 5 and 7.

Figure 6.25 – Iribarren number for cases 2 and 4.

Figure 6.26 – Iribarren number for cases 6 and 8.

Regarding Figure 6.23 to Figure 6.26, below is described, for all cases, what is the development of the Iribarren number along the breaker line from the apex of the structure and in the direction of the shoreline.

For the storm condition, H = 4.0 m, T = 15 s:

Case 1: The Iribarren number is almost constant along the breaker line with a value of 0.65.

Case 3: The Iribarren number is almost constant along the breaker line with a value of 0.70.

Case 5: The Iribarren number is constant in the beginning and in the middle with a value of 0.66 and increases at the end to a value of 0.72.

Case 7: The Iribarren number increases a little along the breaker line, varying from a value of 0.72 at the apex till 0.80 at the end of the breaker line.

For the common condition, H = 1.5 m, T = 9 s:

Case 2: The Iribarren number increases from a value of 0.70 at the apex to a value of 0.82 at the end of the breaker line.

Case 4: The Iribarren number increases in the beginning from 0.72 to 0.82 and stays constant at a value of 0.82 towards the end of the breaker line.

Case 6: The Iribarren number increases in the beginning from a value of 0.69 at the apex to a value of 0.88 in the middle. Then the value decreases till 0.78 and increases again towards the end till a value of 0.90.

Case 8: The Iribarren number is almost constant along the breaker line with a value of 0.74.

Regarding to the Iribarren number, plunging wave with an inshore Iribarren number varying between 0.6 and 0.9 is the best to surf for both amateur and professional surfers (Henriquez, 2004). In order to catch the wave in the beginning it is preferred a smaller wave value of about 0.6 at the beginning of the ride. From Figure 6.23 to Figure 6.26 and taking into account what is described above the following can be concluded:

For the storm condition, H = 4.0 m and T = 15 s:
All cases are good to surf for amateur surfers, and.
- Concerning the reef angle without platform (cases 1 and 5), both cases can be surfed. The difference is minimal;
- Regarding the reef angle with platform (cases 3 and 7), both cases can be surfed. The difference is minimal;
- For the option of yes or no for a platform for the reef angle of 45° (cases 1 and 3), both cases can be surfed. However, case 1 without platform has smaller values of the Iribarren number along the breaker line, which makes catching the wave in the beginning easier for amateur surfers;
- For the option of yes or no for a platform for the reef angle of 66° (cases 5 and 7), both cases can be surfed, however case 5 without platform has smaller values of the Iribarren number along the breaker line, which makes catching the wave in the beginning easier for amateur surfers.

For the common condition, H = 1.5 m and T = 9 s:
- Concerning the reef angle without platform (cases 2 and 6), both cases can be surfed, however case 2 with a reef angle of 66° has smaller values of the Iribarren number along the breaker line, which makes catching the wave in the beginning easier for amateur surfers;
- Regarding the reef angle with platform (cases 4 and 8), both cases can be surfed. The difference is minimal;
- For the option of yes or no for a platform for the reef angle of 45° (cases 2 and 4), both cases can be surfed. The difference is minimal;
- For the option of yes or no for a platform for the reef angle of 66° (cases 6 and 8), both cases can be surfed, however case 8 with platform has smaller values of the Iribarren number along the breaker line, which makes catching the wave in the beginning easier for amateur surfers.

6.5 CONCLUSION

Using the calibrated numerical model COULWAVE, eight cases have been simulated to get insights about the hydrodynamic behavior around a reef in order to find the capability of the reef to protect the local coastline of Leirosa, Portugal, and to increase the local surfing possibilities.

Based on the cases studied it was not possible to define an optimal geometry of an MFAR in terms of coastal protection based only on the indication given by the velocity fields for the eight cases studied. However, the indication for the storm wave conditions (H = 4.0 m and T =15 s) tested, is in most cases erosion near by the shoreline. The indication for common wave conditions (H = 1.5 m and T = 9 s), is unclear for all cases; neither erosion nor sedimentation is a clear indication. A morphodynamic study needs to be executed to get a deeper insight about designs of geometries that give sedimentation near by the shoreline in storm wave conditions. Besides that, a more profound morphodynamic study needs to be conducted to investigate the mode of sedimentation, erosion or sedimentation, under common wave conditions.

Anyway, in terms of coastal protection a reef with platform seem to constitute a good first option.

The optimal geometry of an MFAR in terms of surfability can be divided into four surf parameters:

- Regarding the breaker line, for both the storm condition and the common wave condition, the cases of a reef angle of 45° are better, because they give longer breaker lines, by which the surfers can make a longer ride;
- Regarding the breaker wave height, for both the storm and the common wave condition, the case without platform and a reef angle of 66° is the best option for amateur surfers.
- Regarding the peel angle, for both the storm and the common wave condition, the case without platform and a reef angle of 66° is the best for amateur surfers.
- Regarding the Iribarren number, for the storm condition, the case without platform is the best for amateur surfers. The variation in the reef angle does not seem to make difference. For the common condition, the case without platform and a reef angle of 45° is the best for amateur surfers.

Taking all four surf parameters into account, the case without platform and with a reef angle of 66° is the best choice for the geometry in terms of surfability. Although two of the four parameters give better results for a reef angle of 45°, the angle of 66° is chosen to be better due to the larger importance of the peel angle and the breaker wave height with respect to the Iribarren number and the length of the breaker line. Besides

that, the Iribarren number is good for all tested cases and the variation in this parameter is very small.

Chapter 7 Conclusions and Recommendations

7. CONCLUSIONS AND RECOMMENDATIONS

7.1 CONCLUSIONS

Portugal is one of many countries in the world that suffers from coastal erosion. Conventional ways of protecting a coastline appear to entail some disadvantages. An innovative and interesting way of protecting a local coastal zone is by means of multi-functional artificial reefs. A multi-functional artificial reef is a submerged breakwater which, besides the helping to protect the local coastline, can have other purposes; in particular it may enhance the surfing possibilities and the environmental value of the local area. The structure has several positive side-effects: first, it provides an unimpaired visual amenity; second, it offers tourist and economic benefits by improving the surfing conditions; third, it can enhance the environmental value of the area where it is built, and fourth, with a proper design the down drift erosion can be minimal.

As a result of a theoretical study, a preliminary design, achieved step by step, is proposed for a multi-functional artificial reef making use of the theory and the state of the art. The proposed reef geometry is used as initial design in the numerical and physical tests, which are executed to analyze the hydrodynamics around a multi-functional reef breakwater in order to see the tendencies and obtain preliminary results related with the protection of a stretch of the central coast of Portugal and to increase the local surfing possibilities. The main design parameters for an MFAR are the reef angle, the height of the reef, the form of the reef in plant, the submergence of the reef, the horizontal dimensions and the seaward slope of the reef structure. Taking into account the condition that the proposed geometry function properly on a sea slope bottom of less than 1:50, the main preliminary choices are as follows: the upper part of the structure is a delta shaped with an angle of 66º and a side slope of 1:10, and the lower part consists of a platform whose slopes are as steep as possible. The position of the reef should be such that the distance from the apex of the structure to the undisturbed shoreline is greater than 1.5 the natural surf zone width.

Two design parameters (the submergence of the reef and the length of the reef) have influence on the breaker type that should be determined. Therefore, a physical and a numerical 2DV study have been executed to get insight in the influence of the length of the reef and the submergence on the Iribarren number, which is an indication for the breaker type for the reef functionality. From both studies, it was concluded that for the common wave conditions tested, the design wave height of 1.50 m gives a good surfable plunging wave for a submergence of 1.50 m. From the numerical tests, initial values of several parameters for the simulations carried out in order to find the optimal

geometry were determined: the height of the reef is 3.20 m, the seaward slope of the reef is 1:10 and the reef submergence is equal to the design wave height of 1.50 m.

In order to be able to investigate the other three design parameters (the reef angle, the geometry of the reef (with or without a platform) and the horizontal dimensions in 2DH) for the optimal geometry, the Boussinesq-type COULWAVE model is firstly calibrated. The influences of the bottom friction and of the upwind fraction differences were investigated on the significant wave height and the energy spectrum. The influences of the breaking parameters on the significant wave height were also studied. It can be concluded that the default values of all investigated parameters give very similar results to the laboratory data of a submerged reef in a wave basin (obtained by Poort, 2007). Because of that, it was chosen to set all investigated parameters on the default values for the simulations that were carried out to investigate the design parameters of the MFAR.

An optimal geometry of an MFAR for the local coastline of Leirosa, Portugal, in terms of coastal protection was not possible to define with the indication given by the velocity fields of the eight cases simulated. The indication for storm wave conditions (H = 4 m and T = 15 s) is in most cases erosion near by the shoreline. The indication for the common wave condition (H = 1.5 m and T = 9 s) is unclear for all cases; neither erosion nor sedimentation is clearly indicated. A morphodynamic study is needed to get a deeper insight of the reef geometry on the morphodynamic response.

The optimal geometry of an MFAR in terms of surfability can be divided into four surf parameters;

- Regarding the breaker line, for both wave conditions tested, a reef angle of 45° gives a longer breaker line, by which the surfers can make a longer ride;
- Regarding the breaker wave height, for both wave conditions tested, the case without platform and a reef angle of 66° is the best for amateur surfers;
- Regarding the peel angle, for both wave conditions tested, the case without platform and a reef angle of 66° is the best for amateur surfers;
- Regarding the Iribarren number, for the storm condition, the case without platform is the best one for amateur surfers. The variation in the reef angle does not make much difference. For the common condition, the case without platform and a reef angle of 45° is the best one for amateur surfers.

Taking all four surf parameters into account, the case without platform and a reef angle of 66° is the best choice for the geometry in terms of surfability. Although two of

the four parameters give better results for a reef angle of 45°, the angle of 66° is chosen to be better due to the larger importance of the peel angle and the breaker wave height with respect to the Iribarren number, and the length of the breaker line. Besides that, the Iribarren number is good for all tested cases and the variation in this parameter is very small.

Comparing the results of the 2DH study with COULWAVE model for the optimal geometry and the results of the theoretical study, it can be concluded that, regarding the surfability parameters, a reef angle of 66° is a better choice than the reef angle of 45°. Moreover, in contradiction to the expected results with a platform in the theoretical study, a reef without platform appeared to be better option in the 2DH study. This is a consequence of the wave focusing that couldn't be taken into account in the theoretical study.

7.2 RECOMMENDATIONS

Some research questions were faced during this investigation, which lead to some recommendations for future work:

1. The investigation of the wave shape, in the laboratory study, was carried out on a submerged reef with a smooth slope and a rigid material bottom. However, it is recommended to investigate the wave shape also over porous bottoms, like geotextile sand containers as this is the material which is the most suitable to build an MFAR. Within these containers, the turbulence and the energy dissipation will be different than over a rigid bottom, which is expected to have an influence on the wave shape.

2. The calibration of the numerical COULWAVE model has shown that it can be successfully used to simulate the hydrodynamics around an MFAR. However, improvements are recommended on the actual version of COULWAVE. This improvement includes mainly the introduction of porous flow simulation. This will enables the model to study global coastal areas with submerged porous structures.

3. Even though the velocity patterns give an indication about the sediment transport, they are not sufficient to get a deep insight about the influence of an MFAR on the morphology around the reef. For a proper design of a reef to protect a local coastline a morphological study has to be executed in which longshore currents, correct bathymetry, tide and wave angles have to be taken into account.

4. Even though COULWAVE has appeared to be a numerical model suitable to study the hydrodynamics around an MFAR, it would be even better to use a numerical model in the future that can simulate the wave shape on the reef. In

chapter 4 the use of COBRAS-UC is described. COBRAS-UC is not yet available for 3D studies, but as soon as possible, it is recommended to use a similar model for hydrodynamic studies around an MFAR.

5. In chapter 6, the bathymetry and the wave conditions used are those found in general along the central western coast of Portugal. However, it is recommended to make any case-study taking into account the exact bathymetry and the wave conditions in the area.

6. It is recommended to include an economical study for the construction of an MFAR in the case-study. That should involve, for example, the costs of material and the construction costs using different techniques.

7. As described in this thesis, an MFAR has two main goals. One is protecting the local coastline and the other is increasing the local surfing possibilities. It is recommended to investigate the need for and interest in increasing the local surfing possibilities in front of the coast where the reef is designed.

BIBLIOGRAPHY

Agnon, Y., Madsen, P. A., and Schaffer, H., 1999. A new approach to high order Boussinesq models. *Journal of Fluid Mechanics 399*, 319-333.

Antunes do Carmo, J.S. and Seabra-Santos, F.J., 2002. Near-shore sediment dynamics computation under the combined effects of waves and currents. *Journal of Advances in Engineering Software*, Elsevier Science, Vol. 33, Nº 1, 37-48.

Army Corps of Engineers, 1992. Engineering and Design – Coastal Geology, Department of the U.S. Army, publication number EM 1110-2-1810, CECW-EG.

ASRLtd, Reef construction: geotextile materials, 2008. http://www.asrltd.co.nz/downloads_reef.htm, accessed 25 March 2008.

Balzano, A. 1998 Evaluation of methods for numerical simulation of wetting and drying in shallow water flow models. *Coastal Engineering, 34*, 83-107.

Battjes, J.A., 1974. Surf similarity. *Proc. 14th International Conference on Coastal Engineering*, 466-479.

Black, K., 2000. Artificial surfing reefs for erosion control and amenity: theory and application. *Proc. of the International Coastal Symposium 2000* (www.asrltd.co.nz).

Black, K., Andrews, C., 2001. Sandy shoreline response to offshore obstacles: Part1. Salient and tombolo geometry and shape. *Journal of Coastal Research, Special Issue 29*, 82-93.

Black, K., Mead, S., 2001. Design of the Gold Coast Reef for Surfing, Public Amenity and Coastal Protection: Surfing Aspects. *Journal of Coastal Research, Special Issue 29*, 115-130.

Bleck, M., Kübler, S. and Oumeraci, H., 2003. Sand-filled geotextiles containers for shore protection. In Coastal Structures 2004, Portland, Oregon.

Borrero, J.C. & Nelson, C., 2003. Results of a comprehensive monitoring program at Pratte's reef.. www.surfrider.org.

Bowen, A.J. 1969. Rip currents: 1.Theoretical investigations. *Journal of Geophysical Research*, 74(5467).

Boussinesq J., 1872. Théorie des ondes et des ramous qui se propagent le long d'un canal rectangulaire horizontal. J. Math. Pure et Appl., 2, 17, 55-108.

Bowman Bishow Gorham, 2000. Cables Artificial Surf Reef: 12 Month Post-Construction Monitoring Survey. *Report No. R99132:3*, Department of Transport, Western Australia.

CIRIA (Simm J. D., Brampton, A. H., Beech, NW and Brooke J. S.), 1996. Beach management manual, Report 153, J. D. Simm (editor), ISBN 0-86017 4387.

Capitão, R.; Fortes, C.J.; Carvalho, M.M.; Covas, J.A. (1999). Definição de Regimes de Agitação Marítima - Casos de Estudo. *1ªs Jornadas Nacionais de Engenharia Costeira e Portuária. AIPCN-PIANC*, pp. 31-45. Porto, 1999.

Chen, Q., Dalrymple, R. A., Kirby, J. T., Kennedy, A. and Haller, M. C. 1999 Boussinesq modeling of a rip current system. *Journal of Geophysical Research*, 104, 617 - 637.

Chen, Q., Kirby, J. T., Dalrymple, R. A., Kennedy, A. B., and Chawla, A. 2000 Boussinesq modeling of wave transformation, breaking, and runup. Part I: 2D. *Journal of Waterway, Port, Coastal and Ocean Engineering126(1)*, 57-62.

Corbett, B., Tomlinson, R., 2002, Noosa Main Beach Physical Modelling, *Research Report No. 17*, Griffith Centre for Coastal Management.

Corbett, B.B., Tomlinson, R.B., Jackson, L.A., 2005. Reef breakwaters for coastal protection safety aspects and tolerances. *Proc. of the 17th Australiasian Coastal & Ocean Engineering Conference* (www.coastalmanagement.com.au).

Dias, J.A., Bernardo, P. and Bastos, R., 2002. The occupation of the Portuguese littoral in 19th and 29th centuries, *Littoral 2002*, *The changing coast*. EUROCOAST/EUCC, Porto – Portugal. Ed. EUROCOAST – Portugal, ISBN 972-8558-09-0.

Edwards, R., 2003. A brief description of the Biological Assemblages Associated with Narrowneck Artificial Reef and Non-Woven Geotextile Substratum. Prepared for Soil Filters Australia.

Eurosion, 2004. *Living with coastal erosion in Europe: Sediment and space for sustainability*. A guide to coastal erosion management practices in Europe, 164 pages.

Fortes, C.J.E.M.; Coli, A.B.; Neves, M.G., CAPITÃO, R. (2006) – Porto Santo Island. Offshore wave characterization and propagation. *Journal Coastal Research*, SI 39, 1600-1605.

Fredsøe J. and Deigaard, R., 1995. *Mechanics of coastal sediment transport*. Advances Series on Ocean Engineering – Volume 3. World Scientific Publishing Co., ISBN 9810208405 – ISBN 9810208413 (pbk).

Galvin, C.J., 1968. Breaker type classification on three laboratory beaches. *Journal of geophysical research, 73(12)*, 3651-3659.

Galvin, C.J., 1972. *Wave breaking in shallow water*. Waves on beaches and resultant sediment transport. Academic Press, New York, N:Y., 413-456.

Garcia, N., Lara, J.L. and Losada, I.J. (2004). 2-D Numerical analysis of near-field flow at low-crested permeable breakwaters. Coastal Engineering, 51, 991-1020.

Gobbi, M. F., Kirby, J. T., and Wei, G., 2000. A fully nonlinear Boussinesq model for surface waves. Part II. Extension to O(kh)4) . *Journal of Fluid Mechanics 405*, 182-210.

Goda, Y. 1987. Statistical Variability of Sea State Parameters as a Function of Wave Spectrum. *Proc. IAHR Seminar on Wave Anal. and Gen. in Lab. Basins*, Lausanne, Switzerland.

Gomes, F.V. and Pinto, F.T. (2006). EUROSION Case Study, Vagueira – Mira (Portugal), Instituto de Hidráulica e Recursos Hídricos, FEUP, 18 pages.

Gopalakrishnan, T. C. 1989 A moving boundary circulation model for regions with large tidal flats., *International Journal for Numerical Methods in Engineering , 28*, 245-260.

Gourlay, M.R., 1993. Wave set-up and wave-generated currents on coral reefs. *Coasts 1993: Preprints of Papers: 11th Australasian Conference on Coastal and Ocean Engineering*, 23-27 August 1993, Townsville, Qld. Instn Engrs, Aust., Barton, ACT, Nat. Conf. Publ. 93/4, Vol.2, 479 – 484.

Green, A. E. and Naghdi, P.M. 1976 A derivation of equations for wave propagation in water of variable depth. *Journal of Fluid Mechanics 78*, 237-346.

Henriquez, M., 2004. *Artificial surf reefs*. M.Sc. thesis. Delft University of Technology (www.waterbouw.tudelft.nl).

Henriquez, M., Janssen, T.T., Van Ettinger, E.H.D., Reniers, A.J.H.M, 2006. Refraction-controlled surfability. *Proc. of the 5th International Surfing Symposium.*

Hutt, J.A., Black, K.P. Mead, S.T., 2001. Classification of surf Breaks in Relation to Surfing Skill. *Journal of Coastal Research, special issue 29*, p. 66-81.

Hsiao, S.-C. 2000. *Permeable effects on nonlinear water waves*. Ph. D. Thesis, Cornell University.

Hsiao, S.-C. and Liu, P. L.-F. 2002. *Permeable effects on nonlinear water waves*. Royal Society of London.

Hsu, T.-J., Sakakiyama, T., Liu, P.L.-F., 2002. A numerical model for wave motions and turbulence flows in front of a composite breakwater. *Coastal Engineering 46*, 25– 50.

Jackson, L.A., Reichelt, R.E., Restall, S., Corbett, B., Tomlinson, R., McGrath, J. 2004. Marine ecosystem enhancement on a geotextile coastal protection reef – Narrowneck reef case study. *Proc. of the 29th International Conference on Coastal Engineering* (Lisbon, Portugal), 3940-3952.

Jackson, L.A., Tomlinson, R., Turner, I., Corbett, B., D'Agata, M., McGrath, J., 2005. Narrowneck artificial reef; results of 4 yrs monitoring and modifications. *Proc. of the 4th International Surfing Reef Symposium* (www.coastalmanagement.com.au).

Kanayama, S., Tanaka, H., and Shuto, N. 1998 A multi-level model for nonlinear dispersive water waves. *Coastal Engineering 1998 (ed. Billy L. Edge), vol. 1*, pp.576-588. ASCE.

Kaminsky, G., and Kraus, N.C., 1993. Evaluation of depth-limited wave breaking criteria. *Waves '93*, Amer. Soc. Civil Engrs, 180-193.

Kamphuis, J.W., 2000. *Introduction to Coastal Engineering and Management*, World Scientific Press, 437 pages.

Kennedy, A.B., Chen, Q., Kirby, J.T. & Dalrymple, R.A., 2000. Boussinesq modeling of wave transformation, breaking, and runup. Part I: 1D. *Journal of waterway, port, coastal and ocean engineering 126(1)*, 39-47.

Komar, P.D., 1998. *Beach Processes and Sedimentation* (2nd Edition). Prentice Hall, New Jersey.

Korteweg D. J. and De Vries G., 1895. On the change of form of long waves advancing in a rectangular canal, and on a new type of stationary waves. Phil. Mag. 39/5, 422-443.

Kowalik, Z. and Bang, I. 1987 Numerical computation of tsunami run-up by the upstream derivative method. *Science of Tsunami Hazards, 5(2)*, 77-84.

Lara et al., 2006a J.L. Lara, N. Garcia and I.J. Losada, RANS modelling applied to random wave interaction with submerged permeable structures, *Coastal Engineering 53 (2006)*, 395–417.

Lara et al., 2006b J.L. Lara, I.J. Losada and P.L.-F. Liu, Breaking waves over a mild gravel slope: experimental and numerical analysis, *Journal of Geophysical Research*, AGU 111 (2006), C11019.

Leendertse, J. J. 1987 Aspects of SIMSYS2D, a system for two-dimensional flow computation. R-3752-USGS. Rand Corp., Santa Monica, CA, 80.

Li, Y. and Raichlen, F. 2002 Non-breaking and breaking solitary wave run-up, *Journal of Fluid Mechanics, 456*, 295-318.

Liu, P.L.-F., Lin, P., Chang, K.A., Sakakiyama, T., 1999. Numerical modeling of wave interaction with porous structures. *Journal of Waterway, Port, Coastal and Ocean Engineering 125*, 322– 330.

Liu, P. L.-F., 1994. Model equations for wave propagation from deep to shallow water. In *Advances in Coastal Engineering (ed. P. L.-F. Liu), vol. 1*, pp.125-157. World Scientific.

Lopes, A.M., Nunes, M., Carvalho, T., Caridade, P., Carvalho, J.C. & Graça, T.P. (2003). O litoral da Região Centro de Portugal: Um caso preocupante de risco e de perda de território. Relatório CCDR-Centro, 49 pages (in Portuguese).

Losada et al., 2005 I.J. Losada, J.L. Lara, E. Damgaard and N. Garcia, Modelling of velocity and turbulence fields around and within low-crested rubble-mound breakwaters, *Coastal Engineering 52 (2005)*, 887–913.

Losada, I.J., Lara, J.L., Guanche, R., Gonzalez-Ondina, J.M. 2008. Numerical analysis of wave overtopping of rubble mound breakwaters. *Coastal Engineering 55 (1)*, 47-62.

Lynett, P.J., 2002. A multi-layer approach to modeling of generation, propagation and interaction of water waves. Ph.D. thesis. Cornell University.

Lynett, P. and Liu, P. L.-F., 2002. Modeling Wave Generation, Evolution, and Interaction with Depth Integrated, Dispersive Wave Equations COULWAVE Code Manual Cornell University Long and Intermediate Wave Modeling Package.

Madsen, P. A., and Sorensen, O. R., 1992. A new form of the Boussinesq equations with improved linear dispersion characteristics. Part II: A slowly varying bathymetry. *Coastal Engineering 18*, 183-204.

Madsen, P. A., Sorensen, O. R., and Schaffer, H A. 1997 Surf zone dynamics simulated by a Boussinesq-type model. Part I: Model description and cross-shore motion of regular waves. *Coastal Engineering, 32,* 255-287.

Madsen, P. A., and Schaffer, H. A., 1998. Higher order Boussinesq-type equations for surface gravity waves - Derivation and analysis. *Royal Society of London A 356*, 1-60.

Mead, S.T. and Black, K.P., 2001a. Predicting the Breaking Intensity of Surfing Waves. In: Black, K.P. (ed.), Natural and Artificial reefs for Surfing and Coastal Protection. *Journal of Coastal Research Special Issue No. 29*, 51-65.

Mead, S.T. and Black, K.P., 2001b. Field studies leading to the bathymetric classification of world-class surfing breaks. In: Black, K.P. (ed.), Natural and Artificial reefs for Surfing and Coastal Protection. *Journal of Coastal Research Special Issue No. 29*, 5-20.

Moores, A.E., Black, K.P., and Mead, S.M., 2006. Physical modeling of the Mount Maunganui Artificial Reef. *Proceedings of the First International Conference on the Application of Physical Modelling to Port and Coastal Protection.* (Porto, Portugal), 309-321.

Nwogu, O. 1993 Alternative form of Boussinesq equations for nearshore wave propagation. *Journal of Waterway, Port, Coastal and Ocean Engng. 119(6)*, 618-638.

Over, 2006. Surfability of an ASR in irregular waves. *M.Sc. thesis*. Delft University of Technology (www.waterbouw.tudelft.nl).

Pattiaratchi, C., 2000. Design studies for an Artificial Surfing Reef: Cable Station, Western Australia. *Proc. Coasts and Ports '99*, 485-489.

Peregrine, D. H., 1967. Long waves on a beach. *Journal of Fluid Mechanics 27*, 815-827.

Petera, J., and Nassehi, V. 1996 A new two-dimensional finite element model for the shallow water equations using a Lagrangian framework constructed along fluid particle trajectories, *International Journal for Numerical Methods in Engineering, 39*, 4159-4182.

Pilarczyk, K.W., 2003. Design of low-crested (submerged) structures – an overview. 6th International Conference on Coastal and Port Engineering in Developing Countries, Colombo, Sri Lanka.

Poort, M., 2007. Rip currents. A laboratory study of a rip current in the presence of a submerged reef. *M.Sc. thesis*. Delft University of Technology (www.waterbouw.tudelft.nl).

Press, W.H., Flannery, B.P. and Teukolsky, S.A. 1989. "Numerical Recipes," CambridgeUniversity Press, 569-572.

Ranasinghe, R., Hacking, N., Evans, P., 2001. Multi-functional artificial surf breaks: A review. NSW Department of Land and Water Conservation.(www.asrltd.co.nz).

Ranasinge, R. Turner, I.L., 2006a. Shoreline response to multi-functional artificial surfing reefs: A numerical and physical modeling study. *Journal of Coastal Engineering 53*, 589-611.

Ranasinge, R. Turner, I.L., 2006b. Shoreline response to submerged structures: A review. *Journal of Coastal Engineering 53*, p. 65-79.

Reis, C.S. and Freitas, H., 2002. Rehabilitation of the Leirosa sand dunes. In EuroCoast-Portugal Association (ed.) Littoral 2002, Porto, 22-26 September 2002. Porto, Portugal. III: 381-384.

Reis, C.S., Freitas, H. and Antunes do Carmo, J.S., 2005. Leirosa Sand Dunes: A Case Study on Coastal Protection. Proc. IMAM - Maritime Transportation and Exploitation of Ocean and Coastal Resources, Lisboa, 26-30 de September, 1469-1474. Ed. Taylor and Francis / BALKEMA. ISBN Vol. 2: 0 415 39374 4, cd-rom: 0 415 39433 3.

Restall, S.J., Jackson, L.A., Heerten, G., Hornsey, W.P., 2002. Case Studies showing the growth and development of geotextile sand containers. *An Australian Perspective. Geotextiles & Geomembranes, vol 20*, no 5.

Rey S., I. Alejo J., Alcántara-Carrió and Vilas F., 2002. Influence of Boundary Conditions on Morphodynamics and Sedimentology of Patos Beach (Ría de Vigo, Nw of Spain), Littoral 2002, The Changing Coast. EUROCOAST / EUCC, Porto, Ed. EUROCOAST – Portugal, ISBN 972-8558-09-0.

Serre F., 1953. Contribution à l'étude des ecoulements permanents et variables dans les canaux. La Houille Blanche, 374-388.

Sielecki, A. and Wurtele, M.G. 1970. The numerical integration of the nonlinear shallow-water equations with sloping boundaries. Journal of Computational Physics, 6, 219-236.

Sitanggang, K.I., and Lynett, P., 2005. Parallel computation of a highly nonlinear Boussinesq equation model through domain decomposition. *International journal for numerical methuds in fluid*s, vol 49 (1), 57-74.

Smith, E.R., Kraus, N.C., 1990. Laboratory study on macro-features of wave breaking over bars and artificial reefs. *Tech. Report CERC-90-12*, U.S. Army Engr. Waterways Expt. Station, Coastal Engrg. Res. Center, Vicksburg, Miss.

Smith, E,R. Kraus, N.C., 1991. Laboratory study of wave breaking over bars and artificial reefs. *Journal of Waterway, Port, and Coastal Engineering, 117(4)*: 307-325.

Smit, F. and Mocke, G., 2005. Physical and numerical modelling of morphological and surf parameter response to an artificial reef. *Proc. 2005 Artificial Surfing Reef Conference.*

Sverdrup, H.U. and Munk, W.H., 1946. Theoretical and Empirical Relations in Forecasting Breakers and Surf. *Transactions of American Geophysical Union (27)*, 828-836.

Tao, J. 1983. Computation of wave runup and wave breaking Internal Report, Danish Hydraulics Institute, Denmark.

Ten Voorde M., Neves, M.G.. and Antunes do Carmo, J.S., 2008. Estudo Preliminar da Geometria de um Recife Artificial para Protecção Costeira e para a Prática de Surf na Costa Oeste Portuguesa. Preliminary Study on the Geometry of an Artificial Reef for Coastal Protection and Surfing along the West Coast of Portugal. Revista da Gestão Costeira Integrada 8(1), pp 65-79.

Ten Voorde, M., Antunes do Carmo, J.S., Neves, M.G., 2009. Multi-functional artificial reefs for coastal protection. In book: Agricultural Runoff, Coastal Engineering and Flooding. Novapublishers (in press).

Thurman, H.V, and Trujillo, A.P., 1999. "Essentials of Oceanography", 6th edition, Prentice-Hall, Inc., ISBN 0-13-727348-7.

Trung, L.H., 2006. Interacting Artificial Surf Reefs *M.Sc. thesis*. Delft University of Technology. (www.waterbouw.tudelft.nl).

Turner, I.L., Leyden, V.M., Cox, R.J., Jackson, L.A., McGrath, J.E., 2001. Three-dimensional scale physical model investigations of the gold coast artificial reef. *Journal of Coastal research, special issue 29*, p. 131-146.

Van Ettinger, H.D., 2005. Artificial surf reef design. *M.Sc. thesis*. Delft University of Technology. (www.waterbouw.tudelft.nl).

Van Rijn L.C., 2001. Sand transport and morphology of offshore sand mining pits/areas (EVK3-2001-00053 SAND PIT EU project).

Walker, J.R., 1974. Recreational Surf Parameters. *Tech. rept. 30*. University of Hawaii, James K.K. Look Laboratory of Oceanographic Engineering.

Wei, G. and Kirby, 1995. A time-dependent numerical code for extended Boussinesq equations. *Journal of Waterway, Port, Coastal and Ocean Engineering 120*, 251-261.

Wei, G., Kirby, J. T., Grilli, S. T., and Subramanya, R., 1995. A fully nonlinear Boussinesq model for surface waves. Part I. Highly nonlinear unsteady waves. *Journal of Fluid Mechanics 294*, 71-92.

Woo, S.-B. 2002 Finite element modeling of the fully-nonlinear extended Boussinesq equations. Ph. D. Thesis, Cornell University.

Zelt, J. A. 1991 The runup of nonbreaking and breaking solitary waves. *Coastal Engineering, 15*, 205-246.

PAPERS PUBLISHED WITHIN THE RESEARCH OF THIS THESIS

Journals:

1. Ten Voorde, M., Antunes do Carmo, J.S., Neves, M.G., 2007. Numerical simulations for the design of a multi-functional artificial reef for Leirosa coast, Portugal. *International Journal of Ecodynamics*, Eds. Tiezzi, Jørgensen, Brebbia, Chon & Patten, WITPRESS, Vol. 2, Nº 2, pp. 124-132.

2. Ten Voorde M., Neves, M.G.. and Antunes do Carmo, J.S., 2008. Estudo Preliminar da Geometria de um Recife Artificial para Protecção Costeira e para a Prática de Surf na Costa Oeste Portuguesa / Preliminary Study on the Geometry of an Artificial Reef for Coastal Protection and Surfing along the West Coast of Portugal. *Revista da Gestão Costeira Integrada / Journal of Integrated Coastal Zone Management 8(1)*, pp. 65-79.

3. Ten Voorde, M., Antunes do Carmo, J.S., Neves, M.G., 2009. Designing a Preliminary Multifunctional Artificial Reef to Protect the Portuguese Coast. *Journal of Coastal Research 25(1),* pp. 69-79.

4. Ten Voorde, M., Antunes do Carmo, J.S., Neves, M.G., Mendonça, A. 2009. Physical and numerical study of "breaker types" over an artificial reef. *Journal of Coastal Research, SI 56*, pp. 569-573.

Chapter book:

1. Ten Voorde, M., Antunes do Carmo, J.S., Neves, M.G., 2009. Multi-functional artificial reefs for coastal protection. In book: Agricultural Runoff, Coastal Engineering and Flooding, edited by Ch. A. Hudspeth, T. E. Reeve, ISBN: 978-1-60741-097-3, pp. 153-210, Nova Science Publishers, Inc.

Conferences:

1. Ten Voorde, M., Antunes do Carmo, J.S., Neves, M.G., 2006. Artificial surfing reefs: the preparation of physical tests and the theory behind. *In: Proceedings of 1st International Conference on the Application of Physical Modelling to Port and Coastal Protection* (Porto, Portugal), edited by F. Veloso Gomes, F. Taveiro Pinto, L. das Neves, and G. Iglesias, ISBN: 90-78046-04-X, pp. 425–434.

2. Ten Voorde, M., Antunes do Carmo, J.S., Neves, M.G., 2006. Contribution to the design of artificial surfing reef breakwaters for coastal protection. *In: Proceedings of the International Junior Researcher and Engineer Workshop on Hydraulic Structures (IJREWHS'06)*, Montemor-o-Novo, Jorge Matos and Hubert Chanson Eds., Report CH61/06, Div. of Civil Engineering, The University of Queensland, Brisbane, Australia, Dec., pp. 115-124 (ISBN 1864998687).

3. Ten Voorde, M., Antunes do Carmo, J.S., Neves, M.G., 2007. Modelação numérica do escoamento em torno de um recife artificial para protecção costeira e prática de surf. *IV Congresso sobre Planeamento e Gestão das Zonas Costeiras dos Países de Expressão Portuguesa* (Madeira, Portugal), electronic version.

4. Ten Voorde, M., Didier, E., Neves, M.G., Anselmo, A., Aveiro, L., Gil, L. & Antunes do Carmo, J.S., 2007. Modelação numérica de um recife artificial para a prática de surf: Comparação de resultados obtidos por três modelos matemáticos. *5as Jornadas Portuguesas de Engenharia Costeira e Portuária* (Lisbon, Portugal), electronic version.

5. Reis, M.T.; Neves, M.G.; Hu, K.; ten Voorde, M., 2008. "Numerical and physical modelling of wave overtopping over a porous breakwater". *The 18th International Offshore (Ocean) and Polar Engineering Conference (ISOPE)*, (Vancouver, Canada), electronic version.

6. Ten Voorde, M., Antunes do Carmo, J.S., Neves, M.G., 2008. Numerical investigation of multi-functional artificial reefs for coastal protection. *1ˢᵗ PoCoast seminar on Coastal Research* (Porto, Portugal) *(in press)*.

7. Ten Voorde, M., Antunes do Carmo, J.S., Neves, M.G., Mendonça, A., 2009. Experimental study to multi-functional artificial reef parameters. *Coastal Processes 2009* (La Valetta, Malta) *(in press)*.

8. Mendonça, A., Borrego, M., Ten Voorde, M., Neves, M.G., Antunes do Carmo, J.S., 2009. Ensaios bidimensioniais da rebentração sobre um recife artificial. 6as Jornadas Portuguesas de Engenharia Costeira e Portuária (Funchal, Madeira, Portugal) (in press).

ANNEXES

ANNEX I

Annex I.a - Iribarren number < 0.6

Height reef = 0.19 m	Height reef = 0.36 m

Submergence is 0.24 m

Hm = 0.26 m Tm = 2.44 s S = 0.24 m Ir = 0.60

Submergence is 0.24 m

Hm = 0.31 m Tm = 2.52 s S = 0.24 m Ir = 0.57

Annex I.b - 0.6 ≤ Iribarren number < 0.8

| Height reef = 0.19 m | Height reef = 0.36 m |

Submergence is 0.12 m

Submergence is 0.12 m

| Hm = 0.18 m Tm = 2.52 s S = 0.12 m Ir = 0.75 |

| Hm = 0.18 m Tm = 2.52 s S = 0.12 m Ir = 0.75 |

Submergence is 0.16m

Submergence is 0.16 m

| Hm = 0.24 m Tm = 2.52 s S = 0.16 m Ir = 0.65 |

| Hm = 0.19 m Tm = 2.52 s S = 0.16 m Ir = 0.72 |

Hm = 0.18 m Tm = 2.52 s S = 0.16 m Ir =0.75

Hm = 0.23 m Tm = 2.84 s S = 0.16 m Ir =0.75

Hm = 0.20 m Tm = 2.84 s S = 0.16 m Ir =0.79

Submergence is 0.20 m

Submergence is 0.20 m

Hm = 0.23 m Tm = 2.49 s S = 0.20 m Ir =

181

$Hm = 0.23$ m $Tm = 2.52$ s $S = 0.20$ m $Ir = 0.66$

$Hm = 0.18$ m $Tm = 2.47$ s $S = 0.20$ m $Ir = 0.73$

$Hm = 0.18$ m $Tm = 2.52$ s $S = 0.20$ m $Ir = 0.74$

$Hm = 0.23$ m $Tm = 2.84$ s $S = 0.20$ m $Ir = 0.75$

Submergence is 0.24 m

Hm = 0.26 m Tm = 2.52 s S = 0.24 m Ir = 0.61

Hm = 0.31 m Tm = 2.84 s S = 0.24 m Ir = 0.64

Hm = 0.33 m Tm = 3.16 s S = 0.24 m Ir = 0.69

Hm = 0.26 m Tm = 3.84 s S = 0.24 m Ir = 0.69

Hm = 0.28 m Tm = 3.16 s S = 0.24 m Ir = 0.75

Hm = 0.29 m Tm = 3.16 s S = 0.24 m Ir = 0.74

Hm = 0.17 m Tm = 2.52 s S = 0.24 m Ir = 0.77

Annex I.c - 0.8 ≤ Iribarren number < 1

Height reef = 0.19 m

Submergence is 0.08 m

Height reef = 0.36 m

Submergence is 0.08 m

Hm = 0.12 m *Tm* = 2.40 s *S* = 0.08 m *Ir* = 0.87

Hm = 0.13 m *Tm* = 2.52 s *S* = 0.08 m *Ir* = 0.87

Hm = 0.07 m *Tm* = 1.90 s *S* = 0.08 m *Ir* = 0.91

Hm = 0.06 m *Tm* = 1.84 s *S* = 0.08 m *Ir* = 0.93

Hm = 0.13 m *Tm* = 2.84 s *S* = 0.08 m *Ir* = 0.97

Submergence is 0.12 m

Hm = 0.12 m Tm = 2.52 s S = 0.12 m Ir =0.90

Hm = 0.18 m Tm = 2.84 s S = 0.12 m Ir = 0.83

Hm = 0.13 m Tm = 2.52 s S = 0.12 m Ir =0.86

Hm = 0.18 m Tm = 3.16 s S = 0.12 m Ir =0.94

186

Hm = 0.14 m Tm = 2.84 s S = 0.12 m Ir = 0.97

Hm = 0.14 m Tm = 2.84 s S = 0.12 m Ir =0.97

Submergence is 0.16 m

Submergence is 0.16 m

Hm = 0.19 m Tm = 2.84 s S = 0.16 m Ir =0.82

Hm = 0.23 m Tm = 3.16 s S = 0.16 m Ir = 0.83

Hm = 0.13 m Tm = 2.52 s S = 0.16 m Ir = 0.88

Hm = 0.19 m Tm = 3.16 s S = 0.16 m Ir = 0.92

Hm = 0.17 m Tm = 3.16 s S = 0.16 m Ir = 0.97

Hm = 0.14 m Tm = 2.84 s S = 0.16 m Ir = 0.96

Hm = 0.13 m Tm = 2.84 s S = 0.16 m Ir = 0.97

Submergence is 0.20 m

Submergence is 0.20 m

Hm = 0.24 m Tm = 3.16 s S = 0.20 m Ir = 0.81

Hm = 0.23 m Tm = 3.16 s S = 0.20 m Ir =0.83

$Hm = 0.18$ m $Tm = 3.16$ s $S = 0.20$ m $Ir = 0.93$

$Hm = 0.23$ m $Tm = 3.16$ s $S = 0.20$ m $Ir = 0.83$

Submergence is 0.24 m

$Hm = 0.23$ m $Tm = 3.16$ s $S = 0.24$ m $Ir = 0.83$

Annex I.d - 1.0 ≤ Iribarren number < 1.2

| **Height reef = 0.19 m** | **Height reef = 0.36 m** |

Submergence is 0.08 m   *Submergence is 0.08 m*

| Hm = 0.12 m Tm = 2.78 s S = 0.08m Ir =1.00 | Hm = 0.08 m Tm = 2.47 s S = 0.08 m Ir =1.07 |

| Hm = 0.06 m Tm = 2.05 s S = 0.08 m Ir =1.07 | Hm = 0.13 m Tm = 3.16 s S = 0.08 m Ir =1.09 |

| Hm = 0.08 m Tm = 2.50 s S = 0.08 m Ir =1.10 |

Hm = 0.09 m Tm = 2.81s S = 0.08 m Ir = 1.19

Submergence is 0.12 m

Hm = 0.08 m Tm = 2.52 s S = 0.12 m Ir = 1.09

Submergence is 0.12 m

Hm = 0.13 m Tm = 3.16 s S = 0.12 m Ir = 1.09

Hm = 0.13 m Tm = 3.16 s S = 0.12 m Ir = 1.10

Hm = 0.08 m Tm = 2.52 s S = 0.12m Ir = 1.10

191

Hm = 0.09 m *Tm* = 2.84 s *S* = 0.12 m *Ir* =1.19

Hm = 0.09 m *Tm* = 2.78 s *S* = 0.12 m *Ir* =1.19

Submergence is 0.16 m

Hm = 0.12 m *Tm* = 3.16 s *S* = 0.16 m *Ir* =1.14

Annex 1.e - Iribarren number ≥ 1.2

$$\boxed{\textbf{Height reef} = \textbf{0.19 m}}$$

Submergence is 0.12 m

$$\boxed{Hm = 0.09 \text{ m} \quad Tm = 3.16 \text{ s} \quad S = 0.12 \text{ m} \quad Ir = 1.34}$$
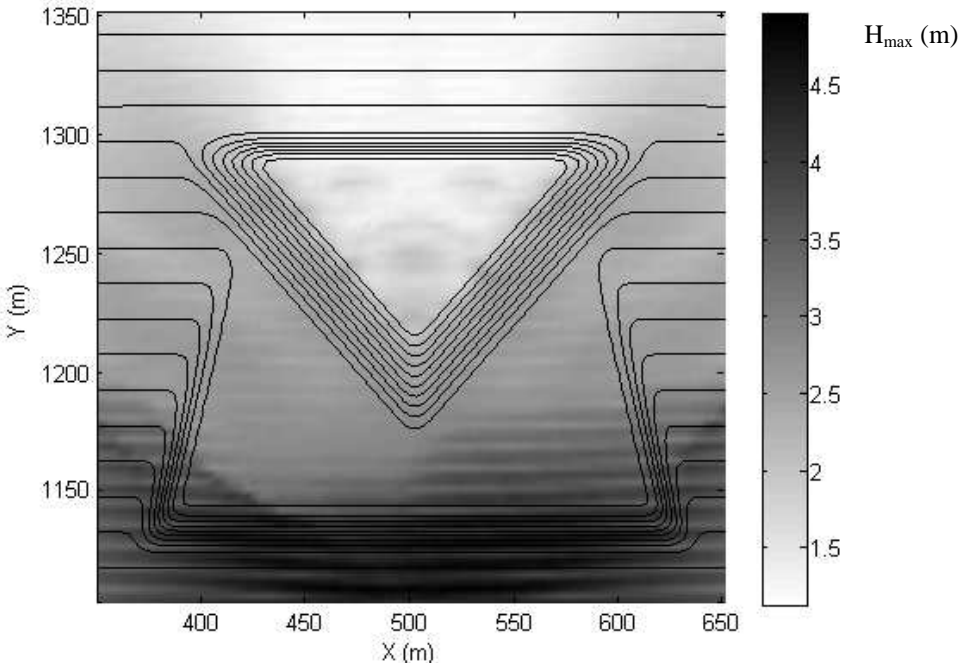
ANNEX II

Case 1

Figure II.1 - Wave height around reef for case 1.

Case 3

Figure II.2 - Wave height around reef for case 3.

Case 5

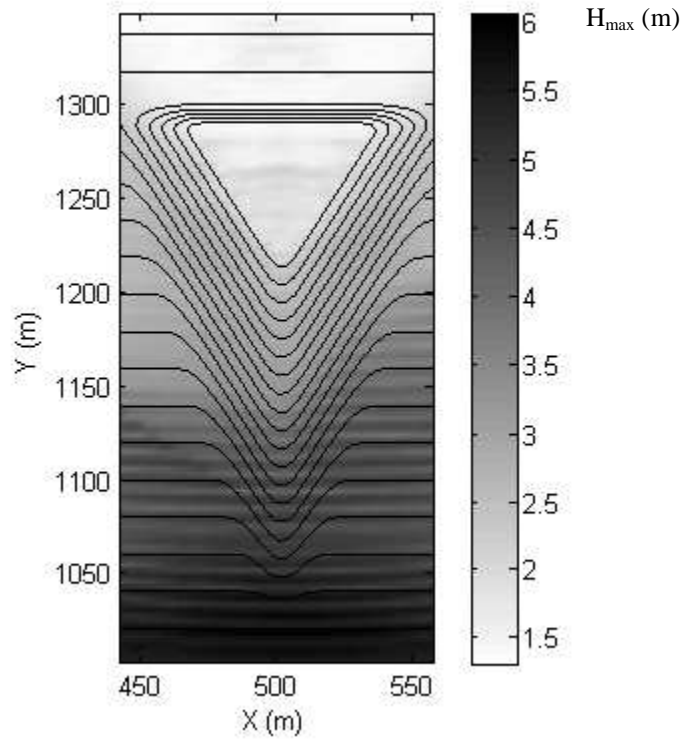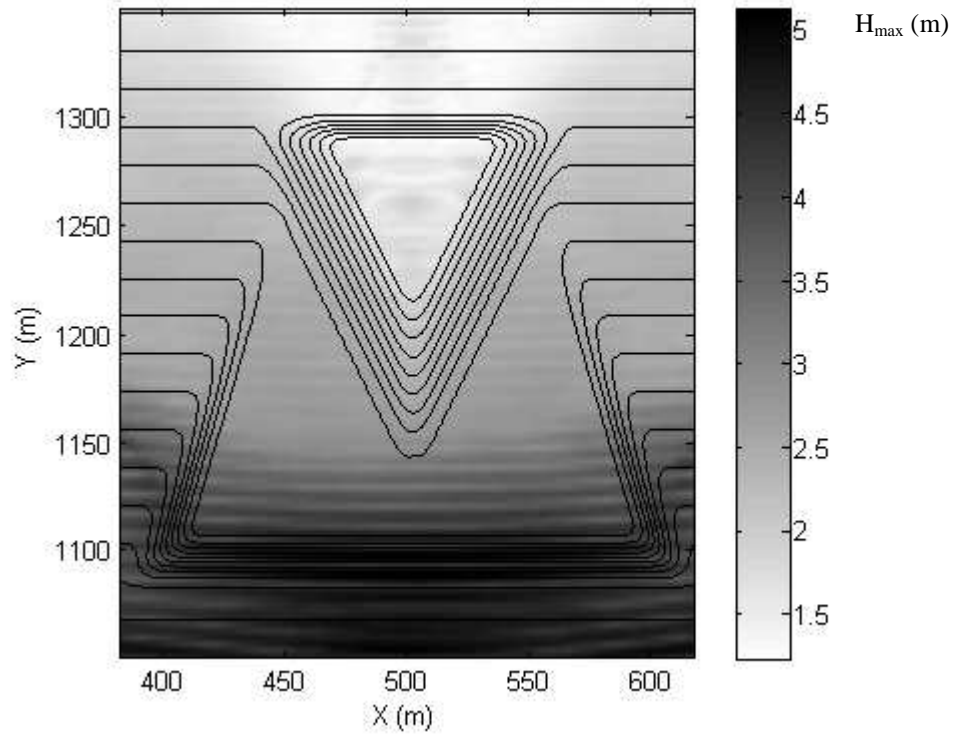Figure II.3 - Wave heights around reef for case 5.

Case 7

Figure II.4 - Wave heights around reef for case 7.